Impact of variable proton relative biological effectiveness on estimates of secondary cancer risk in paediatric cancer patients

Vilde Grandemo

Supervisors: Kristian Smeland Ytre-Hauge and Camilla Hanquist Stokkevåg

Master thesis in medical physics and technology

Department of Physics and Technology

University of Bergen

November 2018

Acknowledgements

First of all, I would like to thank my supervisors, Dr. Kristian S. Ytre-Hauge and Dr. Camilla H. Stokkevåg, for your invaluable help and guidance throughout this project.

Thank you, Kristian, for introducing me to the exciting field of proton therapy, for presenting me with the topic of my thesis and for providing necessary tools to conduct it. Thank you, Camilla, for all your help with secondary cancer risk modelling, for your high-quality proofreading and thorough explanations. Thank you both for your excellent and educational feedback. You have made this a highly enjoyable experience. I would also like to thank Ph.D. candidate Lars Fredrik Fjæra for providing me with the python scripts used in this thesis, as well as helping me with modifications when necessary.

In addition, I would like to thank Turid Husevåg Sulen and Camilla Grindeland Boer at the medical physics department at Haukeland University Hospital for allowing me to observe a national dose planning video conference, as well as showing me the dose planning process and letting me try out a few patient cases with proton therapy treatment in RayStation. It was very inspiring and educational.

Thank you to all my friends and fellow physics students at the institute for your support and encouragement for these past five years. You are truly an amazing group of people and I am very privileged to be a part of your academic and social community.

A special thanks to my mother, father and brother for your endless support in every way and for always keeping my spirits up. Finally, I would like to thank Simen for always being there for me during this period. I really appreciate all you have done.

Bergen, November 2018
Vilde Grandemo

Abstract

Background: Proton therapy has an increased dose-conformity compared to conventional radiotherapy with photons, and paediatric cancer patients receiving cranio-spinal irradiation (CSI) are routinely referred to this treatment modality. With long life-expectancy and enhanced radiosensitivity, children are at a significant risk of developing radiation-induced secondary cancers, emphasising the importance of secondary cancer risk estimations following proton therapy for these patients. Previous comparative studies on secondary cancer risk following proton and photon CSI treatment plans for paediatric cancer patients have based the proton risk estimates on a constant proton relative biological effectiveness (RBE) of 1.1. As the proton RBE varies with factors such as linear energy transfer (LET), dose, and tissue type, it is important to investigate how a variable proton RBE may affect the secondary cancer risk estimates for this patient group.

Materials and methods: Proton CSI treatment plans for ten paediatric medulloblastoma patients were analysed with respect to the risk of radiation-induced secondary cancer of the lungs and thyroid by comparing risks predicted by the clinical proton RBE of 1.1 to the risk predictions of four variable RBE models (LET-weighted dose, the McNamara model, the Rørvik model, and the Wilkens model). By applying the organ equivalent dose (OED) concept to different dose-response scenarios, the lifetime attributable risk (LAR) and the excess absolute risk (EAR) were estimated based on age-, sex-, and site-specific risk coefficients gathered from epidemiological data on the Japanese A-bomb survivors.

Results: All secondary cancer risk estimates were higher for the variable RBE models compared to the constant RBE of 1.1 for both organ sites, independent of dose-response relationship used. The risk predictions were highest with the variable RBE models that used tissue parameters corresponding to late reacting tissues which, depending on chosen organ site and dose-response relationship applied, predicted a 9 to 47% increase in risk from the constant RBE estimates.

Conclusion: Regardless of risk model applied, the estimated risk of radiation-induced secondary cancer of the lungs and thyroid will increase when the proton RBE is variable and not constant. However, the enhanced secondary cancer risk estimates found in this thesis were not high enough to impact the conclusion made by previous studies: that proton CSI is the better option compared to photon CSI with respect to estimated secondary cancer risk for radiotherapy of paediatric medulloblastoma patients.

Contents

List of abbreviations

3D-CRT	3D Conformal Radiotherapy
BEIR	Biological Effects of Ionizing Radiation
CCSS	Childhood Cancer Survival Study
CSI	Cranio-Spinal Irradiation
CTV	Clinical Target Volume
DDREF	Dose and Dose-Rate Effectiveness Factor
DSB	Double-Strand Breaks
DVH	Dose Volume Histogram
EAR	Excess Absolute Risk
ERR	Excess Relative Risk
ICRP	International Commission on Radiological Protection
ICRU	International Commission on Radiological Units and Measurements
IMPT	Intensity-Modulated Proton Therapy
IMRT	Intensity-Modulated Radiotherapy
LAR	Lifetime Attributable Risk
LET	Linear Energy Transfer
LQ	Linear-Quadratic
LSS	Life Span Study
NTCP	Normal Tissue Complication Probability
OED	Organ Equivalent Dose
PS	Passive Scattering
PTV	Planning Target Volume
PY	Person-Year
RBE	Relative Biological Effectiveness
RED	Risk Equivalent Dose
SOBP	Spread-Out Bragg Peak
SSB	Single-Strand Break
TCP	Tumour Control Probability
UNSCEAR	United Nations Scientific Committee on the Effects of Atomic Radiation

1. Introduction

Cancer is the second most important cause of death on a global scale, estimated to account for 9.6 million deaths in 2018 [1]. In Norway, over 32 000 new incidences of cancer were reported in 2016 where the cancer incidence has shown a persistent increase over the past 50 years for all cancer sites [2]. The same trend is shown for cancer survival, reflecting the improvements in both early detection and treatment of cancer.

Radiotherapy is one of the leading modalities used for cancer treatment in developed countries, with more than half of cancer patients receiving radiotherapy either alone or in combination with other modalities, mainly surgery and chemotherapy [3]. In radiotherapy, the dose delivered to the tumour to kill the cancerous cells is in the form of energy deposited by ionising radiation, aiming to deliver high radiation doses to the tumour volume while sparing the surrounding normal (healthy) tissue by keeping the dose here minimal [4].

1.1 Radiotherapy – past and present

The discovery of x-rays by the German physicist Wilhelm Conrad Röntgen in 1895 is considered the starting point of radiotherapy, which has been used in cancer treatment for more than a century [5]. Within the three following years, Antoine-Henri Bequerel and Pierre and Marie Curie discovered radioactivity emitted by radioactive sources, and a few years later radium was employed in cancer treatment. Both Bequerel and Pierre Curie recorded the biological effects of radiation they experienced through accidental (by Bequerel) and intentional (by Curie, allegedly) skin contact with radioactive sources, thus giving an introduction to the study of the action of radiation on living material, called radiobiology [5].

Since the early 1900s, radiotherapy has been undergoing massive improvements, including the invention of the CT scan by Hounsfield in 1971 that introduced computers in treatment planning, shifting it from 2D to 3D planning, and the use of multileaf collimators for 3D dose sculpting [6]. These inventions gave rise to the 3D conformal radiotherapy (3D-CRT). The early 2000s took this further by modulating the photon beam intensity during delivery, using so-called intensity-modulated radiotherapy (IMRT).

Treatment modalities using photons (e.g. 3D-CRT and IMRT) and electrons are the most common in radiotherapy today, with radiotherapy using protons as a promising alternative due to the possibility of reducing the dose to healthy tissues whilst avoiding a decline in the total dose to the tumour volume [4].

1.2 Proton therapy

Protons were first suggested as a possible candidate for particle therapy (radiotherapy with hadrons) in 1946 by Robert R. Wilson [7]. This suggestion was based on the spatial distribution of the proton energy deposition when traversing through material which differ from photons in that the main part of the energy is deposited at the end of the proton beam range, giving rise to what is called the Bragg peak (Figure 1.1) [4, 8]. Despite the promises this energy distribution could hold for conforming dose to the tumour and reduction of healthy tissue dose, proton therapy for treatment of cancer in humans was only used in moderate cases before experiencing an increase in use from the late 1980s and early 1990s [4]. Today, there are currently 71 proton therapy centres in operation around the world, and out of the more than 175 000 patients treated with particle therapy in 2016, about 145 000 received proton therapy [9, 10].

The physical properties of protons are well understood, but there still exist uncertainties regarding how protons affect biological matter. Proton radiation, like other ionising radiation, induce cell killing which makes it efficient at terminating cancerous cells when used as a modality in cancer treatment. Despite having an improved dose-

conformity over other radiotherapy modalities, protons can still irradiate normal tissues. Proton dose deposition in normal tissues can cause a number of serious acute and/or late side effects, which in rare cases includes the manifestation cancer. Radiation-induced cancer is called a long-term or late effect due to the often long latency period between radiation exposure and manifestation of disease [11]. Unlike photons, which have an extended history of use in clinical practice and thereby more experience with possible tissue effects, less is known about proton biological effects. In clinical practice today, protons are assumed 10% more biologically effective than photons, based on results from experiments on cells and animals [12, 13]. How biologically effective one type of radiation is compared to a reference radiation, is termed relative biological effectiveness (RBE), and for protons compared to photons (reference radiation) a constant RBE of 1.1 is used clinically. As it has been established that the RBE value of protons depends on many factors, this is a simplification and the proton RBE can potentially deviate appreciably from the value of 1.1, especially in the distal parts of the proton Bragg curve [13]. Thus, variable RBE models have been developed to account for variations in the proton RBE based on factors such as linear energy transfer (LET), dose, fractionation scheme, and tissue type.

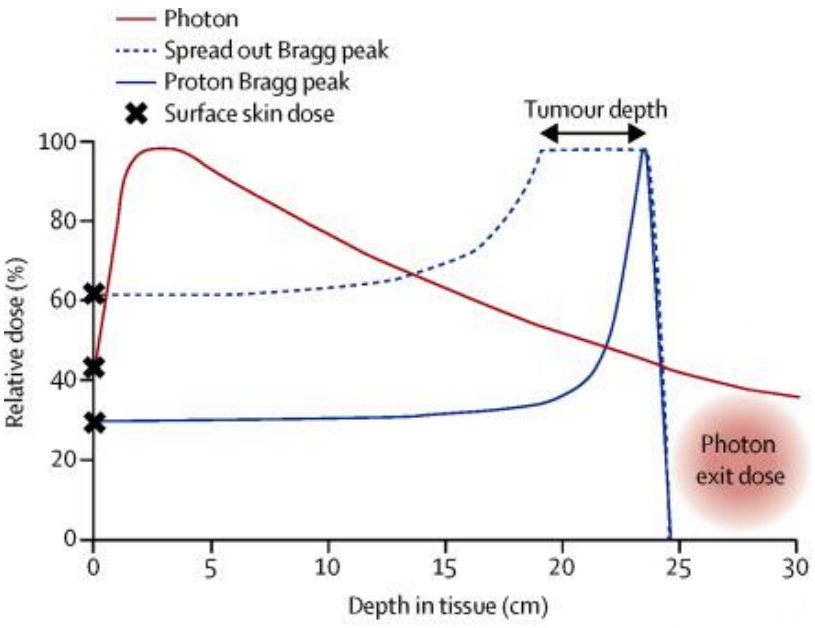

Figure 1.1: Illustration of depth dose depositions of protons (solid blue line) and photons (solid red line) traversing through tissue, with the dashed blue line representing the combination of multiple proton beams, forming a so-call spread-out Bragg peak (SOBP) [14].

1.3 Secondary cancer risk

Over the past several decades, the constant improvements in radiotherapy regarding tumour control and healthy tissue sparing has led to a significant increase in cancer cure rates and life-expectancy after treatment among cancer survivors [15]. Many countries also experience an age increase in the population and thereby a rise in the probability of cancer development, resulting in more cancer to be considered for radiation treatment. When ionising radiation has been used to successfully treat a primary tumour in a patient, the radiation may have caused sufficient amounts of cell damage and mutations in surrounding healthy tissue to increase the risk of inducing a new, or secondary, cancer [16]. The risk of developing a secondary cancer persists throughout life for radiotherapy survivors and, as most secondary cancers have a long latency period, increases with prolonged life after radiation treatment. This enhances the importance of using predictive modelling to estimate the potential increase in radiation-induced secondary cancer risk when evaluating different treatment options

for each patient case [15, 17]. Generally, information gathered from epidemiological[1] studies on irradiated populations and cancer registries from earlier radiotherapy is used as a basis for such secondary cancer risk models [18].

Children have a long life-expectancy after treatment, and thereby an enhanced risk of secondary cancer incidence. Children are also more radiosensitive than adults [15], further elevating the risk of developing a radiation-induced secondary cancer among paediatric cancer patients. Due to the improved dose-conformity of proton therapy compared to other radiotherapy techniques, this modality is routinely considered for the treatment of paediatric cancer patients [4]. Because there currently is no available epidemiological data or secondary cancer registries following proton therapy, predictive modelling of radiation-induced secondary cancer risks following proton therapy treatment is of particular importance to these patients.

1.4 Project objectives

For paediatric cancer patients, the most common malignant brain tumour is medulloblastoma [19]. In addition to surgery and chemotherapy, paediatric medulloblastoma is treated with cranio-spinal irradiation (CSI), with 5-year survival rates in the order of 80% [20]. Paediatric medulloblastoma patients receiving radiation treatment for their disease are at a significant risk of developing radiation-induced secondary cancers after treatment [21-23]. The promise of increased dose-conformity with proton therapy compared to photon therapy has caused many studies to compare proton CSI with photon CSI with respects to secondary cancer risk estimates following these treatment modalities for paediatric medulloblastoma patients [24-31]. All studies used a generic proton RBE of 1.1 for the proton CSI plans, which had the overall best results regarding possible secondary cancer risk compared to the photon CSI plans in

[1] Epidemiology is the study of the distribution of disease and disease-related factors in the human population

every study, without exceptions. It is therefore of interest to investigate how a variable proton RBE may affect the risk estimates for this patient group.

The main objective of this thesis was to estimate the risk of radiation-induced secondary cancer of specific sites following proton CSI treatment with both constant and variable RBE for paediatric medulloblastoma patients, to investigate whether the variations in RBE would result in a different risk compared to the constant RBE of 1.1. The calculations included four variable RBE models in addition to the constant RBE, which all were combined with different dose-response scenarios to estimate risk of radiation-induced secondary cancer of the lungs and the thyroid.

2. Physics of proton therapy

During radiotherapy, energy is transferred to the tissue as a result of the interaction between the beam particles and the traversed material [32]. Radiation is termed ionising radiation if the beam particles have sufficient energy to free electrons completely from the atoms or molecules in the material, i.e. to cause ionisation. Direct ionisation is possible for charged particles (electrons, protons, heavier ions) with enough energy to cause an interaction between the electromagnetic fields of the charged particle and the atomic electrons or nuclei (i.e. electromagnetic interaction), whereas photons and neutrons are termed indirectly ionising as they must first interact with the material to liberate directly ionising particles [32]. This chapter summarises the basic interactions of proton therapy – the interactions of the primary charged particles, i.e. the protons, and the interactions of the secondary uncharged particles that can be produced during proton therapy beam delivery, i.e. photons and neutrons.

2.1 Charged particle interactions with matter

Heavy charged particles interact with matter primarily in three ways: slowed down by electromagnetic (or Coulomb) interactions with atomic electrons, deflected by electromagnetic interactions with atomic nuclei or undergo nuclear interactions with a nucleus [4]. Protons fall into the category of "heavy" charged particles, which include all charged particles with a large rest mass compared to the rest mass of an electron [33].

2.1.1 Stopping power

The main energy loss of heavy charged particles is through electromagnetic interactions with atomic electrons, resulting in ionisation or excitation (i.e. raising the electron to a higher electron shell) of the atom [32, 34]. These electromagnetic interactions are referred to as inelastic collisions and they cause the charged particles to gradually slow down and eventually come to a complete stop. The rate of energy

loss per unit path length (*dE/dx*) is called the stopping power [4]. For the initial beam energies for proton therapy of typically up to 220 MeV/u, the rate of energy loss dominated by these inelastic collisions can be described by the Bethe-Bloch formula (given in the relativistic version by Fano (1963) [35]) [36]:

$$\frac{dE}{dx} = \frac{4\pi e^4 Z_t Z_p^2}{m_e v^2}\left[ln\frac{2m_e v^2}{\langle I\rangle} - \ln(1-\beta^2) - \beta^2 - \frac{C}{Z_t} - \frac{\delta}{2}\right] \quad (2.1)$$

Here, Z_p and Z_t are the charge of the projectile (particle) and the target, m_e and e are the electron mass and charge, $\langle I\rangle$ is the mean ionisation energy of the target atom or molecule, β is the particle velocity, v, relative to the speed of light, C/Z_t is the shell correction and $\delta/2$ is the density effect correction [36].

The stopping power is inversely proportional to the proton velocity which causes the energy loss to increase as the proton slows down, resulting in a maximum energy deposition at the end of the particle track (end-of-range), called the Bragg peak (Figure 1.1) [4, 8]. The range is defined as the depth at which half of the particles in the material have come to rest [37]. As the protons in a monoenergetic beam will experience individual interactions, they will not all stop at the same depth in the material [4]. This is called range straggling and is what defines the width of the proton Bragg peak [37].

2.1.2 Deflection and nuclear interaction

As protons are much heavier than electrons, the interactions with atomic electrons have little effect on the proton trajectory [34]. However, when protons undergo electromagnetic interactions with atomic nuclei, the protons are scattered, resulting in small deflections of the proton trajectories [4]. The sum of all these deflections can cause a significant lateral spread of the proton beam [34].

Although far less likely compared to the electromagnetic interactions, protons may also undergo nonelastic nuclear interactions by head-on collisions with a nucleus [4, 34]. In these collisions, the primary proton is removed from the beam and the nucleus absorbs

some of the proton energy which can cause an emission of secondary particles, such as protons and neutrons, that can travel relatively large distances and further increase the energy deposition in the material [34, 37].

2.1.3 Linear energy transfer

The ionisation density of protons varies with the proton energy, and thus with the position/depth in the patient. The ionisation density is related to the rate of energy loss per unit path length along the proton track, known as the linear energy transfer (LET) (Figure 2.1), which is inversely proportional with the proton energy and therefore increases with depth, in particular near the Bragg peak [38]. The LET ranges from 0.39 keV/µm for 250 MeV protons (highest therapeutically used energy for protons), rising with decreasing energy and reaching a maximum of 83 keV/µm at proton energies of 0.08 MeV [39]. The high-LET values in the Bragg peak region are related to an enhanced biological effectiveness when it comes to cell killing and may result in more severe biological damage than e.g. photon radiation (more on this in chapter 3).

In 1952, Zirkle et al. defined the LET as the average energy, dE_Δ, transferred to the material from a charged particle traversing the distance, dl [40, 41]:

$$L_\Delta = \frac{dE_\Delta}{dl} \tag{2.2}$$

L_Δ, usually expressed in units of keV/µm, refers to the restricted LET which excludes the energy carried away by secondary (i.e. freed) electrons with energies greater than Δ, i.e. with an energy cutoff of Δ [41]. When no energy cutoff is enforced, the unrestricted LET is equal to the stopping power, often denoted L_∞ or simply L.

In most experimental situations, there is a range of LET values, which the definitions above are unable to account for as they only apply to single particles or monoenergetic beams [42]. Therefore, the mean LET value is often reported, either as the track-averaged LET (LET_t) or the dose-averaged LET (LET_d). Of these two averages, the

LET_d is the most common to use in proton therapy and in modelling the biological effects of protons (chapter 3.3.1). LET_d is the mean value of the individual proton LETs, each weighted by the dose it deposits [42]. It accounts for both dose and LET, which is important when considering the biological outcome of radiotherapy [43].

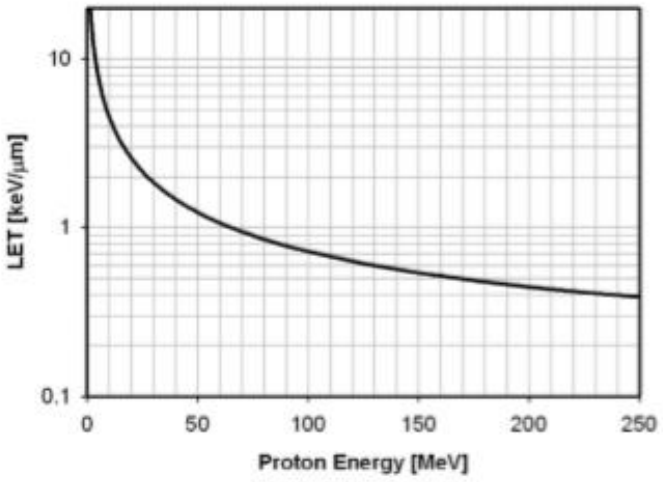

Figure 2.1: LET as a function of proton beam energy through water [13].

2.2 Photon interactions

Photons (x-rays and γ-rays) passing through matter may interact with the atoms of the traversing material – through interactions involving either the atomic electrons or the atomic nucleus – resulting in the photon being either completely absorbed or scattered [32, 44]. The number of photons that undergo such interactions is proportional to the number of incident photons and the thickness of the traversing material, and for a monoenergetic photon beam can be expressed as the decrease of photon beam intensity, *I(x)*, in the material of thickness *x*:

$$I(x) = I_0 e^{-\mu x} \tag{2.3}$$

where I_0 is the initial photon beam intensity and μ is the linear attenuation coefficient that yields the probability of photon absorption or scattering per unit path length [32, 45].

There are three principal processes of photon interaction which cause the attenuation of a photon beam in matter: photoelectric absorption, Compton scattering and pair production [32]. In photoelectric absorption, the photon is completely absorbed by the atom resulting in the ejection of one of the orbital electrons. In Compton scattering, the photon collides with a "free" atomic electron (atomic electron with binding energy much less than the incident photon energy), ejecting the electron from the atom and scatters with reduced energy [32]. For energies exceeding 1.022 MeV (the energy equivalent of the mass of an electron/positron pair) pair production may also occur, i.e. a photon is absorbed in the vicinity of an atomic nucleus and an electron/positron pair is created [45, 46].

2.3 Neutron interactions

Neutrons interact with atomic nuclei through three principal processes: elastic scattering, inelastic scattering and neutron capture [46]. The scattering processes (where inelastic scattering dominates at neutron energies above 10 MeV, and elastic scattering dominates at lower energies) cause the neutrons to slow down until they reach thermal energies and are completely absorbed (i.e. captured) by the nuclei and replaced by secondary radiations [4, 45, 46]. Secondary protons can also be produced by elastic scattering of fast neutrons with hydrogen nuclei, and the deposition of kinetic energies attained from the collision will contribute to the total energy deposition in the material [44, 46].

2.4 Dosimetry and depth dose curves

2.4.1 Absorbed dose

The radiation energy that is absorbed by matter is referred to as radiation absorbed dose. The absorbed dose is the basic physical dose quantity used for reporting dose in clinical radiotherapy as well as in radiological protection and radiation biology [47]. The absorbed dose, *D*, is defined as the mean energy, $d\bar{\varepsilon}$, imparted to a unit mass, *dm*, by ionising radiation [41]:

$$D = \frac{d\bar{\varepsilon}}{dm} \tag{2.4}$$

in SI units of J/kg, with special unit name gray (Gy). This definition applies to all types of ionising radiation of all energies traversing through a material [32]. The absorbed dose only gives information regarding the energy deposition of a particle and must therefore be modified by additional factors to account for different biological effects of each specific radiation type as well as the type of irradiated biological material/tissue [47]. For radiation protection purposes regarding low-dose exposure, the average absorbed dose in a tissue or an organ (T) is weighted by a radiation weighting factor w_R with respect to the biological effect of the radiation (R), called the equivalent dose, the sum of which can further be weighted by a tissue weighting factor w_T to account for the sensitivity of the exposed tissue or organ, called the effective dose [47]. Both terms are expressed in units of J/kg, with special unit name Sievert (Sv). For the high-dose exposures of particle therapy, different modifications to the absorbed dose are recommended (explained in chapter 3) [48].

2.4.2 Dose deposition and the Spread-out Bragg peak

An illustration of the depth dose curves of protons and photons is given in Figure 1.1, showing that the proton deposits less energy traversing through matter compared to the photon, until the end of the track where the maximum of the proton energy is deposited,

i.e. the Bragg peak. The photon depth dose curve, on the other hand, has a maximum energy deposition near the entrance of the material, or tissue, decreasing exponentially with depth (in accordance with eq. (2.3)) [49]. The goal for proton therapy is to have the Bragg peak positioned inside the target volume, i.e. the tumour. To ensure that the entire target volume is receiving the prescribed proton dose, the combination of many different mono-energetic proton beams is used in the treatment delivery, forming what is called a spread-out Bragg peak (SOBP), also illustrated in Figure 1.1 [4]. This SOBP can be achieved by what is called passive scattering (PS); using filters adapted to the patient and target volume, adjusting the proton beam to spread laterally to fit the target and to give a uniform dose distribution in the depth direction [4]. It can also be done by delivering the proton beam into the patient with less filters, steering the beam laterally with the help of e.g. magnetic fields and adjusting the beam energy to deliver the beam in different depths of the target volume. This is called pencil beam scanning, or intensity-modulated proton therapy (IMPT) [4].

3. Radiobiology of protons

Radiobiology is the study of how ionising radiation interacts with living matter [5]. It is well-established that ionising radiation is a carcinogen, i.e. it promotes the formation of cancer as a result of changes in the molecular structures caused by radiation damage to the cells [18]. The initial phase of radiobiological cell damage is set in motion by the physical process of interactions between ionising radiation and the atoms or molecules within a cell [16]. All subsequent processes (i.e. biological effects) are included in the biological phase. This includes how damage to the DNA of the cell can cause cell death or genetic mutations that may lead to cancer induction (carcinogenesis) [11].

3.1 The radiobiological impact of ionising radiation

The critical target in a cell is the DNA and damage to the DNA causes most biological effects of ionising radiation [5]. This includes cell killing, DNA mutations and carcinogenesis. There are two ways for ionising radiation to interact with biological matter [5]. The first is by ionising or exciting the target atoms, called direct action (the most common interaction for high-LET radiations), which starts the process that leads to biological alterations. The second is by interaction with other cellular atoms or molecules, called indirect action (which is around two thirds of the biological damage from photon radiation), generating highly reactive molecules that can cause damage to the DNA.

The most common radiation-produced lesions of DNA damage are single-strand breaks (SSB) and double-strand breaks (DSB) [49]. With DSB, both strands of the DNA helix are severed, making it impossible for one strand to act as a template for the repair of the broken strand (which is possible for SSB). Thus, DSB can be seen as critical lesions that may lead to most of the early and late radiation-induced effects. Several studies have proposed that the induction of DSB is higher for protons than for photons at clinically relevant energies, especially where protons have higher LET values (i.e. near

the Bragg peak) [49]. To assess the effect on cell killing, measurement of surviving cells after irradiation is performed in *in vitro*[2] studies [38].

The carcinogenic effect is stochastic, meaning that the probability of cancer formation is dose dependent, but the severity of the induced cancer itself has no relation to the dose [5]. In contrast, deterministic effects, such as radiation-induced skin redness, occur above a threshold dose, where the severity of the effect increases with dose [50]. Incorrectly repaired damage in a cell may lead to genetic mutation, where such mutations in somatic cells could be involved in cancer formation [11].

Radiation carcinogenesis is a multistage process, occurring over a long time period, where the induction of the initial mutation is called the initiation stage [17]. This is followed by a promotion phase expressing the acquired mutations. The last stage of the carcinogenesis process is the malignant progression phase. Here, the cells attain further mutations and thus become invasive. It may take several years, even decades, from starting the initiation stage until the clinical manifestation of the disease occurs.

3.2 The linear-quadratic model

Cell experiments quantifying cell survival after irradiation have been used to assess biological effects of ionising radiation. For instance, the number of surviving tumour cells can be used to model the tumour control probability (TCP), and normal tissue cell lines can be used to model the normal tissue complication probability (NTCP) [16]. The resulting cell survival curves are plotted as the surviving fraction against radiation dose, usually on a semi-logarithmic scale (Figure 3.1a) [16]. Radiobiological models are often applied to describe and analyse the relationship between cell survival and radiation dose in order to relate experimental data to clinical cancer treatment. The

[2] Experiments and procedures done outside living organisms, e.g. laboratory examinations of tissues and cell cultures done in test tubes. This is opposed to *in vivo* studies – experiments and procedures done inside a living organism

linear-quadratic (LQ) model [51] is frequently used to give a mathematical description of the continually downward bending shape of the cell survival curve (Figure 3.1b), fitting the curve by an exponential second-order polynomial, thus yielding the formulae for cell survival as a function of absorbed dose *D* [16]:

$$S(D) = e^{-\alpha D - \beta D^2} \tag{3.1}$$

The ratio of the parameters α and β determines the shape of the curve. To give the LQ model a mechanistic justification, an interpretation that the linear component $e^{-\alpha D}$ comes from single-track events and the quadratic component $e^{-\beta D^2}$ comes from double-track events has been proposed [16]. A single-track event is when a single hit from a particle track damages a site within a cell, whereas a double-track event is when two consecutive particle tracks hit and damage the same site within a cell. The quadratic component is therefore dependent on the dose-rate as a higher dose-rate will give less time for cell repair between hits. Thus, the α/β ratio gives the deposited radiation dose where the linear damage contribution is equal to the quadratic contribution, i.e. when $\alpha D = \beta D^2$ [16].

The α/β values are dependent on tumour or tissue type, with high α/β ratio for early responding tissues and fast growing tumours (expression of damage occurring days to weeks after irradiation) and low α/β ratio for late responding tissues and some slow growing tumours (expression of damage occurring months to years after irradiation) [16, 52]. The α/β ratios of the different tissue- and tumour types are used to describe fractionation[3] sensitivity and to make decisions regarding fractionation schemes in radiotherapy. Although several publications list α and β values obtained from the proton radiation survival curves, these are often characterised by large uncertainties,

[3] Dose fractionation – delivering the total radiation dose is divided into several fractions with lower dose – is a common practice in radiotherapy

and most of the literature therefore primarily use the α/β ratios for the reference x-ray/photon radiation when referring to cell/tissue type [13]. α/β values obtained from photon radiation survival curves will hereby be referred to as $(\alpha/\beta)_x$, in accordance with literature.

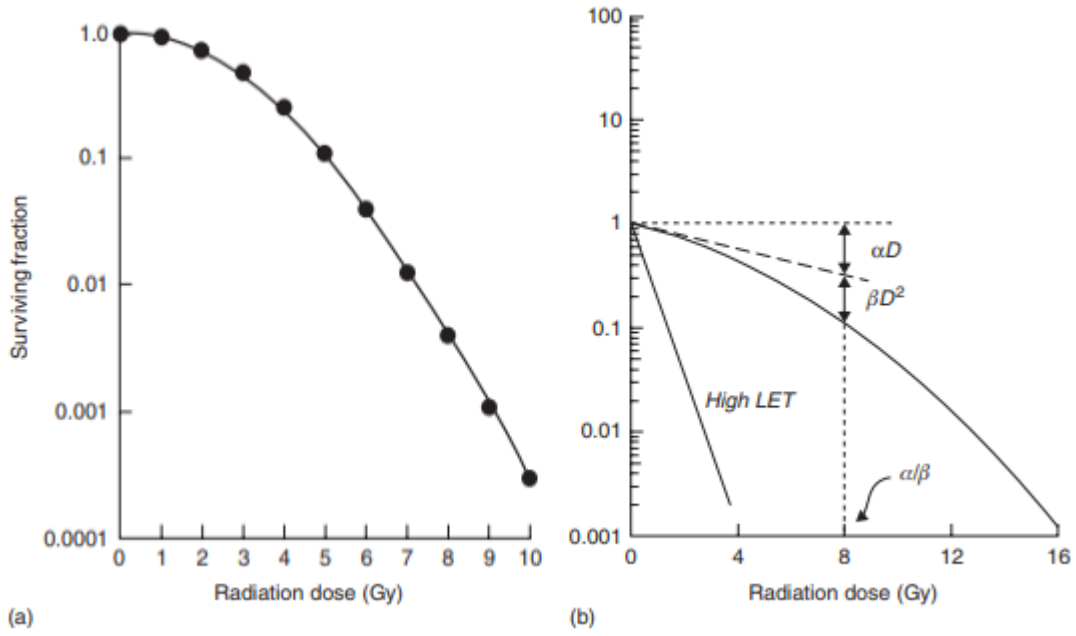

Figure 3.1: Cell survival curves, where a) show a typical cell survival curve for cells irradiated in tissue culture with low-LET radiation and b) show cell survival curves and parameters of the LQ model for both high-LET (straight solid line) and low-LET (bended solid line) [16].

There are some limitations to the LQ model, due to unclear validity at low doses (< approx. 1 Gy) and at high doses (> approx. 10 Gy) [13]. Other cell survival models based on the LQ model have been proposed to account for these limitations.

3.3 Relative biological effectiveness – RBE

The relative biological effectiveness, or RBE, of protons is a measure of how biologically effective proton radiation is compared to a reference radiation (e.g. ^{60}Co photons) when applying the same physical dose. The radiation doses should, per definition, be given under identical conditions to make the definition of RBE valid. The International Commission on Radiological Units and Measurements (ICRU)

recommends using the RBE-weighted dose with units Gy(RBE) (i.e. the proton absorbed dose, D_p, multiplied with the proton RBE) to represent the corresponding dose of photons, D_x, that will produce the same biological effect under the same conditions [48]. The proton RBE can therefore be described as the ratio of isoeffective absorbed doses of the reference radiation and the proton radiation that generate the same biological effect:

$$RBE = \frac{D_x}{D_p} \tag{3.2}$$

In clinical proton therapy, a generic value for proton RBE of 1.1 is used, meaning that proton radiation is assumed 10% more biologically effective than photon radiation for the same absorbed dose. This value of 1.1 has been obtained from experimental data as an average of measured RBE values, which mainly comes from *in vivo* studies on animal systems in the 1970s [12, 13]. RBE values obtained from *in vitro* data on the endpoint[4] of cell survival are typically somewhat higher.

The proton RBE is dependent on the total dose and dose fractionation, beam quality, tissue type and biological endpoint, and may thus vary with these factors. There have been several advances in understanding and determining proton RBE values since the animal studies in the 1970s, including increased clinical experience, published RBE values that deviate from the generic value and new models developed to determine how RBE may vary with additional factors. Such advances brings into question whether this value should be implemented as a variable and not a constant in treatment planning and optimisation [12]. If the proton RBE deviates from the generic value of 1.1, this could have clinical implications and impact on the estimation of radiation-induced side effects, including secondary cancer risk for proton therapy. To describe this further,

[4] Clinical endpoints represent or describe the outcomes of interest

one must look at the different RBE dependencies and how these may contribute to variations of the proton RBE.

3.3.1 RBE as a function of LET

The combination of dose-averaged LET (LET_d) and RBE-weighted dose contribute to the proton RBE at each point in the SOBP. Figure 3.2 illustrates how LET_d distributions of a proton beam show a slight increase throughout the SOBP, with a significant increase in LET_d value, and thus in RBE value, at the distal end of the SOBP [12, 13]. This effect becomes greater for proton beams with lower initial energy and smaller modulation widths, potentially reaching a maximum LET_d value of around 20 keV/µm in the fall-off region [13]. In general, the proton RBE has shown an increase with increasing LET_d and the variable RBE models in Figure 3.2 demonstrate that the proton RBE is potentially much larger than 1.1 at LET_d values approaching the maximum LET_d of around 20 keV/µm.

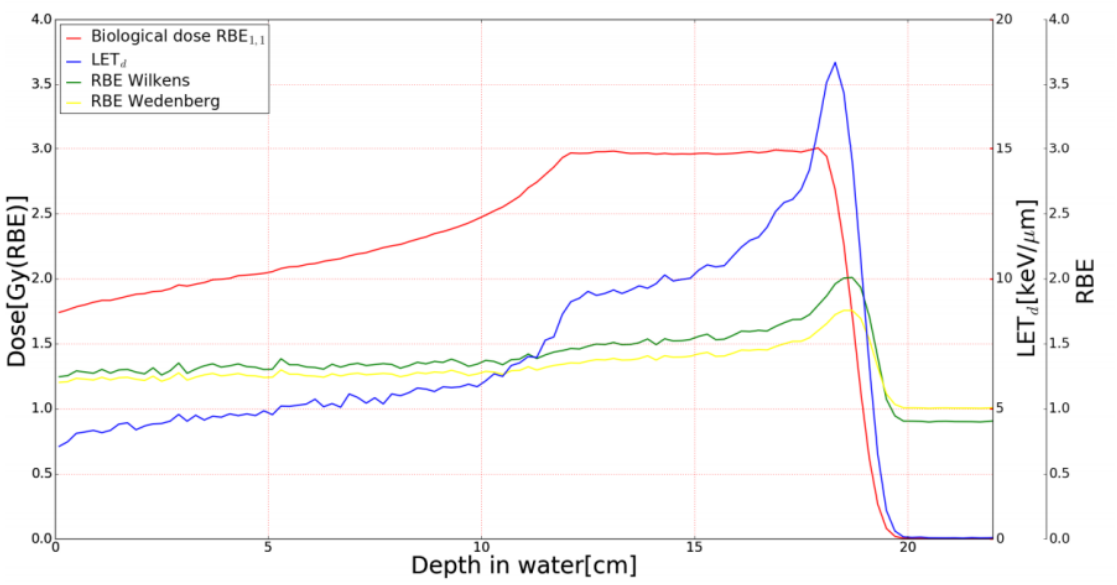

Figure 3.2: Illustration of a proton SOBP depth dose distribution with clinical RBE of 1.1 (red line) and the respective LET_d distribution (blue line). The relationship between RBE and LET_d is demonstrated by the curves for the two variable RBE models of Wilkens (green line) and Wedenberg (yellow line) with corresponding RBE values shown by the RBE scale on the far right [53].

3.3.2 Other RBE dependencies

There has been established an RBE dependency on $(\alpha/\beta)_x$, on dose and dose fractionation, and on clinical and biological endpoints. In general, an increase in RBE is observed with decreasing $(\alpha/\beta)_x$ [13, 54]. The higher α/β shown in proton experiments compared to photon experiments leads to an increase in RBE with decreasing dose [54]. Lastly, the clinical proton RBE value of 1.1 is for the endpoint of cell inactivation and tumour response, and other clinical and biological endpoints may have additional variations in proton RBE values [55].

3.3.3 RBE models

There have been several phenomenological models[5] proposed to account for possible RBE variations as an alternative to using the generic proton RBE of 1.1. Most of these models are derived from fits to experimental data points and calculate the proton RBE using RBE formalisms based on the LQ model. Using equation (3.2) within the LQ framework (eq. (3.1)), RBE can be expressed as a function of the proton dose, D_p, and the tissue parameters α and β for protons and α_x and β_x for photons [13, 56, 57]:

$$RBE\left(D_p, \alpha, \alpha_x, \beta, \beta_x\right) = \frac{D_x}{D_p}$$

$$= \frac{1}{2D_p}\left(\sqrt{\left(\frac{\alpha}{\beta}\right)_x^2 + 4D_p\left(\frac{\alpha}{\beta}\right)_x \frac{\alpha}{\alpha_x} + 4D_p^2 \frac{\beta}{\beta_x}} - \left(\frac{\alpha}{\beta}\right)_x\right) \tag{3.3}$$

From this, the RBE in the higher limit of surviving fraction (RBE_{max}) can be obtained when $D_p = 0$ [58], and the RBE in the lower limit (RBE_{min}) can be obtained when $D_p \to \infty$ [59]:

$$RBE_{max} = \frac{\alpha}{\alpha_x} \tag{3.4}$$

$$RBE_{min} = \sqrt{\frac{\beta}{\beta_x}} \tag{3.5}$$

From these two functions, describing the extreme RBE at low and high doses, respectively, equation (3.3) can be written as

[5] Phenomenological models describe the empirical relationships of phenomena observed in experiments without explaining the underlying cause of these relationships

$$RBE\left(D_p, (\alpha/\beta)_x, RBE_{max}, RBE_{min}\right) = \frac{1}{2D_p}\left(\sqrt{\left(\frac{\alpha}{\beta}\right)_x^2 + 4D_p\left(\frac{\alpha}{\beta}\right)_x RBE_{max} + 4D_p^2 RBE_{min}^2} - \left(\frac{\alpha}{\beta}\right)_x\right) \quad (3.6)$$

Equation (3.6) is common for all LQ-based RBE models, whereas the differences between these models occur in their definition of RBE_{max} and RBE_{min}. Results have shown varying degrees of RBE dependence on LET_d, either through a linear relationship (e.g. McNamara, Wilkens, Wedenberg, Carabe) [39, 60] or a non-linear (e.g. Rørvik) [61]. Other models have had a stronger focus on variations in LET_d for proton therapy plans by using the LET_d distribution directly, assuming a linear dependency of LET_d on RBE (Unkelbach) [62]. Different variable RBE models are shown in relation to a constant RBE of 1.1 in Figure 3.3. Here, the model predictions of variable proton RBE values could affect risk estimations of radiation-induced secondary cancer for proton therapy in a way that may differ from such estimations calculated using the clinical value of 1.1.

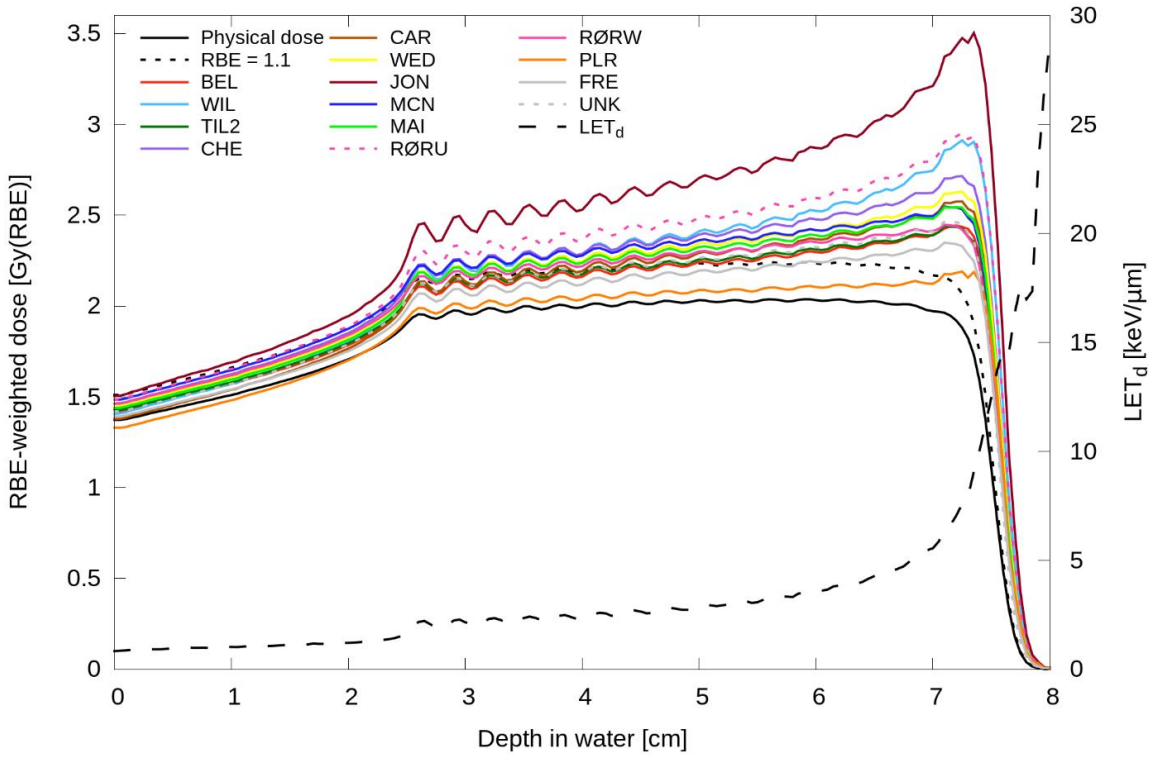

Figure 3.3: Depth dose distributions of SOPBs in water calculated by different RBE models using an $(\alpha/\beta)_x$ value of 3.76 Gy. The RBE estimates of the different RBE models (in colours) are shown in relation to the clinical RBE value of 1.1 (dotted black line), with the LET_d distribution (dashed black line) on the right y-axis [63].

4. Estimating radiation-induced secondary cancer for proton therapy

Developing a radiation-induced secondary cancer after the successful treatment of a primary cancer has been a concern for many years, dating back to the first decades of radiotherapy. In the following years, many epidemiological studies have therefore been conducted regarding the carcinogenic effect of radiotherapy, and they have shown that radiotherapy leads to a small but significant risk of secondary cancer induction [17]. Several of these studies have also pointed out different factors that may influence the risk of secondary cancer incidence following radiotherapy. These factors include for instance genetic susceptibility, hormonal mechanisms, lifestyle and age [11]. The age factor underlines that the risk of secondary cancer induction is of particular importance to paediatric patients due to their long life expectancy after treatment as well as increased radiosensitivity. These patients also have high long term survival rates (the 5-year relative survival rate for children of 0-14 years from 2005-2011 was 83.4% for all childhood cancers [64, 65]) which emphasises the relevance of secondary cancer risk for this patient group [27, 29, 66]. Literature investigating the potential benefits of proton therapy compared to photon therapy exist for paediatric patients [24-31, 66-68] and exhibit indications that proton therapy may be a better option in reducing potential side effects, at least for specific cancer sites. To establish whether there truly is an advantage in using proton therapy over photon therapy in treatment of paediatric cancers, long-term post-treatment follow-up studies are needed.

Generally, epidemiological studies on radiation aim to describe the different effects of ionising radiation in exposed populations [18]. There is little to no data on secondary cancer incidence following proton therapy that can be used for risk assessments for this modality. Therefore, data from epidemiological studies on (non-proton) radiation combined with theoretical modelling can be used to estimate the risk of secondary cancer incidence following a successful proton therapy treatment. Epidemiological studies directly concerning the carcinogenic effect of radiotherapy are only a fraction

of the epidemiological studies on the effects of radiation in exposed populations. Other radiation exposed groups can include those subjected to accidental exposure, professional exposure, and medical exposure for diagnostic purposes [11]. Due to the statistical power of some of these studies (which include large cohorts, thorough follow-up, large ranges of radiation doses etc.), they form the basis for many risk estimations on secondary cancers following radiotherapy, including risk estimations made by the Biological Effects of Ionizing Radiation (BEIR) VII report and the United Nations Scientific Committee on the Effects of Atomic Radiation (UNSCEAR) report [18, 69]. However, these epidemiological data mostly concerns irradiated populations exposed to radiation doses quite different to what is commonly used in radiotherapy (e.g. more uniform dose distributions, and whole body irradiation) [11, 70]. Furthermore, the radiation techniques from data on the follow up of cancer patients are no longer in use and are also quite different from the radiation techniques used today. Thus, theoretical models for predicting the risk of radiation-induced secondary cancer have been developed to extrapolate such epidemiological data to modern day radiation treatment techniques and dose-ranges relevant for radiotherapy as well as using the proton RBE to make the doses from e.g. photon irradiation applicable to proton therapy [17, 54].

4.1 Epidemiological data

Data from epidemiological studies can be used to quantify the risk of developing a radiation-induced cancer as well as to determine the different factors that can affect this development. There has also been a focus on finding a relationship between the risk of developing certain types of cancer and the average dose relevant for these cancer inductions [70]. Epidemiological studies that can be used for cancer risk estimations following radiotherapy are presented below. The information about the studies presented here are gathered primarily from the BEIR VII report [18] and the UNSCEAR report [69] and concern the follow-up of the Japanese A-bomb survivors and patients irradiated for medical purposes. Studies on occupational exposure and

environmental exposure are not included because of the difficulty in assessing the risk of radiation-induced cancers following these types of exposure, either due to lack of information regarding the received radiation dose (occupational) or inability to provide reliable risk estimates (environmental).

4.1.1 The Life Span Study cohort

The follow-up of Japanese survivors of the atomic-bombings of Hiroshima and Nagasaki, also referred to as the Life Span Study (LSS) cohort, is deemed the most important cohort of irradiated populations studied for the development of cancer risk estimates for irradiated populations [5, 18]. This is mainly due to its large population size of approx. 120 000 people, where the 93 000 persons who were in one of the cities during the bombings have been the primary cohort for analyses since the early 1970s [18]. Other factors that make this cohort valuable in radiation epidemiology is the long and thorough follow-up, that the cohort consists of persons of both sexes and of all ages, and that the cohort received short-term exposure to different doses of high- and low-LET radiation [11]. The LSS cohort received doses of γ- and neutron radiation at high dose-rates, where around 50 000 of the survivors received doses between 5 mSv and 2 Sv [5, 18]. The survivors that were exposed at low doses are often used in assessing the biological effects at these dose levels, and the many survivors exposed at higher dose levels form a basis for estimating risks that can be related to therapeutic irradiations [18]. Despite that there exist uncertainties regarding exact dose received by the survivors as well as the pattern of irradiation, the data from this group has formed the basis for many radiation-induced secondary cancer risk estimations. Specifically, for the doses ranging from around 0.1 Gy to 2.5 Gy, a linear dose-response relationship has been produced by the data from this cohort, which is referred to as the “gold standard” and viewed as a good estimation for secondary cancer risk following these doses (Figure 4.1) [71].

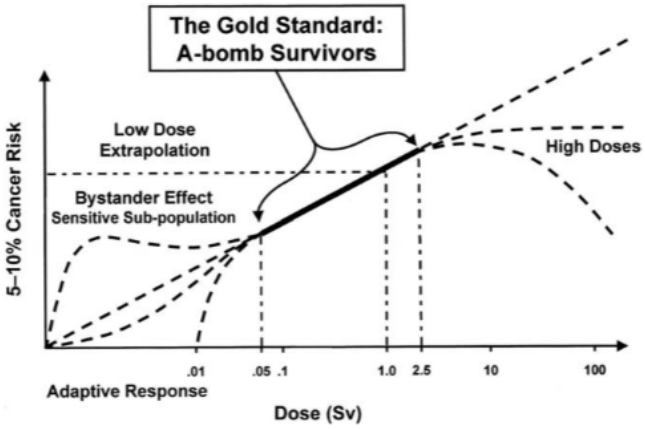

Figure 4.1: Schematic dose-response relationship for radiation-induced carcinogenesis in humans. The atomic-bomb data represents the “gold standard” – the best quantitative data over a dose range of approximately 0.1-2.5 Gy. There are considerable uncertainties in the dose-response relationship above and below this dose range [71].

Because the LSS cohort received whole-body irradiations, reports on health risks following radiation exposure, like BEIR VII and UNSCEAR, have been able to assess risks for specific cancer sites and evaluate the comparability of these site-specific risks [18, 69].

4.1.2 Medical exposure

One of the largest populations that provide epidemiological data on the effects of radiation is patients irradiated for medical purposes, either by diagnostic examination or through treatment of benign or malignant disease [11, 18]. Patients receiving radiation for diagnostic purposes make up the largest subgroup, and are typically exposed to low radiation doses of about 0.5 mSv annually, with examinations occurring at least twice a year on average [18]. Because of this low dose exposure, the findings of studies on diagnostic irradiation regarding risk of cancer induction may be difficult to apply to radiotherapy patients receiving much higher doses over a shorter time period. Thus, epidemiological data on follow up of cancer patient cohorts that have undergone curative radiotherapy have been suggested as the data that can provide the

best estimates of radiation-induced secondary cancer risk [11]. The higher doses that are delivered to the target volume are typically in the 50-60 Gy dose-range, and the low doses that can be received by organs further away from the target area are usually 100 mGy or less [18]. These studies can therefore provide information on secondary cancer risk following both high and low radiation doses as well as the effects of fractionation used in radiotherapy and site-specific secondary cancer risk [18, 69]. The effects of cell killing and fractionation have been assumed to be largely the reason for the generally lower risk estimates following radiotherapy compared to those for the LSS cohort [69].

Clinical evidence

Generally, studies that aim to estimate secondary cancer risk following radiotherapy have focused on patients receiving radiation treatment for malignant diseases who have a high chance of long-term survival, such as patients with cervical cancer, breast cancer, Hodgkin's disease, and childhood cancers [18]. Studies on the risk of radiation-induced secondary cancer for cervical cancer patients have provided risk estimates for breast cancer, leukaemia, and stomach cancer and have generally shown an increase in risks for cancers of the stomach, rectum, urinary bladder, bone and joints [18, 69]. Another studied group is patients treated for Hodgkin's disease, or Hodgkin's lymphoma, which is a special case of lymphoma[6] that has mostly been treated with a combination of radiotherapy and chemotherapy [18]. A number of cohort and case-control studies on the treatment of Hodgkin's disease has been conducted, showing a general increase in secondary cancer risks of the lungs and breast [69]. Secondary cancer risks following radiation treatment of childhood cancers have been evaluated by combining data gathered by different groups world-wide [18]. The risks were suggested to be as high as 12% during the first 25 years after diagnosis. One study of

[6] Cancer that starts in the lymphocytes (white blood cells)

a larger patient cohort concerning secondary cancer[7] following treatment of a primary childhood cancer is the Childhood Cancer Survival Study (CCSS), consisting of 14 363 5-year (at least) survivors of childhood cancer treated between 1970 and 1986 [72]. The study showed that radiotherapy increased the risk of all secondary cancers, with relationships between secondary cancer risk and dose estimated for specific cancer sites. This included a linear-exponential relationship between radiation dose and secondary thyroid cancer risk, where the risk increased up to doses of 29 Gy and then decreased for doses > 30 Gy, as well as a linear relationship between dose and risk of both secondary brain tumours and secondary breast cancer [72].

4.2 Predictive modelling

Theoretical models can be used to extrapolate the risk estimation data from relevant epidemiological studies, making estimates from accidental irradiations applicable to radiation therapy doses and estimates from earlier and outdated radiotherapy treatment techniques applicable to modern radiation techniques, including proton therapy. The purpose of these models is to provide reasonable estimations of risk of radiation-induced secondary cancer for the different techniques used in modern radiotherapy, for dose-ranges relevant for patients undergoing curative radiotherapy, and for site-specific cancer induction in tissues with different radiosensitivities. The probability of secondary cancer induction as a function of dose, known as a dose-response relationship, forms the basis for these theoretical models. There is much debate on how this dose-response relationship is shaped for higher doses, with proposed shapes including a continuous linear increase with dose, the formation of a plateau where the cell kill is balanced by cell repopulation and repair, an exponential risk reduction due

[7] The reports from the CCSS use the term subsequent neoplasm rather than secondary cancer, but as most neoplasms turn into tumours, the term secondary cancer has been kept throughout this summary and only the statistics on malignant secondary neoplasms are listed

to the competition between cell mutation and cell kill, or alterations to these shapes due to fractionation effects (Figure 4.2 and Figure 4.3).

4.2.1 Quantification of radiation-induced cancer risk

The quantification of radiation-induced cancer risk in epidemiological studies is done by comparing the rate of cancer incidence in exposed populations to the rate of cancer incidence in unexposed populations [18]. This is also done for cancer mortality. The difference between the risk of cancer incidence with radiation exposure and the risk of cancer incidence without radiation exposure, i.e. the baseline risk, is called the excess absolute risk (EAR) (eq. (4.1)), and by dividing the EAR by the baseline risk one obtains the excess relative risk (ERR) (eq. (4.2)) [69]. For cancer incidence, the EAR is often expressed as the number of these cases per person-year (PY), whereas the ERR is dimensionless [18]. Both these terms are used in radiation epidemiology, often expressed per unit dose, and are dependent on variables such as sex (s), age at exposure (e), attained age (a), and time since exposure (y):

$$EAR(s,e,a,y,D) = \frac{R_e(s,e,a,y,D) - R_n(s,e,a,y)}{PY} \tag{4.1}$$

$$ERR(s,e,a,y,D) = \frac{EAR(s,e,a,y,D)}{R_n(s,e,a,y)}$$

$$= \frac{R_e(s,e,a,y,D) - R_n(s,e,a,y)}{R_n(s,e,a,y)} \tag{4.2}$$

where R_e is risk in exposed subjects and R_n is risk in unexposed subjects [18, 69]. There is a danger of overrepresentation of changes for very small absolute risks which the EAR avoids, and is therefore the preferred measurement used for reporting risk in radiotherapy [17]. Because baseline risks can be different for one population compared to another, both ERR and EAR are used to make risk estimates obtained from one population applicable to the population of interest, known as risk transport [18]. This

is usually done by combining the ERR and EAR estimates, weighted according to their relevance for each chosen organ site. The EAR and ERR calculations that are transported to the population of interest can be used to express the radiation risks in terms of lifetime risk, called lifetime attributable risk (LAR) [18, 73]. LAR gives the probability of cancer incidence (or mortality) for a person exposed to radiation from the age of exposure, *e*, added a risk-free latency period, *L*, to an attained age, *a*, of 100 years:

$$LAR(D, e) = EAR \cdot \frac{S(a)}{S(e)} \tag{4.3}$$

Here, *S(a)* is the survival function yielding the probability at birth to survive until the age *a*, and the ratio *S(a)/S(e)* is the probability of reaching age *a* on the condition of survival to age *e* (both *S(a)* and *S(e)* refer to the survival function of the unexposed population) [18, 73]. Equation (4.3) is an example of how LAR can be calculated based on EAR estimations [18]. EAR, ERR and LAR estimates can be used together with different dose-response relationships to model absolute, relative and lifetime risk of radiation-induced secondary cancer, respectively.

4.2.2 Linear dose-response relationship and modifying factors

The linear dose-response relationship obtained from the LSS cohort data (Figure 4.1) forms the basis for risk models used by committees concerned with radiation protection (e.g. the International Commission on Radiological Protection (ICRP) and BEIR) [74]. The LSS data is related to high doses and high dose-rates which can overestimate the radiation risks associated with low doses[8] and low dose-rates for low-LET radiations [5, 18]. The risk estimates for exposure to high doses and dose-rates are therefore divided by a dose and dose-rate effectiveness factor (DDREF) to give the risk estimates relevant for exposure to low doses and dose-rates (recommendations are e.g. a DDREF

[8] Low dose is defined by the BEIR VII report as doses ranging from near zero to around 0.1 Sv of low-LET radiation

of 2 for doses below 0.2 Gy at any dose-rate and for higher doses at dose-rates less than 0.1 Gy/h (ICRP) and maximum 3 for tumour induction based on available data (UNSCEAR report from 1993) used together with linear dose-response models) [5, 18, 69]. The DDREF may however not be applicable to radiotherapy as it is primarily used for doses and dose-rates much lower than the high (fractionated) doses and dose-rates in external-beam radiotherapy [16, 75]. As these linear dose-response models are developed with respect to radiation protection, and only have a clear validity at lower doses, they are not recommended to be used in risk estimations following radiotherapy for tissues receiving higher doses (> 2.5 Gy in Figure 4.1) [18, 69].

4.2.3 Linear-exponential dose-response relationship

A bell-shaped dose-response relationship was proposed by Gray in the 1960s, where the risk of cancer incidence increases in proportion to cell mutation induced in normal cells for a lower dose-range, and then falls off at higher dose-ranges due to the increase in the probability of killing these mutated cells [5]. The relationship describing this competition between carcinogenic mutation induction and cell kill is also referred to as the linear-exponential dose-response relationship [76], and the UNSCEAR reports from 1993 and 2000 include a version of this (called the competition model) based on the LQ model:

$$Effect = (\alpha_1 D + \beta_1 D^2) \times e^{-(\alpha_2 D + \beta_2 D^2)} \quad (4.4)$$

where D is the radiation dose, and the LQ parameters α_1 and β_1 represent the effect of carcinogenic mutation induction, and α_2 and β_2 represent the effect of cell killing [17]. When the radiation dose is low, equation (4.4) reduces to a linear dose-response relationship ($Effect \approx \alpha_1 D$), which corresponds to that observed for e.g. the LSS cohort, with α_1 describing the rate of secondary cancer incidence for lower doses. This linear-exponential dose-response relationship has been observed both for the induction of leukaemia in the LSS cohort and for site-specific cancer induction in certain patient

cohorts [17]. Modifications to the dose-response relationship in equation (4.4) has been done by Schneider et al. (2005) (Figure 4.2) [76], with the linear-exponential dose-response relationship as a function of dose (eq. (4.5)) and employing the EAR to this relationship (eq. (4.6)):

$$f(D) = De^{-\alpha_{org}D} \tag{4.5}$$

$$EAR^{org} = \beta De^{-\alpha_{org}D} \tag{4.6}$$

Here, the organ-specific cancer incidence rates β, also referred to as the initial slope (i.e. the slope of the dose-response curve at low doses, described by the LSS cohort), is given in units of per 10 000 PY per Gy, EAR^{org} is given in units of per 10 000 PY and α_{org} is an organ-specific cell sterilisation parameter [76]. Relating this version of the linear-exponential dose-response relationship to epidemiological data, the β values were obtained from the UNSCEAR report of 2000 and the EAR^{org} and D values were obtained using data from epidemiological studies on Hodgkin's patients treated with (fractionated) radiotherapy. All these values were then used in equation (4.6) to determine the α_{org} parameter values.

Another variation of this dose-response relationship was introduced by Schneider et al. (2011) to account for the effects that can result from fractionation schemes used in radiotherapy (Figure 4.3 – here called the bell-shaped dose-response relationship in accordance with literature) [77]. This was done by having the α_{org} parameter proportional to the number of cells that is reduced by cell killing and defined using the LQ model with the α and β parameters from equation (3.1):

$$\alpha_{org} = \alpha + \beta d = \alpha + \beta \frac{D}{D_T} d_T \tag{4.7}$$

Here, the fractionation schedule is implemented by the prescribed target dose, D_T, and the fractionation dose, d_T. As different tissues have different α/β values, equation (4.7) can be rearranged to account for this:

$$\alpha_{org} = \alpha\left(1 + \frac{d_T}{\alpha/\beta}\frac{D}{D_T}\right) \tag{4.8}$$

Thus, the α parameter values can be determined for different α/β values [78].

4.2.4 Plateau dose-response model

The bell-shaped dose-response relationship differentiates from the linear-exponential dose-response relationship in equation (4.6) as it accounts for fractionation schemes employed in radiotherapy. However, it does not account for the cell repopulation effects that can occur during fractionated radiotherapy. The balance between cell kill and cell repopulation can result in a dose-response relationship that levels off in a continuous plateau for higher doses. This type of plateau dose-response relationship has been described by Schneider and Kaser-Hotz (2005) (Figure 4.2) [79], based on a model by Davis from 2004 [80], as a function of dose (eq. (4.9)), and employing the EAR to this relationship (eq. (4.10)) using the same variables as for the linear-exponential dose-response relationship in equation (4.6):

$$f(D) = \frac{\left(1 - e^{-\delta_{org}D}\right)}{\delta_{org}} \tag{4.9}$$

$$EAR^{org} = \frac{\beta\left(1 - e^{-\delta_{org}D}\right)}{\delta_{org}} \tag{4.10}$$

The $\delta_{org}$is an organ-specific model parameter, obtained in the same way as the α_{org} parameter from equation (4.6) [79]. The δ_{org} parameter values were thus determined based on the Hodgkin's patient cohort values for EAR^{org} and D, as well as the β values which were obtained from the UNSCEAR report of 2000 and from the LSS cohort study by Thompson et al. (1994) [81]. The plateau dose-response relationship can also

account for fractionation effects and tissue types by representing the δ_{org} parameter in the same way as the α_{org} parameter with equation (4.8) and finding the α parameter values for the plateau dose-response relationship (Figure 4.3) [77].

4.2.5 Full model dose-response relationship

To account for the cases of cell repopulation effects that are somewhere between the full repopulation effect from the plateau dose-response relationship and no repopulation effect from the linear-exponential (or bell-shaped) dose-response relationship, Schneider (2009) [82] developed a mechanistic model for a dose-response relationship that includes a repopulation/repair parameter, *R*, to determine the size of the repopulation effects. This is hereafter referred to as the full model (Figure 4.3), with the dose-response relationship shown as a function of dose in equation (4.11), and employing the EAR and parameters used by Schneider et al. (2011) in equation (4.12):

$$f(D) = \frac{e^{-\alpha' D}}{\alpha' R}\left(1 - 2R + R^2 e^{\alpha' D} - (1-R)^2 e^{-\frac{\alpha' R}{1-R}D}\right) \tag{4.11}$$

$$EAR^{org}(D, agex, agea) = \beta\, f(D)\, \mu(agex, agea) \tag{4.12}$$

Here, the α' parameter in equation (4.11) is represented as in equation (4.8) to account for cell killing, fractionation and different tissue types (i.e. α/β values) [77]. As for equation (4.12), the β values are the initial slopes for the LSS cohort taken from Preston et al. (2007) [83] in units of (10 000 PY-Gy)$^{-1}$, and μ is a modifying function containing population dependent variables:

$$\mu(agex, agea) = e^{\gamma_e (agex - 30) + \gamma_a \ln\left(\frac{agea}{70}\right)} \tag{4.13}$$

where *agex* is age at exposure, *agea* is attained age and γ_e and γ_a are age modifying parameters for the LSS cohort at age of exposure of 30 and attained age of 70 years taken from Preston et al. (2007). When equation (4.11) is derived in the limit of $R = 0$,

i.e. if no cell repopulation occurs, the dose-response relationship becomes linear-exponential (or bell-shaped):

$$f(D) = De^{-\alpha' D} \tag{4.14}$$

And deriving equation (4.11) in the limit of $R = 1$, i.e. if full cell repopulation occurs, the dose-response relationship turns into a plateau one:

$$f(D) = \frac{1 - e^{-\alpha' D}}{\alpha'} \tag{4.15}$$

To derive the values of α and R for different organs at risk, Schneider et al. (2011) used a combined fit of the LSS cohort and a Hodgkin's patient cohort [77].

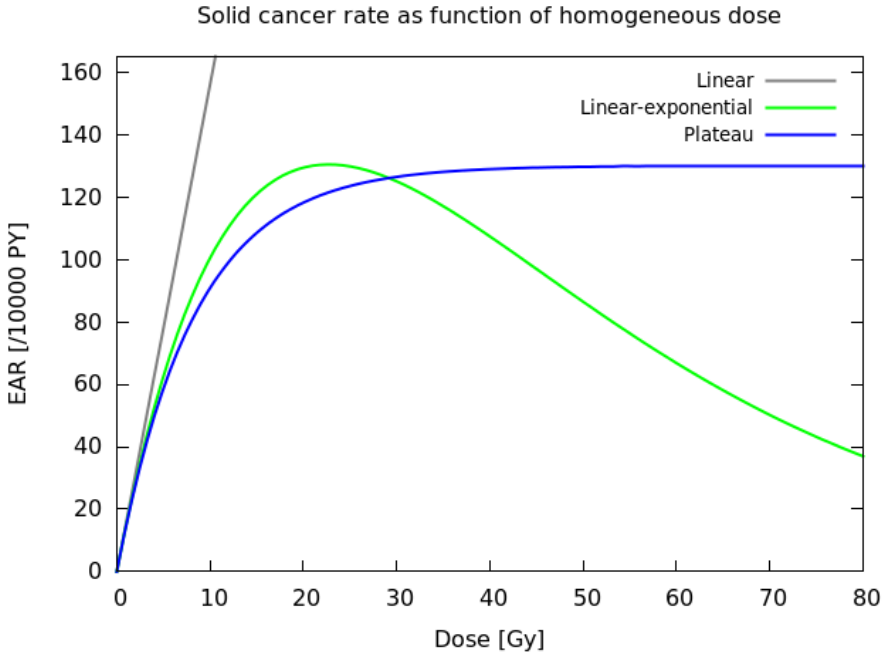

Figure 4.2: Illustration of dose-response relationships for solid cancer excess absolute risk as a function of homogeneous dose. Parameter values are chosen according to Schneider and Kaser-Hotz (2005) [79].

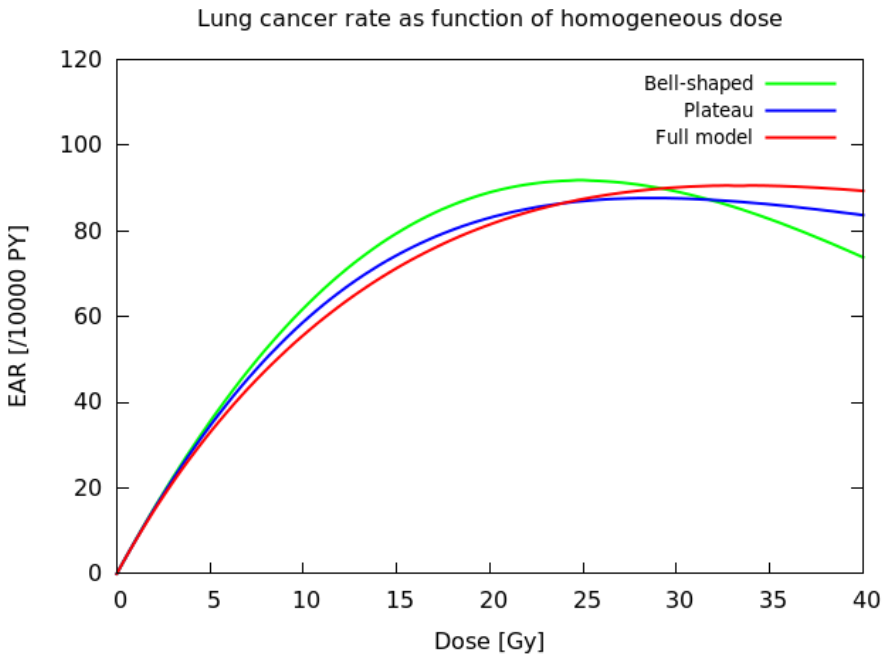

Figure 4.3: Illustration of dose-response relationships for lung cancer excess absolute risk as a function of homogeneous dose. Parameter values are chosen according to Schneider et al. (2011) [77].

4.2.6 The organ equivalent dose concept

Inhomogeneous dose distributions occur in both proton and photon therapy and becomes a problem when one employs the average organ dose in secondary cancer risk estimations. This may lead to erroneous risk estimates as it does not account for the cell sterilisation effects that can occur at higher doses. Schneider et al. (2005) proposed a solution to this problem by implementing the concept of organ equivalent dose (OED) when estimating the risk of radiation-induced secondary cancer [76]. This concept states that any dose distribution within an organ is equivalent and corresponds to the same OED if it causes the same radiation-induced risk of cancer incidence, allowing this risk to be estimated from inhomogeneous three-dimensional dose distributions. The dose in each voxel can therefore be converted into so-called risk equivalent dose (RED), which represents the dose-response relationship function *f(D)* from the equations in chapters 4.2.3-4.2.5 [77]. As the RED only yields the risk of radiation-induced secondary cancer as a function of dose in each voxel inside an organ, the OED

concept can either be applied to obtain risk estimates for the whole organ by taking the sum over all RED calculation points (*N*), representing the same constant organ volume (eq. (4.16)), or determined for an organ of total volume V_T, based on the RED and the dose volume histogram, *V(D)*, for that organ (eq. (4.17)).

$$OED_{org} = \frac{1}{N}\sum_{i=1}^{N} f(D_i) \tag{4.16}$$

$$OED_{org} = \frac{1}{V_T}\sum_{i} V(D_i)\, f(D_i) \tag{4.17}$$

Thus, the OED is the dose-response relationship (or RED) weighted dose variable averaged over the whole organ volume [77]. For a linear RED weighted dose, the OED becomes the average organ dose, which is also the case for non-linear RED at low doses.

5. Material and methods

5.1 Patient data and treatment planning

5.1.1 Patient data

The patient cohort selected for this thesis consisted of 10 paediatric medulloblastoma patients, 5 boys (8-12 years old) and 5 girls (5-9 years old). All patients had received cranio-spinal irradiation (CSI) as a part of the treatment. All structures of relevance in this thesis were individually delineated by an experienced oncologist. This included the clinical target volume (CTV), consisting of the brain and spinal canal, which was further used to define the planning target volumes (PTVs), as well as the organs at risk that were chosen for radiation-induced secondary cancer risk estimations.

The sites included for estimation of secondary cancer risk following proton therapy were the lungs and the thyroid. These sites were chosen for the following reasons:

- Both sites are at risk of receiving high doses during CSI treatment of medulloblastoma as they are placed close to the target volume (Figure 5.1)
    - The lungs and thyroid are located distally and laterally to the target volume and beam direction, in the vicinity of the higher LET components associated with the distal part of the SOBP, and thereby at risk of receiving doses with increased probability of RBE values larger than 1.1
- Photon CSI can cause significant dose delivered to these two structures, which can be largely avoided with proton CSI and is therefore particularly beneficial for this patient group with regards to long term effects and secondary cancer [4]
    - This also makes it interesting to investigate risk predictions for these organs made by RBE values beyond 1.1
- Both sites (thyroid especially) have shown great variations in risk based on sex and age of the patient [18]

- Radiation exposure, especially during childhood, is a well-established factor in increasing thyroid cancer incidence, which is also the second most common cancer in young women (after breast cancer) [84]
- Lung cancer has a high mortality rate, especially if diagnosed at a late stage [85]

The proton CSI treatment plans with both constant and variable RBE described in the next two sections were all created prior to this thesis. These treatment plans were then used together with each of the dose-response relationships in chapters 4.2.2-4.2.5 to estimate the risk of secondary cancer induction for proton therapy, employing the OED concept to account for inhomogeneous dose distributions in normal tissues [17].

5.1.2 Treatment planning

For all the patients in the cohort, the CSI treatment plans were optimised in the Eclipse treatment planning system (Varian Medical Systems, Palo Alto, CA, USA) using the conventional radiotherapy dose prescription for standard risk medulloblastoma: 23.4 Gy delivered in 13 fractions to the CTV. Using the principles of proton RBE related to the isoeffective absorbed doses for protons and photons (eq. (3.2)) discussed in chapter 3.3, the dose and LET distributions were converted into distributions of RBE-weighted doses. From this, a biologically weighted dose of 23.4 Gy(RBE) was used for the proton plans based on the clinical RBE of 1.1. The technique used for the proton CSI treatment delivery was intensity-modulated proton therapy (IMPT) with pencil beam scanning.

5.1.3 Variable RBE models

The treatment plans were recalculated using FLUKA Monte Carlo code [86, 87] coupled to in-house python based scripts [88] to obtain LET_d, RBE, and RBE-weighted doses for the four variable RBE models used in this thesis: LET-weighted dose, the McNamara model, the Rørvik model and the Wilkens model; further details can be found in Rørvik et al. (2018) [63] and SOBPs presented in Figure 3.3. An example of

the dose distribution with constant and variable RBE is shown for one of the patients in Figure 5.1.

LET-weighted dose is often referred to as the Unkelbach model as it was proposed by Unkelbach et al. in 2016 [62]. The model is here referred to as LET-weighted dose (abbreviated LWD) because it uses the LET distribution in the proton plan directly, independent of tissue or patient-specific RBE. The model assumes an increase in RBE with increasing LET, and do not account for the assumption of a steeper RBE increase with LET for normal tissues with low $(\alpha/\beta)_x$ values than for tumours with higher $(\alpha/\beta)_x$ values.

The McNamara model [60] shows a linear increase in RBE with LET_d and increasing RBE with decreasing $(\alpha/\beta)_x$ values. The calculations using the McNamara model in this thesis has been done with $(\alpha/\beta)_x$ = 2 Gy (abbreviated MCN_{2Gy}) and $(\alpha/\beta)_x$ = 10 Gy (abbreviated MCN_{10Gy}).

The Rørvik model [61] is the only variable RBE model in this thesis with a non-linear RBE-LET_d relationship. As with the McNamara model, the Rørvik model accounts for RBE variations with tissue type, which is why the calculations using this model has also been done with $(\alpha/\beta)_x$ = 2 Gy (abbreviated $RØR_{2Gy}$) and $(\alpha/\beta)_x$ =10 Gy (abbreviated $RØR_{10Gy}$).

The Wilkens model [39] is based on data points from in vitro experiments using V79 cell lines. The model (abbreviated WIL) has a linear dependency of RBE on LET_d (RBE increasing with increasing LET_d up to 20 keV/µm), and also describes RBE as a function of dose and tissue specific parameters for protons. The model has a fixed $(\alpha/\beta)_x$ = 3.758 Gy.

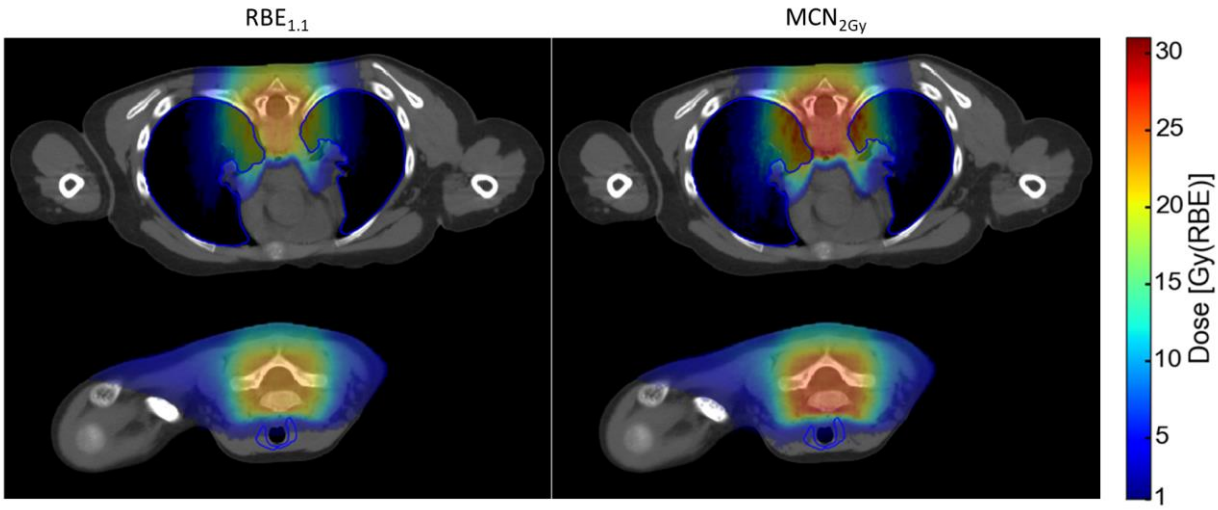

Figure 5.1: Dose distribution in patient 4 (8-year-old female) with constant RBE of 1.1 (left) and variable RBE model (right) for contoured organs at risk – lungs (top) and thyroid (bottom).

5.2 Modelling risk of radiation-induced cancer

In this thesis, two approaches were used to estimate the risk of radiation-induced (lung and thyroid) cancer for each patient. The first approach was to calculate the LAR based on the OED concept and the dose-response relationships by Schneider et al. (2005) [76, 79]. This was done for both lung and thyroid. The second approach was to calculate the EAR using the OED concept for the lungs using the dose-response relationships by Schneider et al. (2011) [77]. No EAR thyroid model was reported from the latter.

5.2.1 Obtaining the OED

The RBE-weighted dose distributions in the proton plans for each RBE model (both clinical RBE of 1.1 – hereby referred to as $RBE_{1.1}$ – and the four variable RBE models) were recalculated to RED distributions using an in-house developed python script [88]. The python script was modified to calculate the RED for each organ at risk and each RBE model using the dose-response relationships in chapters 4.2.2-4.2.5. The resulting RED-weighted proton plans were then imported to 3D Slicer (version 4.8.0) [89] where the dose volume histograms (DVHs) could be created from the RED distributions for

the lungs and thyroid of each patient from all RBE models, thus yielding the OED according to eq. (4.17) for each organ. The RED distributions obtained for each organ, RBE model and risk model was used together with the CT images of one of the patients to illustrate the respective RED distributions in each organ.

5.2.2 Lifetime attributable risk calculations

To calculate the LAR for the lungs and thyroid of each patient, the OED was estimated for each organ with respect to each RBE model and each of the linear, linear-exponential, and plateau dose-response relationship functions in equations (4.5) and (4.9) using organ-specific parameters for each organ at risk (Table 5.1). The OED values obtained using 3D Slicer were then multiplied with a risk coefficient, *l*, derived from table 12D-1 in BEIR VII report [18] to yield the LAR in % for each patient and organ at risk:

$$LAR = l \cdot OED_{org} \tag{5.1}$$

The table values in the BEIR VII report are given as LAR per 100 000 persons per 0.1 Gy dose, divided by a DDREF of 1.5. As the use of a DDREF is not appropriate for the high doses and dose-rates in radiotherapy (see chapter 4.2.2), the DDREF was removed from the calculations. Thus, the following equation was used to derive the risk coefficient *l*:

$$l = 100\% \cdot \frac{table\ value}{100\,000\ persons} \cdot 1.5\ (DDREF) \cdot \frac{1}{0.1\ Gy} \tag{5.2}$$

As the table values were given for the ages at exposure 0, 5, 10 and 15 years, the values for ages at exposure not listed were derived through linear interpolation. The resulting values for the risk coefficient *l* are listed in Appendix A for lungs (Table A.1) and in Appendix B for thyroid (Table B.1). To represent the uncertainties in the risk estimates, a 95% confidence interval was calculated for both organs using the procedure

explained in Annex 12C of the BEIR VII report and based on uncertainty values listed in the BEIR report (excluding the uncertainty related to the DDREF) [18].

Table 5.1: Organ-specific parameters from table 1 in Schneider et al. (2005) [76, 79].

Organ	$\alpha_{org}\ [Gy^{-1}]$	$\delta_{org}\ [Gy^{-1}]$
Lung	0.129	0.15
Thyroid	0.033	0.69

To make a general comparison of estimated LAR of the lungs and the thyroid for the whole patient cohort, the median value was calculated for each RBE model and each dose-response relationship. And lastly, the ratio of the LAR estimates made by the variable RBE models were normalised to the LAR estimates made by $RBE_{1.1}$ to find the relative change in LAR of secondary lung and thyroid cancer with the variable RBE models. The median value was calculated for comparison of predicted relative change in LAR between the variable RBE models across the different dose-response relationships.

5.2.3 Excess absolute risk calculations

To calculate the EAR for each patient and organ at risk, the OED was estimated with respects to each RBE model and each of the functions for the bell-shaped, plateau, and full model dose-response relationship in equations (4.11), (4.14) and (4.15), as well as for a linear dose-response relationship, using site-specific model parameters. As there was no reported thyroid model, the calculations could only be done for the lungs (with R = 0.83) using the following α parameters:

Table 5.2: Lung model parameters from table 4 in Schneider et al. (2011) [77].

RED function	*α [Gy^{-1}]*
Full model (eq. (4.15))	0.042
Bell-shaped (eq. (4.11))	0.022
Plateau (eq. (4.14))	0.056

The patient fractionation dose of 1.8 Gy(RBE) was used to find α' according to equation (4.8). As Schneider et al. (2011) assumes α/β = 3 Gy for all tissues, this was also done here for lung tissue. The resulting OED values obtained using 3D Slicer was multiplied with a risk coefficient, *r*, to yield the EAR for the lungs of each patient:

$$EAR^{org} = r \cdot OED_{org} \tag{5.3}$$

where the risk coefficient, *r*, contains the information from the β- and μ-values in equation (4.12):

$$r = \beta_{EAR} \cdot \mu(agex, agea)$$

$$= \beta_{EAR} \cdot e^{\gamma_e(agex-30)+\gamma_a \ln\left(\frac{agea}{70}\right)} \tag{5.4}$$

As with Schneider et al. (2011), the β-values, along with a 90% confidence interval to represent the uncertainties in the risk estimates, were taken from Preston et al. (2007) [83] using the male/female values instead of the sex-averaged, and transferred to a Western population by using the ERR-EAR weighting factor (established according to ICRP 103) for lungs of 1.07 from Schneider et al. (2011) (Table 5.3) [77]. To adjust the EAR estimations to fit the patient cohort, the modifying function μ was calculated based on equation (4.13) using patient data age at exposure (*agex*) and attained age

(*agea*) = average life expectancy in Norway 2017 (Table 5.3) [90]. The resulting values for the risk coefficient *r* are listed in Appendix C (Table C.1).

Table 5.3: Parameters for EAR calculations: β-values with a 90% confidence interval (in parenthesis) for lungs from Preston et al. (2007), transported to a Western population by weighting factor from Schneider et al. (2011), and average life expectancy in Norway 2017 as attained age.

	Male	*Female*
β_{EAR}	6.420 (2.461, 11.770)	9.737 (6.848, 12.840)
Attained age (agea)	80.91	84.24

As with the LAR values, the median EAR for the whole patient cohort was calculated for each RBE model and each dose-response relationship for a general comparison. And lastly, the ratio of the EAR estimates made by the variable RBE models were normalised to the EAR estimates made by $RBE_{1.1}$ to find the relative change in EAR of secondary lung cancer with the variable RBE models. The median value was calculated for comparison of predicted relative change in EAR between the variable RBE models across the different dose-response relationships.

6. Results

The calculated risk estimates for the patient cohort, both individual and collective, regarding radiation-induced secondary lung and thyroid cancer are presented in this chapter, with the risk model (LAR and EAR) results for each organ (lungs and thyroid) described separately.

6.1 Lifetime attributable risk

To illustrate the difference between the three dose-response relationships, the LAR as a function of homogeneous proton dose is shown for one of the patients in the cohort, in Figure 6.1.

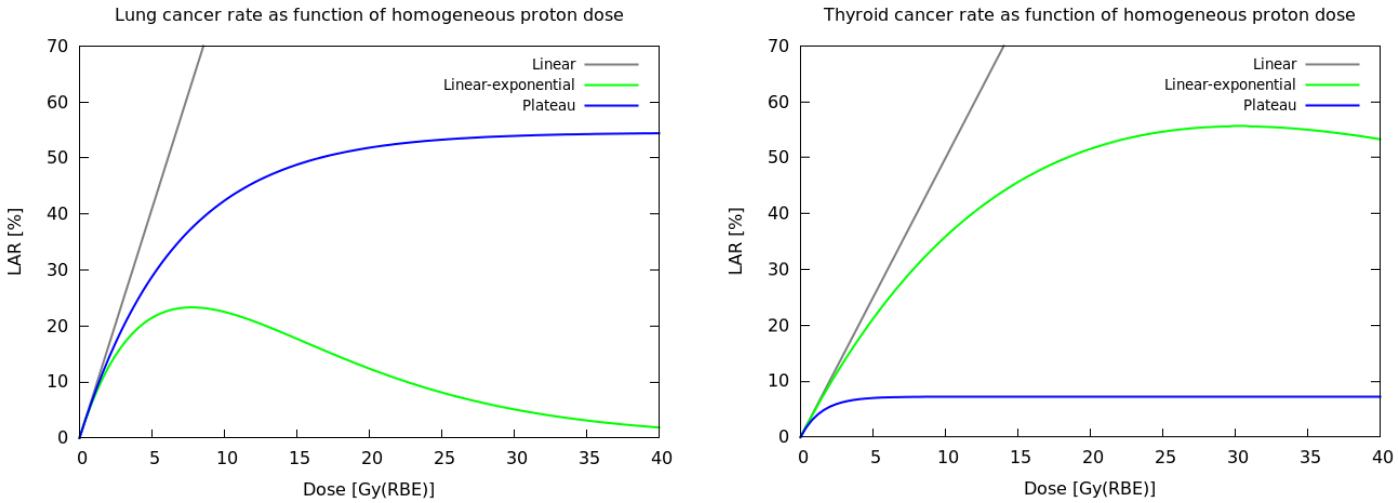

Figure 6.1: Lifetime attributable risk of secondary lung cancer (left) and thyroid cancer (right) as a function of homogeneous dose estimated for patient 4 (8-year-old female), using the linear (grey line), linear-exponential (green line) and plateau (blue line) dose-response relationship. The prescription dose to the target volume is 23.4 Gy(RBE) and the contributions of higher doses are therefore small for the patients in this cohort; the higher dose levels are included only to illustrate the differences between the dose-response relationships at these dose levels.

Both plots show that the linear dose-response relationship gives the highest risk for radiation doses > 2 Gy(RBE) for lungs and > 3 Gy(RBE) for thyroid. The differences between the two organs using the two non-linear dose-response relationships are due

to the differences in the values for the organ-specific cell sterilisation parameter α_{org} and the organ-specific model parameter δ_{org} (Table 5.1). Here, the peak of the linear-exponential dose-response relationship risk prediction is reached at about 7 and 30 Gy(RBE) for lungs and thyroid, respectively. The secondary thyroid cancer risk predictions for the plateau dose-response relationship reaches the plateau already at about 5 Gy(RBE), whereas the dose level at which the risk predictions for secondary lung cancer reach this plateau is not present in the dose range displayed in the figure.

Using both the RBE models and the dose-response relationships, the estimated OEDs and LARs for each of the ten patients in regards to secondary lung cancer are shown in Figure 6.2 and Figure 6.3, respectively.

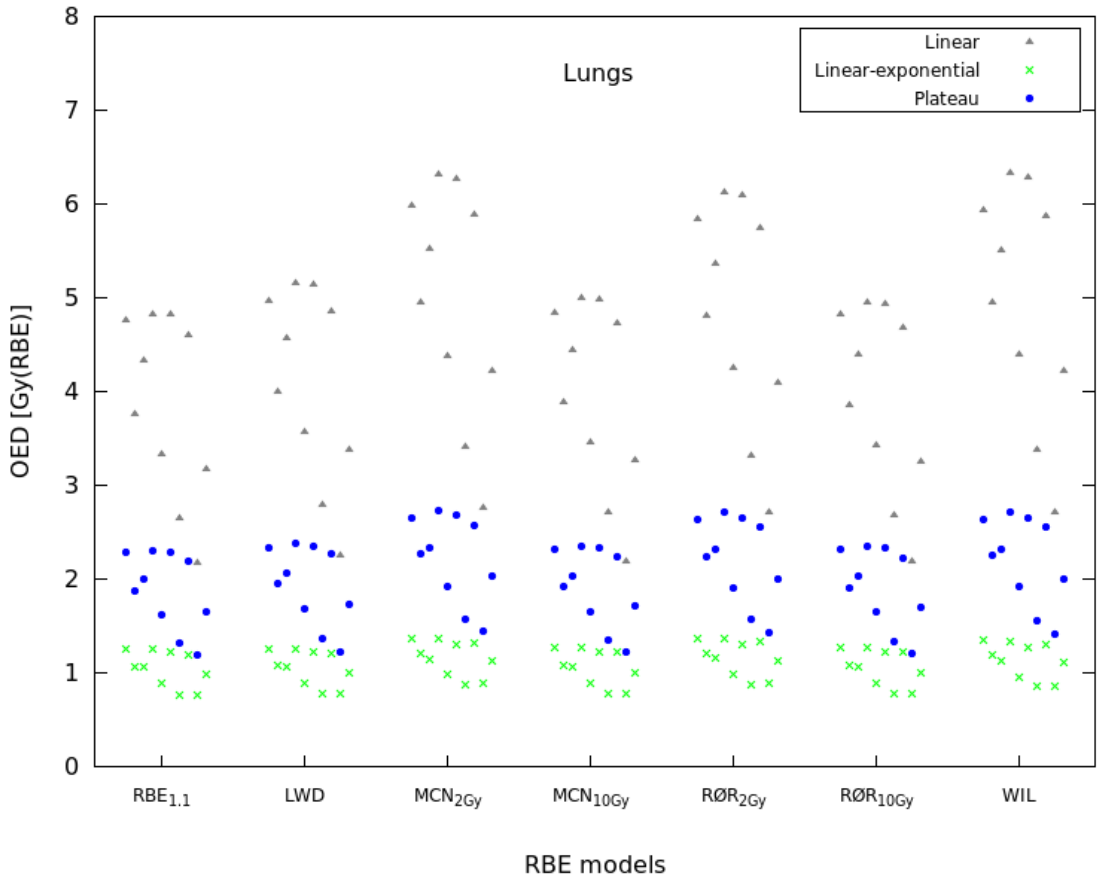

Figure 6.2: Organ equivalent doses for the lungs in Gy(RBE) using the different RBE models and dose-response relationships. The results are shown for patient 1-10 in succession from left to right for each RBE model.

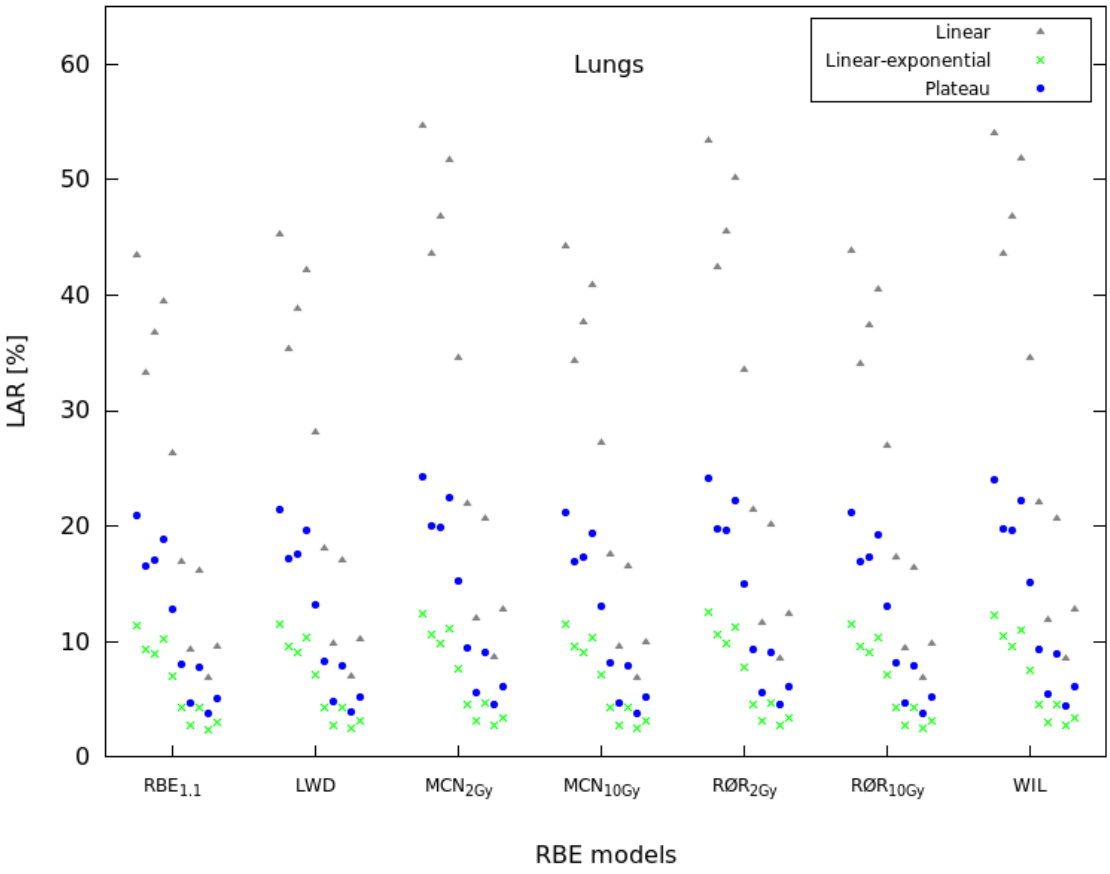

Figure 6.3: Lifetime attributable risks of secondary lung cancer in % using the different RBE models and dose-response relationships. The results are shown for patient 1-10 in succession from left to right for each RBE model.

The highest OED values were found among female patients 1 and 4 (5 and 8 years of age, respectively) and male patients 6 and 8 (both 8 years old), while the lowest OED values were found among male patients 7 and 9 (8 and 11 years of age, respectively). The distinction between the three dose-response relationships were quite clear for the ranges of OED estimates: 0.76 to 1.37 Gy(RBE) (linear-exponential), 1.20 to 2.74 Gy(RBE) (plateau), and 2.17 to 6.29 Gy(RBE) (linear). Each individual OED value is listed in Table A.2 in Appendix A.

All secondary cancer risk dose-response relationships showed a higher LAR of radiation-induced lung cancer for the variable RBE models compared to the constant $RBE_{1.1}$. The risks were highest for the WIL and the MCN_{2Gy} models for the linear model, while the $RØR_{2Gy}$ and the MCN_{2Gy} models gave the highest risks for the linear-

exponential and plateau models, respectively. With respect to each dose-response relationship applied, the highest LAR estimates were made with the linear model, followed by the plateau model, and with the linear-exponential model yielding the lowest risk estimates. This was the case for all patients, independent of RBE model used. Across all dose-response relationship applied, the highest LARs were found for patient 1 (5-year-old female) and the lowest LARs were found for patient 9 (11-year-old male). Collectively, the LARs of secondary lung cancer were higher for the female patients (1-5) compared to the male patients (6-10). Each individual LAR value is listed in Table A.3 in Appendix A.

The median LAR values for the patient cohort are shown in Figure 6.4. Each median LAR estimate, including the range consisting of the minimum and maximum LAR, is listed in Table A.4 in Appendix A. The $RBE_{1.1}$ model had the lowest median risk of secondary lung cancer, regardless of dose-response relationship applied. For the different dose-response models, the highest median risk predictions were with the WIL model (linear), the $RØR_{2Gy}$ model (linear-exponential), and the MCN_{2Gy} model (plateau). The linear-exponential dose-response relationship had the overall lowest median risk estimates for all RBE models, where the $RØR_{2Gy}$ and MCN_{2Gy} models showed the highest median risk increase of 10% relative to the $RBE_{1.1}$ (Figure 6.5). For the plateau model, the highest median relative LAR was 19%, and a 30% median relative LAR for the linear model. The two latter relative LARs were predicted by the MCN_{2Gy} model, which were followed by slightly smaller increases predicted by the WIL and $RØR_{2Gy}$ models, in succession with the linear model and equal with the linear-exponential model. The variations in the estimated relative risks were highest for these three variable RBE models, where the largest ranges were from 24 to 33% (linear, WIL), from 7 to 16% (linear-exponential, $RØR_{2Gy}$), and from 15/16 to 21/22% (plateau, WIL/MCN_{2Gy}). The median relative LARs predicted by the remaining variable RBE models were much lower, with much smaller variations in predicted relative risks. The overall lowest median predictions were given by the remaining variable RBE models, where all median relative LARs were under 3% for the $RØR_{10Gy}$ model. Each median

relative LAR, including the range consisting of minimum and maximum relative LAR, is listed in Table A.5 in Appendix A.

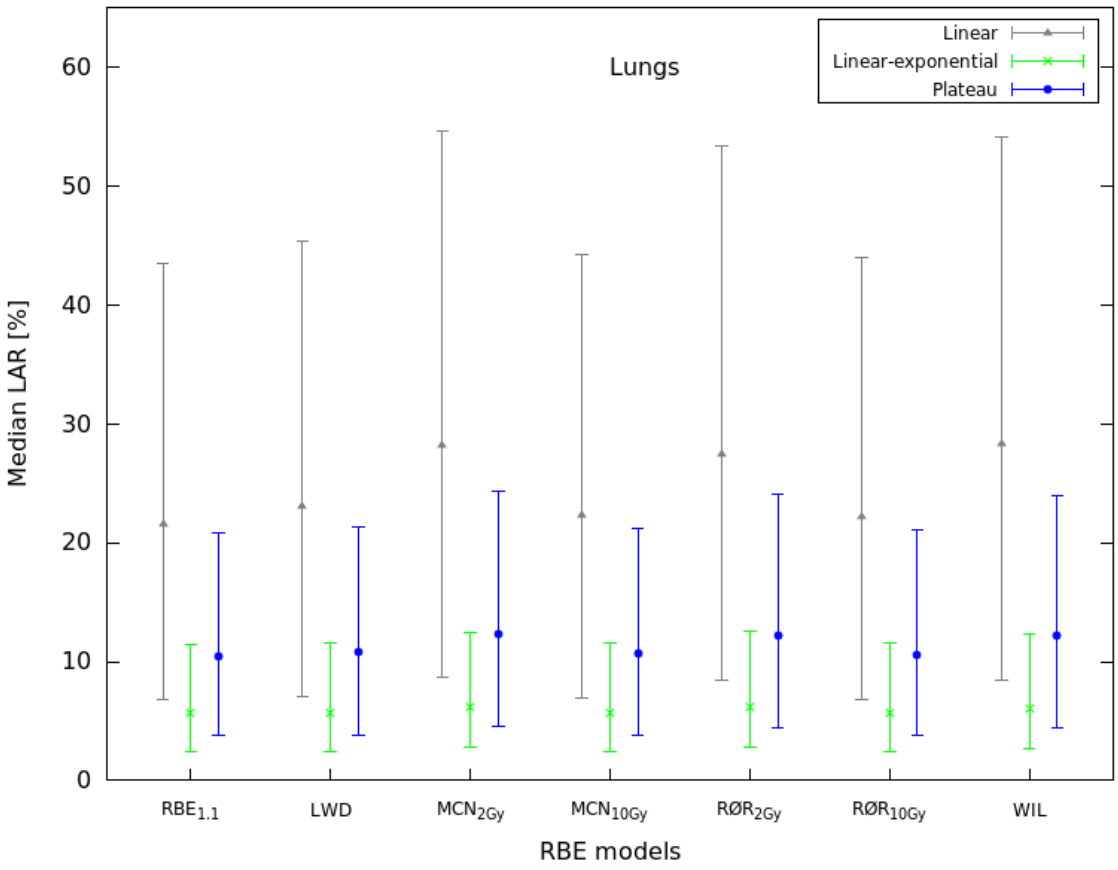

Figure 6.4: Median lifetime attributable risk of radiation-induced lung cancer in % of ten patients for each RBE model and each dose-response relationship. The error bars represent the range in terms of minimum and maximum LAR estimate.

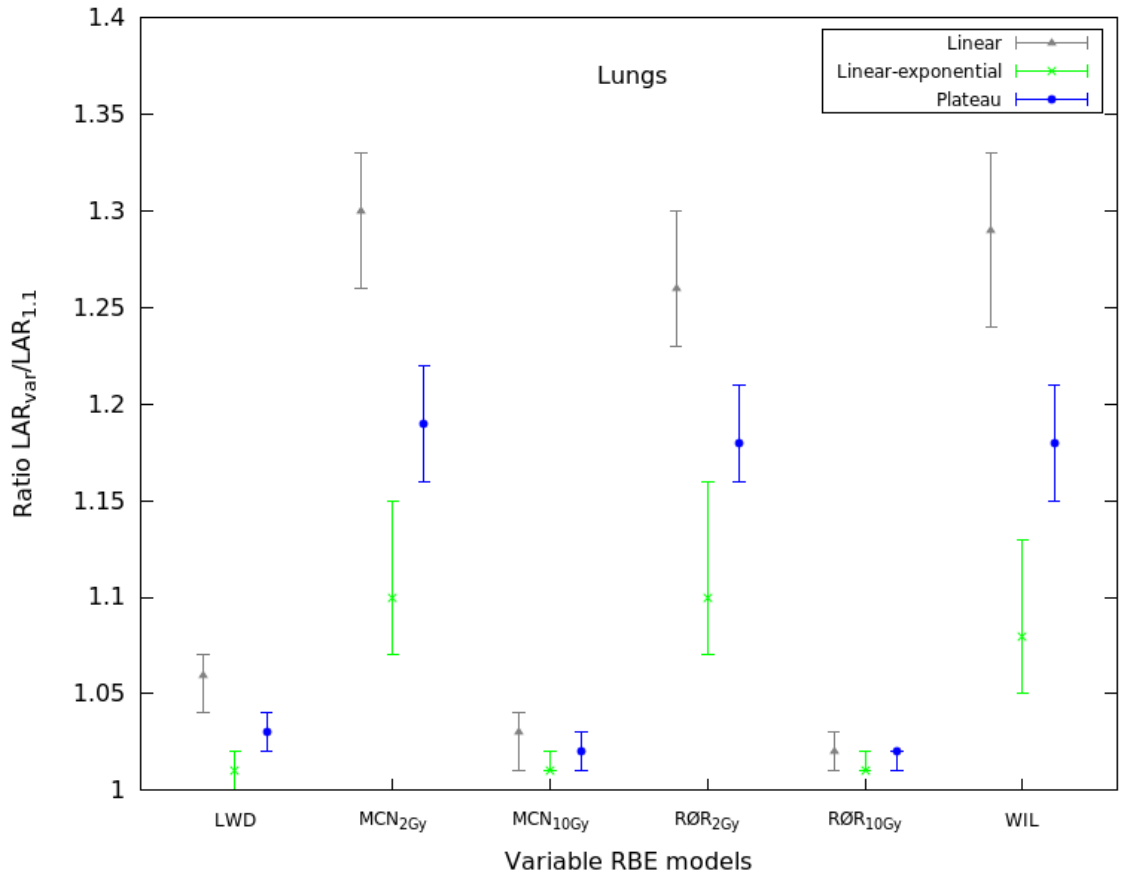

Figure 6.5: The ratio between the variable RBE model LAR estimates and the LAR estimates made by $RBE_{1.1}$ for each dose-response model. The points are the median ratio values of ten patients with error bars representing the range in terms of minimum and maximum LAR ratio.

Figure 6.6 shows an example of the RED distribution in patient 4 for each of the three dose-response relationships using the MCN_{2Gy} model. Both the linear and the plateau dose-response relationship predicted the highest risk of secondary lung cancer to be located in the lung tissue close to the target volume, with the plateau dose-response relationship showing a larger high-RED distribution (although with lower values) further away from the target volume than the linear. The linear-exponential dose-response relationship, however, predicted the highest risk in a more ring-shaped area further away from the target volume. This distance from the target volume was dependent on the RBE model used and was furthest away for the WIL and MCN_{2Gy} models.

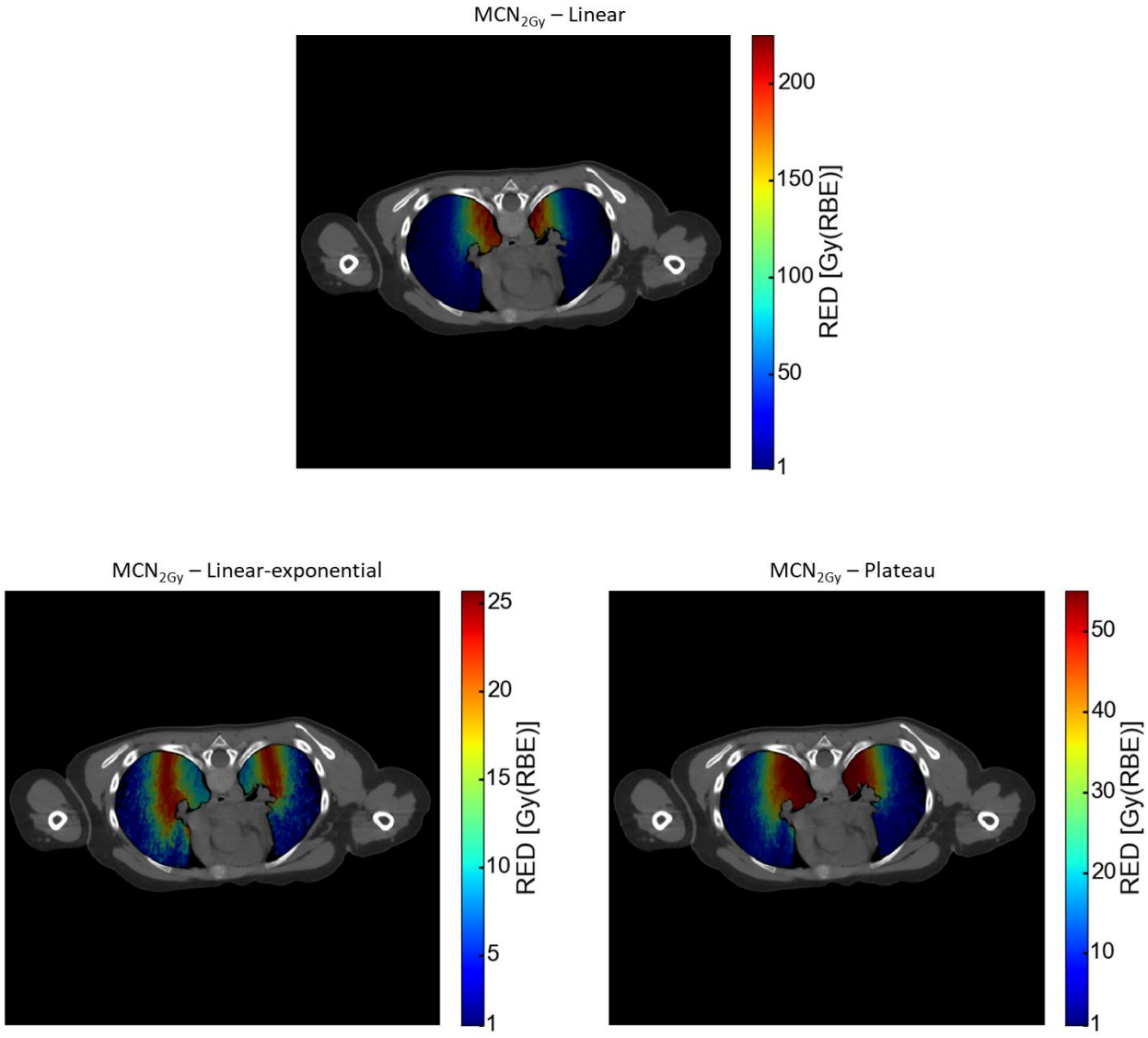

Figure 6.6: Distribution of risk equivalent dose (RED) in the lungs of patient 4 (8-year-old female) with a variable RBE model (MCN_{2Gy}) using the linear (top), linear-exponential (bottom left) and plateau (bottom right) dose-response relationship. RED is given in units of Gy(RBE) which is proportional to the LAR in each voxel.

The estimated OEDs and LARs for each patient regarding secondary thyroid cancer are shown in Figure 6.7 and Figure 6.8, respectively.

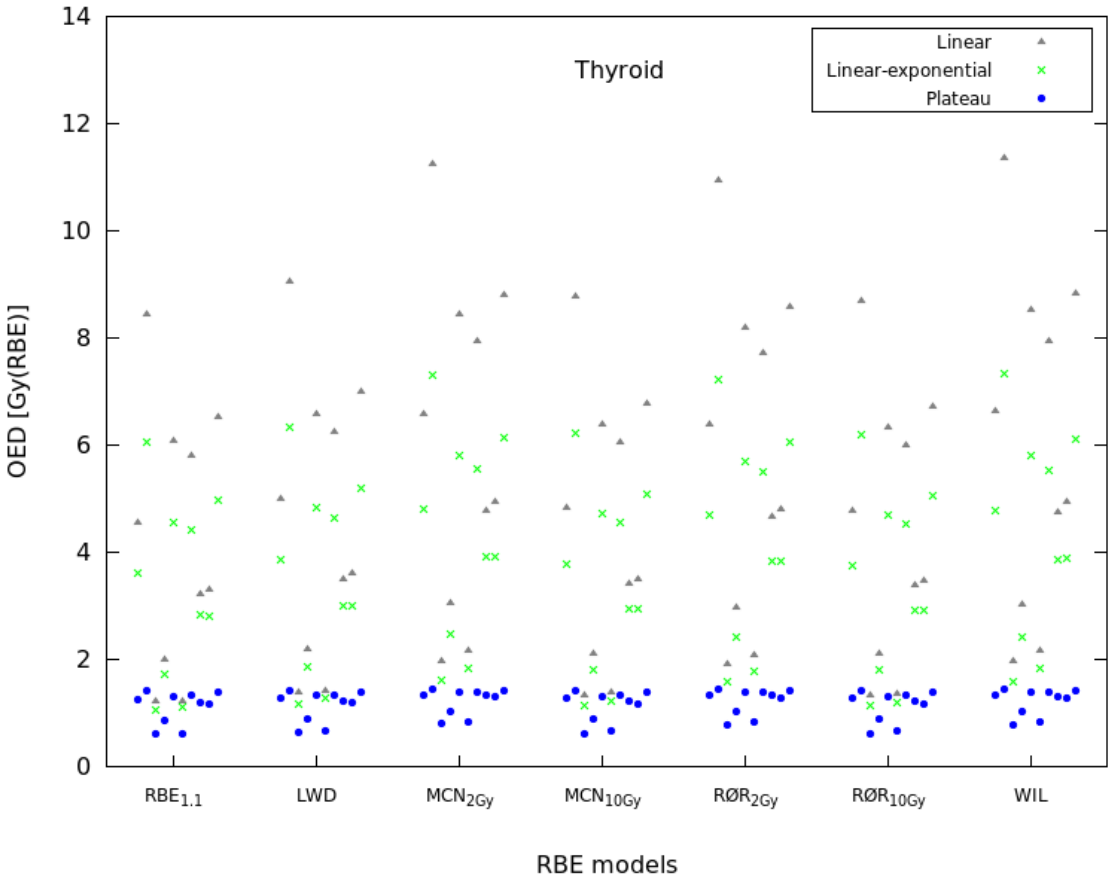

Figure 6.7: Organ equivalent doses for thyroid in Gy(RBE) using the different RBE models and dose-response relationships. The results are shown for patient 1-10 in succession from left to right for each RBE model.

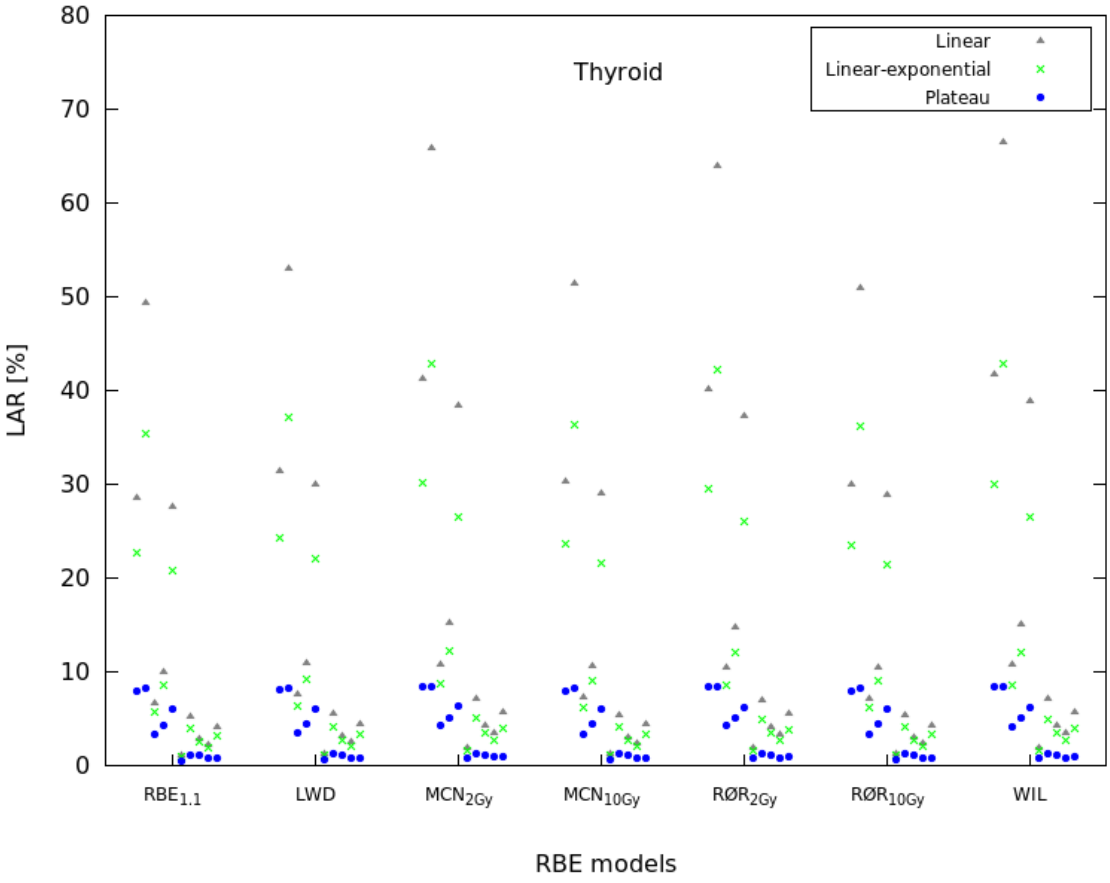

Figure 6.8: Lifetime attributable risks of secondary thyroid cancer in % using the different RBE models and dose-response relationships. The results are shown for patient 1-10 in succession from left to right for each RBE model.

The higher OEDs were found for the linear and linear-exponential dose-response relationships. The variations between OEDs were also much larger for these two dose-response relationships, ranging from 1.24 to 11.37 Gy(RBE) (linear) and from 1.07 to 7.33 Gy(RBE) (linear-exponential), compared to the plateau dose-response relationship, which predicted the overall lowest OEDs ranging from 0.61 to 1.44 Gy(RBE). Each individual OED value is listed in Table B.2 in Appendix B.

All three dose-response relationships showed an overall higher LAR of radiation-induced secondary thyroid cancer for the variable RBE models compared to the $RBE_{1.1}$. The risks were highest for the WIL and the MCN_{2Gy} models using the linear dose-response relationship, while the MCN_{2Gy} model generally gave the highest risks for

both the linear-exponential and the plateau dose-response relationships. For all patients, regardless of RBE model employed, the predicted LARs of secondary thyroid cancer were highest using the linear dose-response relationship, followed by the linear-exponential, and with the plateau dose-response relationship predicting the lowest risks. For all dose-response relationship applied, the highest LARs were found for female patients 1 and 2 (5 and 6 years of age, respectively) and the lowest LARs were found for patient 6 (8-year-old male). Overall, the female patients had higher estimated LARs of secondary thyroid cancer compared to the male patients. Each individual LAR value is listed in Table B.3 in Appendix B.

The median LAR values for the patient cohort are displayed in Figure 6.9 (each individual value with range is listed in Table B.4 in Appendix B). The $RBE_{1.1}$ model had the lowest median risk of secondary thyroid cancer for each of the dose-response relationships. The MCN_{2Gy} model had the highest median risk estimates for all three dose-response relationships, with the WIL model estimating an equally high median risk only for the linear dose-response relationship. The plateau model had the overall lowest median risk estimates for all RBE models, as well as the smallest increase in LAR with the variable RBE models relative to $RBE_{1.1}$ (Figure 6.10). Here, the highest median relative LAR was predicted by the MCN_{2Gy} model of only 9%, as opposed to the 36% and 47% median relative LARs for the linear-exponential model (MCN_{2Gy}) and the linear model (WIL), respectively. These two variable RBE models, followed closely by the $RØR_{2Gy}$ model, showed the largest variations in relative LAR predictions. The median relative LARs were much lower for the remaining variable RBE models, which also had much smaller variations in their relative LAR estimations. The $RØR_{10Gy}$ model predicted the overall lowest median relative LAR, as well as variations in the predicted relative risks, with 5% (range: 3 to 10%) for the linear model, 4% (range: 2 to 9%) for the linear-exponential model, and only 1% (range: 0 to 5%) for the plateau model. Each median relative LAR, with the range of min and max relative LAR, is listed in Table B.5 in Appendix B.

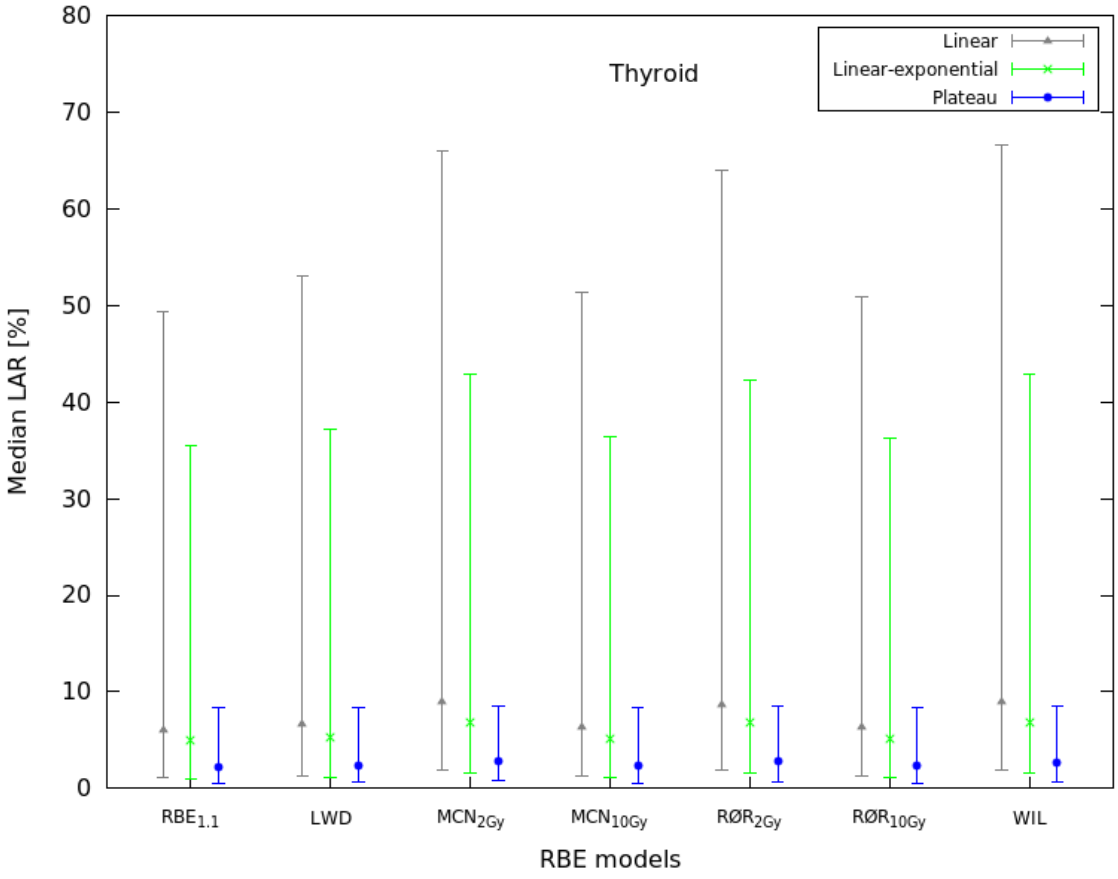

Figure 6.9: Median lifetime attributable risk of radiation-induced thyroid cancer in % of ten patients for each RBE model and each dose-response relationship. The error bars represent the range in terms of minimum and maximum LAR estimate.

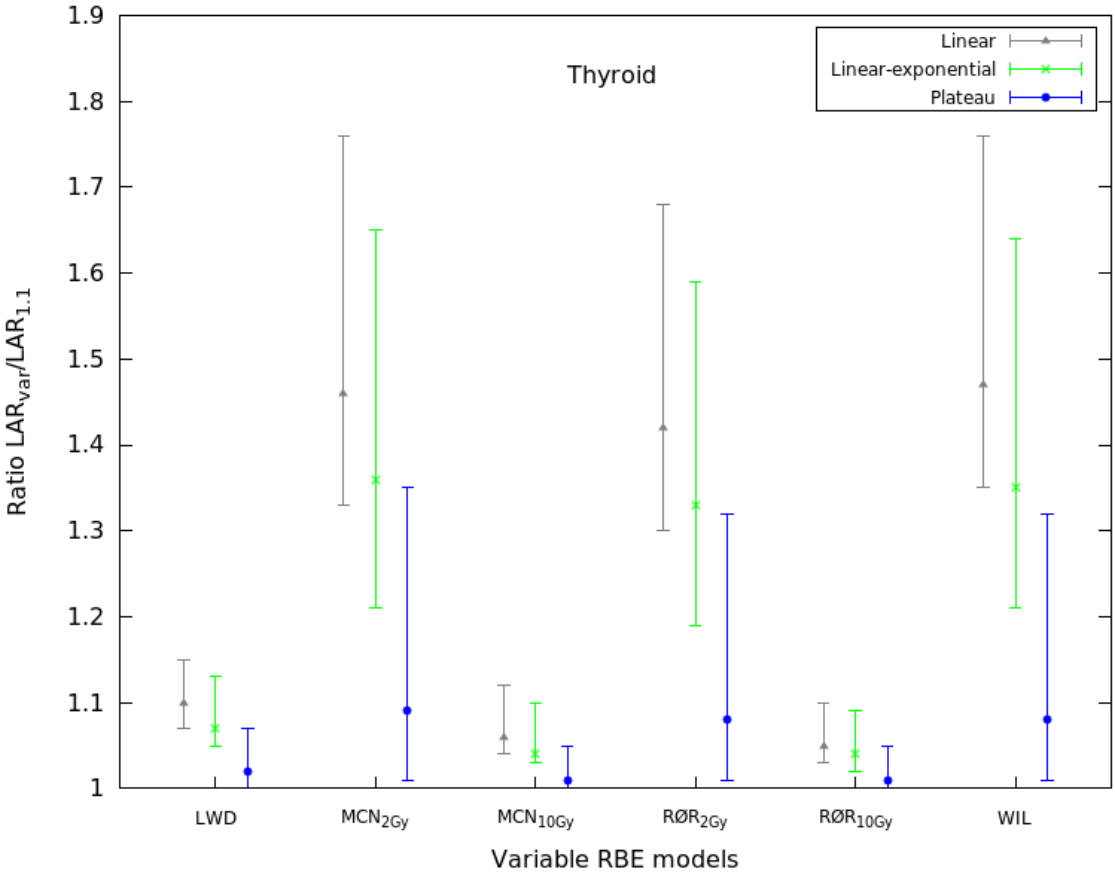

Figure 6.10: The ratio between the variable RBE model LAR estimates and the LAR estimates made by $RBE_{1.1}$ for each dose-response model. The points are the median ratio values of ten patients with error bars representing the range in terms of minimum and maximum LAR ratio.

Figure 6.11 shows an example of the RED distribution in patient 4 for each of the three dose-response relationships using the MCN_{2Gy} model. All three dose-response relationships predicted the risk of secondary thyroid cancer to be highest near the target volume on the left side of the body (right side in the plots) where the thyroid is closest to the target. The spatial risks of the linear and linear-exponential dose-response relationship show very little difference in RED distribution and values, with a small higher-RED region at the edge of the thyroid and mostly lower-RED values in the rest of the organ, whereas the plateau dose-response relationship show a more even decrease in RED with distance from the target volume. The RED values are also generally much lower than for the other two dose-response relationships.

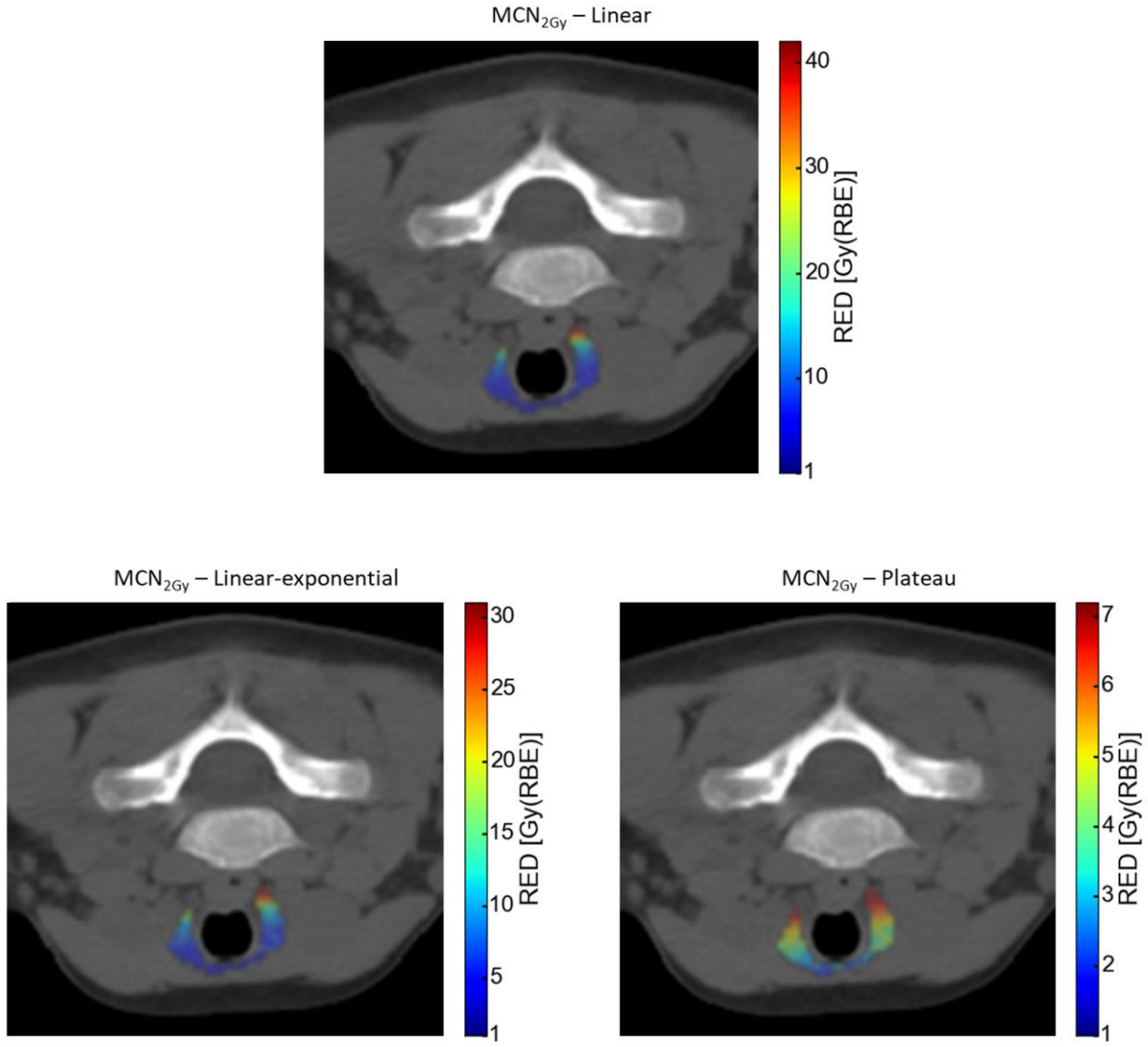

Figure 6.11: Distribution of risk equivalent dose (RED) in the thyroid of patient 4 (8-year-old female) with a variable RBE model (MCN_{2Gy}) using the linear (top), linear-exponential (bottom left) and plateau (bottom right) dose-response relationship. RED is given in units of Gy(RBE) which is proportional to the LAR in each voxel. The CT scan has been zoomed inn to clearer see any difference in RED distribution (original size displayed in Figure 5.1).

6.2 Excess absolute risk

The EAR of radiation-induced lung cancer as a function of homogeneous dose is shown in Figure 6.12 to illustrate the difference between the four dose-response relationships for one of the patients in the cohort.

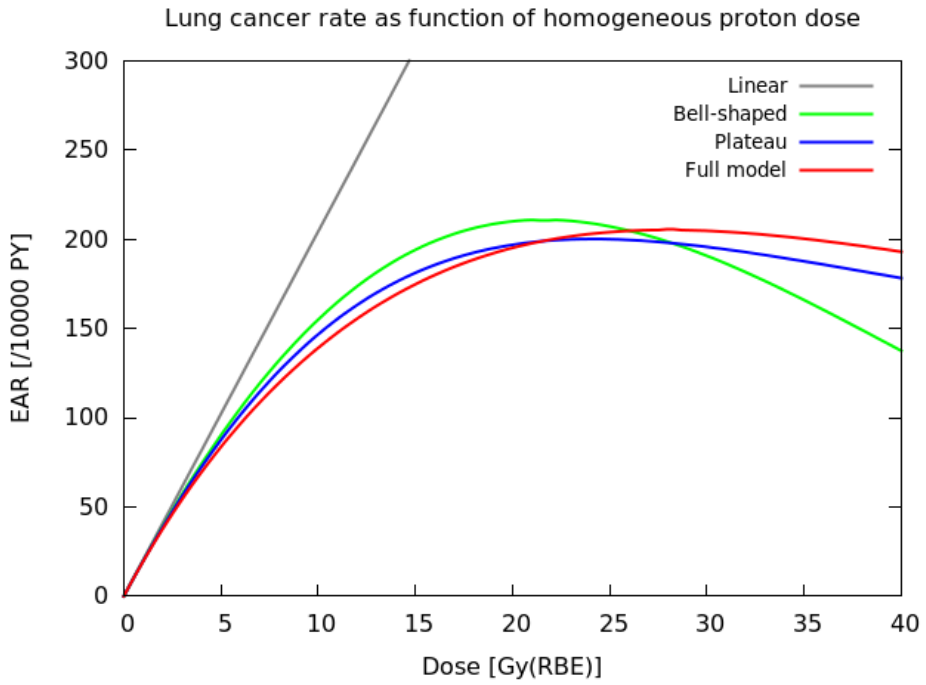

Figure 6.12: Excess absolute risk of secondary lung cancer as a function of homogeneous dose in [/10000 PY] estimated for patient 4 (8-year-old female), using the linear (grey line), bell-shaped (green line), plateau (blue line) and full model (red line) dose-response relationship. The prescription dose to the target volume is 23.4 Gy(RBE) and the contributions of higher doses are therefore small for the patients in this cohort; the higher dose levels are included only to illustrate the differences between the dose-response relationships at these dose levels.

The EAR is similar for all dose-response relationships up to about 2 Gy(RBE). For doses higher than 2 Gy(RBE), the EAR is highest for the linear dose-response relationship, followed by the bell-shaped, plateau and full model in succession from highest to lowest risk up to about 21 Gy(RBE). For doses exceeding approximately 21 and 26 Gy(RBE), the full model predicts higher risks than the plateau and the bell-shaped dose-response relationships, respectively. The plateau dose-response relationship also yields higher risk predictions than the bell-shaped above around 28 Gy(RBE).

Employing each of the RBE models and each of the four dose-response relationships, the estimated OED and EAR of secondary lung cancer for each patient are shown in Figure 6.13 and Figure 6.14, respectively.

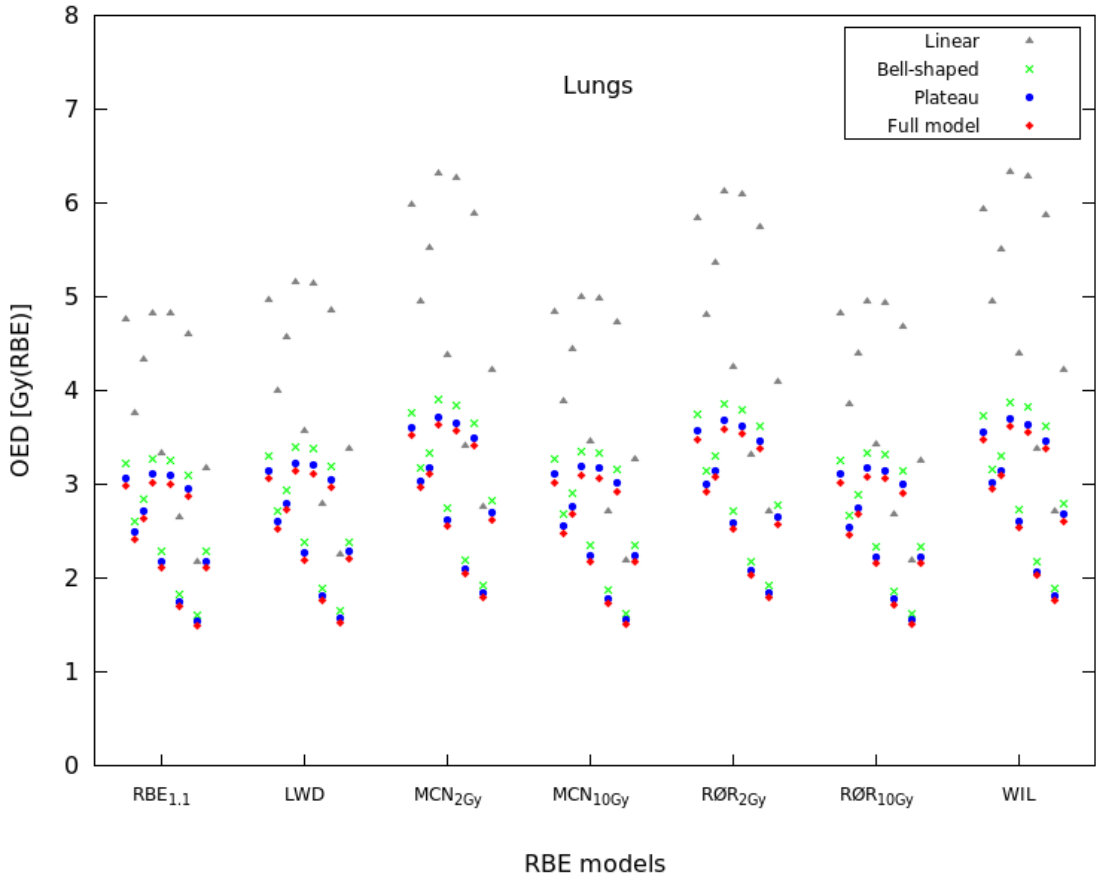

Figure 6.13: Organ equivalent doses for the lungs in Gy(RBE) using the different RBE models and dose-response relationships. The results are shown for patient 1-10 in succession from left to right for each RBE model.

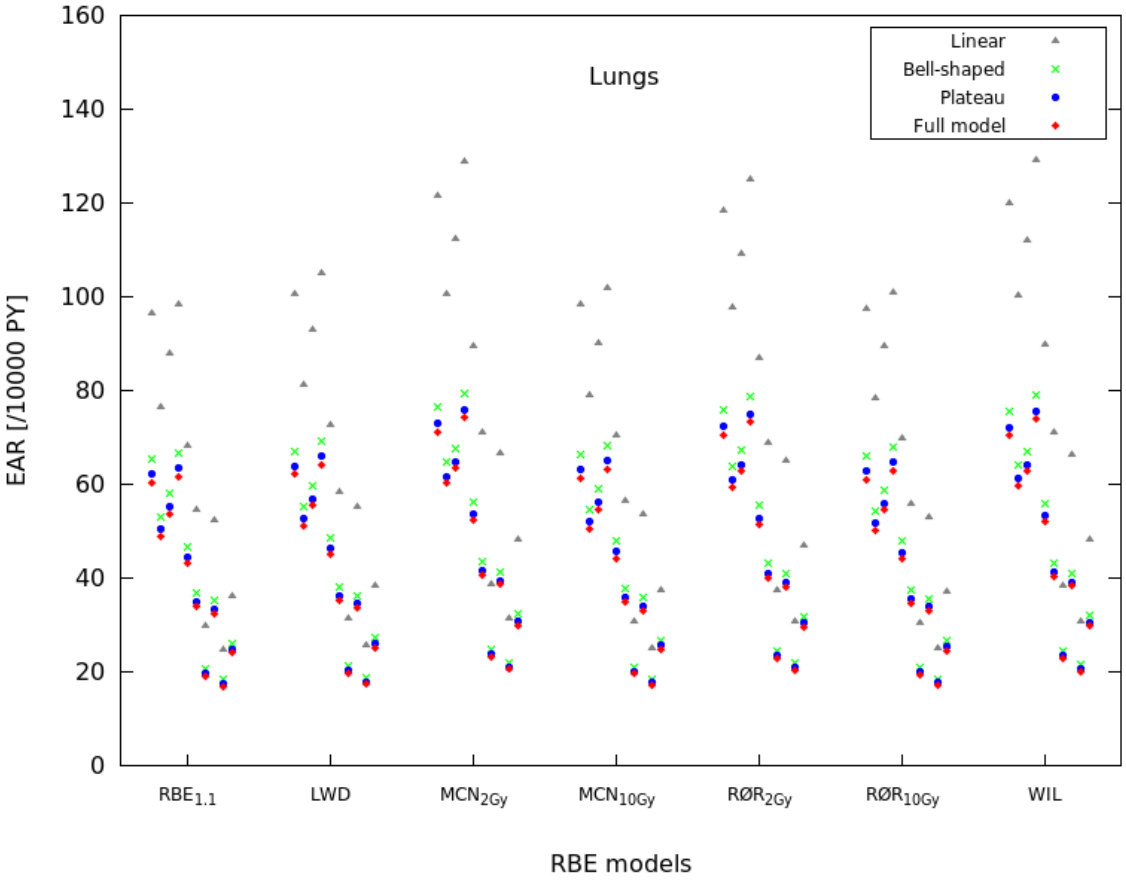

Figure 6.14: Excess absolute risks of secondary lung cancer in $(10000\ PY)^{-1}$ using the different RBE models and dose-response relationships. The results are shown for patient 1-10 in succession from left to right for each RBE model.

As with the LAR of secondary lung cancer, the highest OED values were found for the female patients 1 and 4 and for the male patients 6 and 8, and the lowest OED values were found for patients 7 and 9. There was however a less clear distinction between the non-linear dose-response relationships for the ranges of OED estimates for EAR of secondary lung cancer compared to the previous LAR (lung) calculations (the linear values were of course identical). Here, the lower OED values for the three non-linear dose-response relationships were rather close and ranged from 1.49 ($RBE_{1.1}$ for patient 9 using the full model dose-response relationship) to 3.90 Gy(RBE) (MNC_{2Gy} for patient 4 using the bell-shaped dose-response relationship). Each individual OED value is listed in Table C.2 in Appendix C.

For the estimated EARs of secondary lung cancer, the variable RBE models all showed higher risk estimates compared to the constant $RBE_{1.1}$ model. Overall, the risk estimates were highest for the MCN_{2Gy} model for all four dose-response relationships, with the only exception being the three higher risk estimates for patients 4-6 by the WIL model using the linear dose-response relationship. Across all RBE models, the highest risks were estimated using the linear dose-response relationship for all the patients in the cohort. The three non-linear dose-response relationships had more similar risk estimates, where the bell-shaped have the highest risks of the three, followed by the plateau, and with the full model estimating the lowest risks of all four dose-response relationships. Collectively, the EAR estimates were higher for the female patients compared to the male patients for all RBE models and dose-response relationships applied. The EAR estimates showed the same tendencies as the estimated LAR values of secondary lung cancer, with almost twice as high risk estimates for 8-year-old female patient 4 compared to 8-year-old male patient 6. Any relationship between the EAR estimates and the patient age could not be determined for either of the patients in the cohort. Each individual EAR value is listed in Table C.3 in Appendix C.

The median EAR values for the patient cohort are presented in Figure 6.15 (and listed along with the range in Table C.4 in Appendix C). The $RBE_{1.1}$ model had the lowest median risk of secondary lung cancer for all four dose-response relationships. The WIL model had the highest median risk estimate for the linear model and the MCN_{2Gy} model had the highest median risk estimates for all three non-linear models. Of the four dose-response models, the full model had the overall lowest median risk estimates for all RBE models, and the linear model had the highest. Regarding the median relative EAR with respect to each dose-response relationship (Figure 6.16), the MCN_{2Gy} model predicted the highest median risk increase relative to $RBE_{1.1}$ for all four dose-response relationships, as well as the largest variations in estimates, with 31% median relative EAR for the linear model (ranging from 26% to 33%), 20% for the bell-shaped and plateau model (ranging from 17% to 24%), and 21% for the full model (ranging from 18% to 24%). The WIL and RØR2Gy models, predicting the second and third highest

median relative EARs, respectively, had similar variations in estimates. The lowest relative EAR was made by the $RØR_{10Gy}$ model with respect to both median value and the range, with a median relative EAR of 2% for all dose-response relationships applied. Each median relative EAR, with the range of min and max values, is listed in Table C.5 in Appendix C.

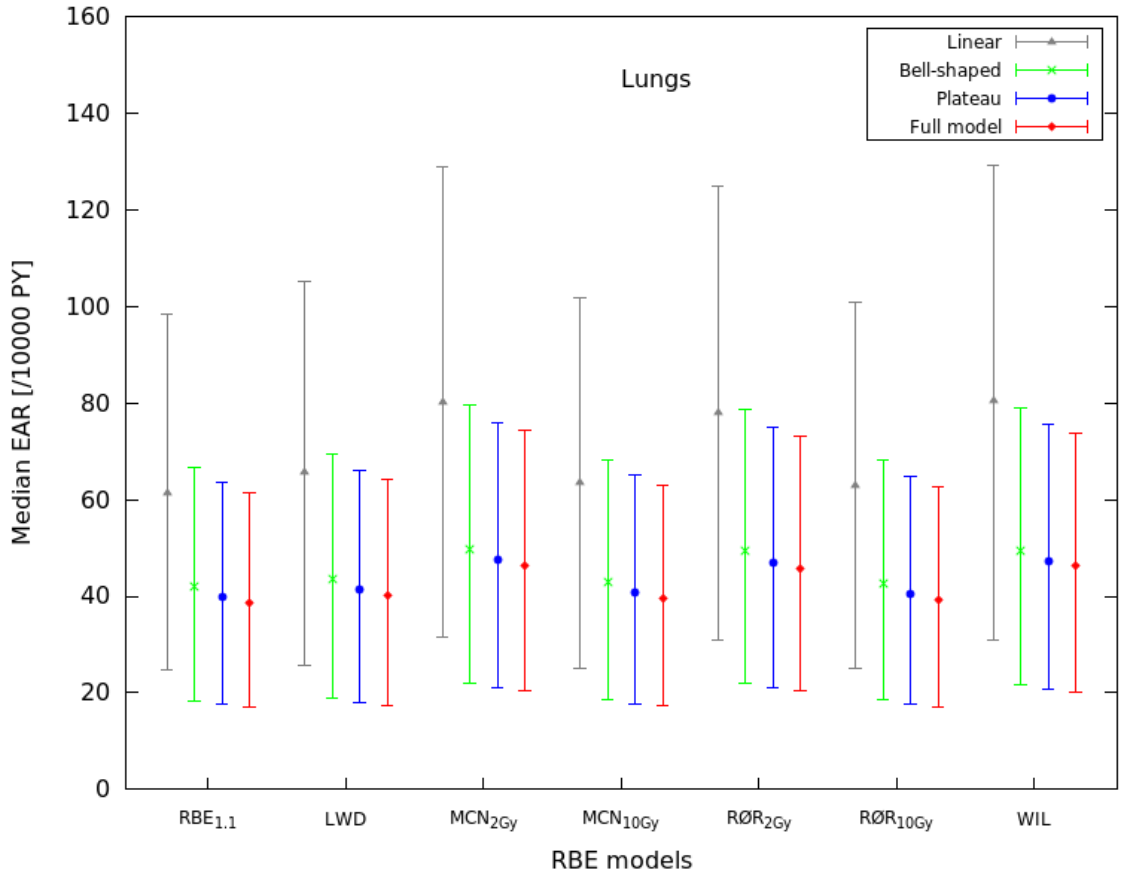

Figure 6.15: Median excess absolute risk of radiation-induced lung cancer in $(10000\ PY)^{-1}$ of ten patients for each RBE model and each dose-response relationship. The error bars represent the range in terms of minimum and maximum EAR estimate.

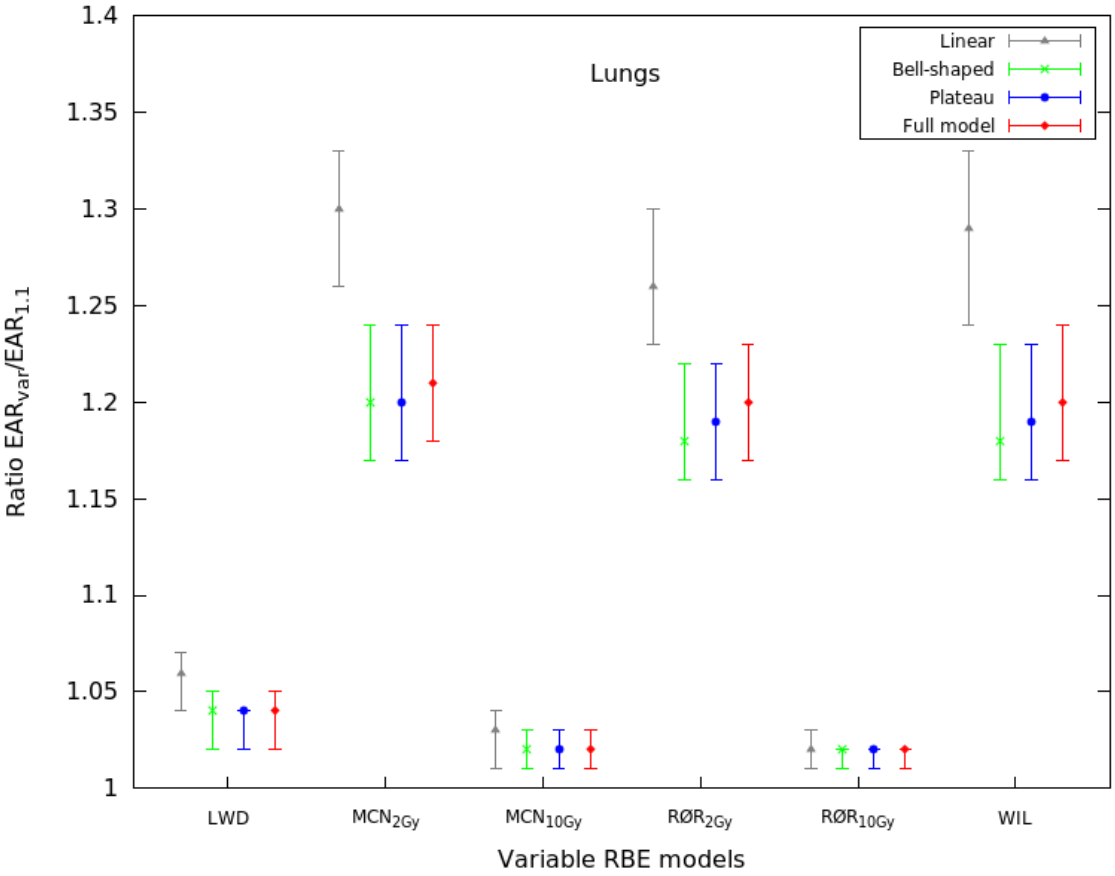

Figure 6.16: The ratio between the variable RBE model EAR estimates and the EAR estimates made by $RBE_{1.1}$ for each dose-response model. The points are the median ratio values of ten patients with error bars representing the range in terms of minimum and maximum EAR ratio.

Figure 6.17 shows an example of the RED distribution in patient 4 for each of the four dose-response relationships using the MCN_{2Gy} model. All four dose-response relationships predicted the highest risk of secondary lung cancer in the lung tissue closest to the target volume, with the highest RED values predicted by the linear dose-response relationship and similar RED values predicted by the non-linear dose-response relationships. In the RED distribution further away from the target volume, the linear dose-response relationship showed a steeper decrease in RED values than the three non-linear dose-response relationships. No clear ring-shaped RED distribution similar to the one in Figure 6.6 could be seen for any of the non-linear dose-response relationships regardless of RBE model employed.

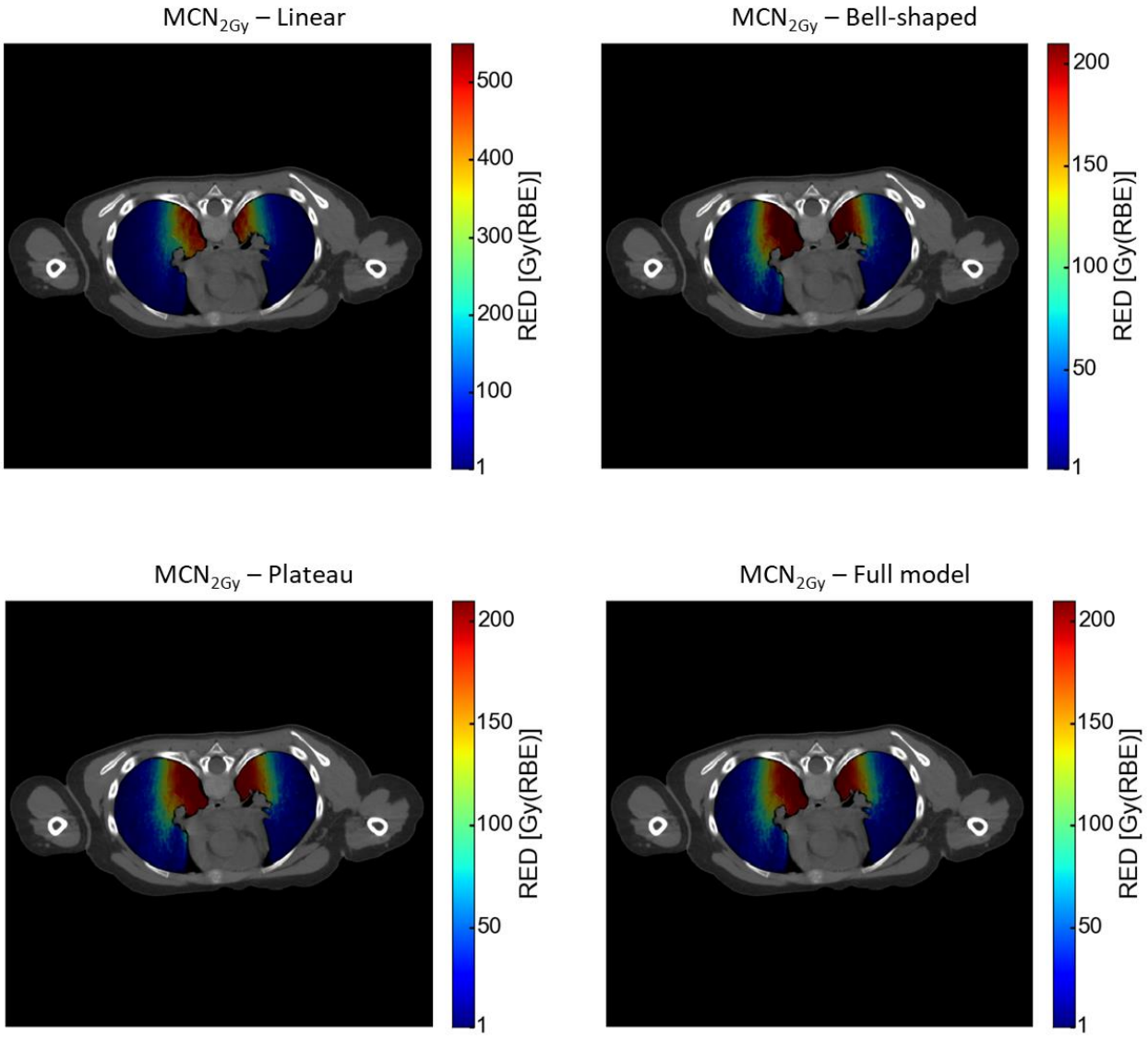

Figure 6.17: Distribution of risk equivalent dose (RED) in the lungs of patient 4 with a variable RBE model (MCN_{2Gy}) using the linear (top left) bell-shaped (top right), plateau (bottom left) and full model (bottom right) dose-response relationship. RED is given in units of Gy(RBE) which is proportional to the EAR in each voxel.

7. Discussion

The results have shown an overall increase in estimated radiation-induced secondary cancer risk with variable proton RBE compared to the generic value of 1.1. Depending on the choice of dose-response relationship, the median increase in risk estimates for the variable RBE models were 1 to 47% relative to the RBE of 1.1. The linear models with respect to both LAR and EAR predicted the highest risk with variable RBE compared to 1.1 for both organs at risk. The variations in risk estimates were also much larger for the linear models. The difference in risk variations between the non-linear dose-response relationships were dependent on the risk model applied, showing little variation for EAR estimates and larger variations for LAR estimates, especially for LAR of secondary thyroid cancer. The variations in risk estimates across the different RBE models were much smaller compared to those seen across the different dose-response relationships. The validity of the absolute risk estimates therefore had a stronger dependency on dose-response relationship than RBE model applied. For the relative increase in risk, on the other hand, the variations in estimates were much smaller across all dose-response relationships applied, with the larger variations in relative risk predictions were seen across the variable RBE models used. This was also where the median relative risk estimates varied most across the different dose-response relationships. Thus, the validity of the relative increase in risk with variable RBE has an overall stronger dependency on the chosen variable RBE model than the chosen dose-response relationship.

Most of the organ doses in these calculations exceeded the threshold value of 2.5 Gy(RBE) where the risk estimates made by linear models start exceeding those made by the non-linear models (Figure 6.1 and Figure 6.12). The EAR estimates using the non-linear dose-response relationships were the most similar to each other of all non-linear model estimates. The ranges of risk estimates were between 18 and 80 (10 000 PY)$^{-1}$ for the bell-shaped model, between 18 and 76 (10 000 PY)$^{-1}$ for the plateau model and between 17 and 74 (10 000 PY)$^{-1}$ for the full model. These similarities are due to

the plateau dose-response relationship falling off at higher doses similar to the bell-shaped dose-response relationship, which differs from the plateau shape seen in the LAR dose-response curves for both lung and thyroid. Also, with the full model representing a combination of these two, it is not unexpected that the EAR estimates vary as little as they do between the non-linear dose-response relationships. Even though there is an agreement that paediatric medulloblastoma have a significant increase in risk of developing radiation-induced secondary cancer after radiotherapy, all LAR and EAR estimates in this thesis are relatively high compared to registered secondary cancers for this patient group [21-23]. There has been recorded a significant increase in risk of developing secondary thyroid cancer where 2 out of 379 patients developed thyroid cancer at 8 and 10 years after treatment in the study by Packer et al. (2013), and Strodtbeck et al. (2013) found a statistically significant relative risk of secondary thyroid cancer at least 5 years post treatment [22, 23]. However, the risks are still lower than the lowest median LAR estimate of secondary thyroid cancer of 2.25% in this thesis, and as no records of observed secondary lung cancer was listed explicitly, it can be assumed that this risk was higher in this thesis as well. On the other hand, the follow-up time for the patients in these studies did not exceed 21 years and can therefore not provide extensive information regarding lifetime risks of secondary cancer induction, which could possibly be much higher due to the latency period of most solid cancers.

Several differences in the predicted risks were seen between the variable RBE models for each of the dose-response relationships. Regarding the variations between the models with differences in chosen $(\alpha/\beta)_x$ value, both the McNamara model and the Rørvik model predicted higher median absolute and median relative risks with $(\alpha/\beta)_x$ = 2 Gy than with $(\alpha/\beta)_x$ = 10 Gy. The Wilkens model also had some of the higher risk predictions in the results, and as this model uses $(\alpha/\beta)_x$ = 3.76, i.e. higher $(\alpha/\beta)_x$ value than the MCN_{2Gy} and $RØR_{2Gy}$ models, this indicates that the risk does not necessary increase with lower $(\alpha/\beta)_x$ values across models. Although there are no definite answers to the $(\alpha/\beta)_x$ value of lung and thyroid tissue, there are indications in literature

suggesting that 3 Gy could be suitable. The thyroid has usually been given an $(\alpha/\beta)_x$ value corresponding to late reacting tissue, whereas $(\alpha/\beta)_x$ values for lung tissue have been listed in the form of range of 2.0-6.3 Gy, and 2.4-6.3 Gy, as well as a fixed 4.0 ± 0.9 Gy [5, 91-93]. Therefore, arguments could be made for the higher validity of variable RBE models with $(\alpha/\beta)_x$ values corresponding to late responding tissues rather than those with $(\alpha/\beta)_x$ corresponding to early responding tissues of 10 Gy, increasing the importance of the larger relative risks predicted by the MNC_{2Gy}, $RØR_{2Gy}$ and WIL models. The highest predicted median relative risks by these RBE models ranged from 9 to 47%. Concerning other variable RBE model aspects, there seemed to be no clear difference between the risk predictions for the non-linear RBE-LET_d relationship of the Rørvik model and those for the linear RBE-LET_d relationships of the other variable RBE models, albeit the $RØR_{10Gy}$ predicting the lowest relative risks of all the variable RBE models, followed closely by the MCN_{10Gy} and the LWD models.

According to the BEIR VII report [18], the risk of radiation-induced lung and thyroid cancer is higher for females than for males, both for LAR and EAR estimations. This was also evident from the results in this thesis. In addition, the report shows an increase in LAR with decrease in age at exposure, of which these results did not show any clear indication. This was likely due to the individual size of the patients and thereby the dose distribution provided by the different proton plans for each patient. For instance, the individual OED values for thyroid (with $RBE_{1.1}$) ranged from ≈ 2.0 to 19.2 Gy(RBE) for patient 10 (12-year-old male) and ≈ 0.9 to 14.9 Gy(RBE) for patient 8 (8-year-old male). For the EAR, the risk estimates are expected to increase with higher attained age and lower age at exposure. The EAR was higher for the female patients with the higher attained age, but this can also be attributed to the sex-specific higher risk for females. The EAR results did not verify any relationship between increase in risk with lower age at exposure, most likely due to the influence of dose distributions on the results as with the LAR estimates. Thus, the individual dose distributions seem to have a higher impact on risk estimates than the age at exposure for this patient group, due to the small age span of 5-12 years. Because of the magnitude in difference between

boys and girls, the sex-specific risk ratios are less sensitive to the inter-patient variations in dose distributions.

There are presently no published studies that have calculated secondary cancer risk following proton therapy with inclusion of possible variations in the proton RBE. Thus, the results from this thesis can only be compared to studies that have estimated radiation-induced secondary cancer risks for proton therapy with a generic RBE of 1.1. Three studies estimating lifetime risk of lung and thyroid cancer using IMPT plans for proton CSI of medulloblastoma patients were found for comparison: Miralbell et al. (2002) [24], Mu et al. (2005) [25] and Stokkevåg et al. (2014) [29]. The results are presented in Table D.1 in Appendix D in comparison with the median risk estimates (including range) from this thesis. The adjusted risk estimates of these three studies all fall within the range of the risk estimates of this thesis, despite the median risk estimates being generally higher compared to all the adjusted risks from these studies. The lowest risk estimate was by Mu et al., but as this study only focussed on spinal irradiation this could potentially cause a lower risk estimates than studies that also include irradiation of the cranium. The patient cohorts were also smaller for these studies compared to the patient cohort of this thesis, with 1, 5 and 6 patients in Miralbell et al., Mu et al. and Stokkevåg et al., respectively. Also, only Stokkevåg et al. included risk estimates based on non-linear dose-response relationships that could be used for comparison, but the average organ risks were weighted according to the higher frequency of medulloblastoma in boys compared to girls, which could be a reason for the small deviation between these results and the results of this thesis.

Several studies have compared secondary cancer risk estimates for proton therapy and photon therapy for paediatric medulloblastoma patients receiving CSI [24-31]. All these studies have shown lower risk predictions for all studied cancer sites following proton therapy compared to photon therapy, independent of dose-response relationship and risk model applied. Although these studies did not necessarily use the exact dose-response relationships chosen for this thesis and also based their risk estimations on the clinical RBE of 1.1 only, it is still interesting to investigate whether the relative increase

in predicted risks with variable RBE seen in this thesis would change the preference of proton therapy over photon therapy in either of these studies. The risk estimates in each of these studies are presented in Table D.2 and Table D.3 in Appendix D. Overall, none of the risk estimates adjusted with the variable RBE model risk increase exceeded the estimated risks for photon therapy. This indicates that the variations that can be found in the proton RBE might not be large enough to prevent proton therapy plans from being the better option compared to photon therapy plans for paediatric medulloblastoma patients, at least for estimated risks of radiation-induced lung and thyroid cancer. The adjusted ratios of proton risk estimates over photon risk estimates were still very low for secondary thyroid cancer, where the ratios ranged from 0.03 to 0.16. However, the adjusted ratios of secondary lung cancer risk estimates were much higher, approaching 1 in the case of Mu et al. (2005), Zhang et al. (2004), and Taddei et al. (2018) with risk ratios of 0.96, 0.98 and 0.95 (including secondary neutrons), respectively.

Uncertainties and limitations

The use of absolute risk estimations has been associated with very large uncertainties [18, 94, 95]. The BEIR VII report considers the uncertainties in the parameters estimated based on the LSS cohort data, the uncertainties that comes with applying this data to another population, and the uncertainty in the DDREF value to be of highest importance [18]. For the EAR estimates, the uncertainty lies mainly in the initial slope parameter β [77]. The uncertainties of relevance (which excludes the uncertainty in the DDREF) are displayed in the confidence intervals for each risk estimate in the tables of Appendix A, Appendix Band Appendix C. In addition, a major contributor to the uncertainty in the results of this thesis is the shape of the dose-response relationship for each organ at risk [96]. When it comes to the shape of the dose-response relationship, there is a clear increase in risk estimates for the linear dose-response relationship compared to the non-linear dose-response relationships. Using the linear dose-response relationship could thus lead to an overestimation of secondary cancer risk for higher dose ranges. On the other hand, the lower risk estimates provided by the non-linear

dose-response relationships may be an underestimation, and there also exists several additional uncertainties with the non-linear dose-response relationships used in this thesis. Both the linear-exponential and the plateau dose-response relationship described by Schneider et al. (2005) [76, 79] are derived from the same epidemiological data on patients receiving radiotherapy for Hodgkin's disease and the EAR dose-response relationships, although based on another patient cohort, are also derived from Hodgkin's patient data [77]. This could make it difficult to transfer these risk estimates to patients treated with radiotherapy for other malignancies, in this case medulloblastoma. Also, it has been pointed out that the dose reconstruction from the Hodgkin's patients treated decades ago suffers from inaccuracy [76]. Lastly, there have only been a few indications and no clear definition of dose-response supporting these relationships in radiation epidemiology literature to date which leads to the possibility that these dose-response relationships are incorrect to use for secondary cancer risk estimations. The present inability to provide reasonable dose-response relationships for proton therapy therefore causes limitations in using the OED concept to account for inhomogeneous dose distributions associated with this modality [13, 17]. The indications to a possible shape of the dose-response relationship in literature have been regarding the evidence of a linear-exponential, or bell-shaped, dose-response relationship for thyroid cancer induction [97] and of a linear dose-response relationship for lung cancer [98]. Thus, there is a possibility that the risks predicted by the linear-exponential dose-response model for secondary thyroid cancer induction are likely, and that there could be incentive for a linear dose-response relationship for secondary lung cancer, perhaps given a less steep slope than the one used in this thesis.

It should also be emphasised that these dose-response relationships are theoretical, proposed to account for the biological effects in cells induced by ionising radiation, which the linear dose-response relationship does not consider, and there may be evidence supporting either of these dose-response relationships in future epidemiological studies. For this reason, theoretical dose-response relationships are viewed as complimentary to epidemiological studies by exploring aspects that can

affect the risk of secondary cancer incidence [17]. In any case, several studies have demonstrated that by using relative risk estimates the effect of the uncertainty in both shape of dose-response relationship as well as the interpatient variations in absorbed dose can be minimised [96, 99]. Therefore, the results in this thesis regarding the ratios and risk estimates relative to each other could be seen as more robust than the actual values of each risk estimate.

Another factor of uncertainty is provided by the estimation of the proton RBE value. The alternative estimation of proton RBE values to the clinical value of 1.1 provided by the variable RBE models used in this thesis all exhibit uncertainties in how RBE varies with factors like LET, tissue type, endpoint and dose. Thus, the uncertainties in the estimation of a variable proton RBE will propagate into the dose-response models used to estimate secondary cancer risks following proton therapy. In a recent review, it was also pointed out that risk estimates in proton therapy (and heavy ion therapy) based solely on RBE for the endpoint of cell kill may be oversimplified [55].

The results in this thesis are also experiencing limitations regarding factors that have not been taken into consideration in the process of calculating the predicted risks. One of these factors is the additional dose contribution from secondary scattered neutrons. As mentioned in chapter 2.3, these secondary particles are present to a certain but not completely ascertained degree during proton therapy beam delivery. There are presently no reliable methods able to account for the secondary neutron dose in proton therapy that comes from scattered neutrons either leaking from the treatment apparatus or produced inside the patient [37]. Although the severity of secondary neutron dose in proton therapy is not yet determined, it may provide an additional increase in risk of secondary cancer incidence for proton therapy. Studies have simulated this additional secondary neutron dose in literature to examine whether there would be a significant impact on secondary cancer risk estimations [25, 26, 30, 31, 68]. The results showed an increase in overall dose from proton therapy modalities, and thus in the risk estimations. However, the magnitude of the increase in dose was not large enough to result in risk estimations that caused a preference of photon therapy modalities over

those of proton therapy, even when using a radiation weighting factor for neutrons up to five times higher than recommended by the ICRP [68]. Another factor that might increase the risk of radiation-induced secondary cancer is the dose that comes from diagnostic imaging with ionising radiation. This risk in comparison to the one from the radiotherapy is however considered to be quite small and might not give much of an increase in the risk estimates in this thesis, and as such risks most likely will not be additive to the risk estimates from the radiation treatment, they would be difficult to study independently [11]. Lifestyle and genetics will also play a role in possibly increasing the risk estimates in this thesis, which are difficult to quantify in order to account for them in risk estimations.

8. Conclusion

As paediatric medulloblastoma patients are at a particularly high risk of developing radiation-induced secondary cancers after treatment, the objective of this thesis was to investigate possible changes in risk estimations following use of variable RBE models compared to constant RBE for proton therapy. Of all the RBE models in this thesis, the $RBE_{1.1}$ displayed the lowest risk estimates for all dose-response relationships and secondary cancer risk models employed. The risk will therefore increase compared to previous estimates when the proton RBE deviates from 1.1, with the size of this increase being dependent on variable RBE models employed. The relative increase in risk estimates with the variable RBE models was fairly insensitive to the choice of dose-response relationship, and also to the inter-patient variations in dose, which are both factors that influenced the absolute risk estimates greatly. By applying these relative increases in risk to estimations made for paediatric medulloblastoma patients following proton therapy with $RBE_{1.1}$ in comparison with photon therapy made by other studies, the overall increase in risk estimates did overtake the values estimated for photon therapy. This indicates that proton CSI is the better treatment option for these patients with respect to secondary cancer risk estimates, regardless of a potentially higher proton RBE than the clinical value of 1.1.

Bibliography

1. WHO. *World Health Organization Cancer*. 2018 [cited 2018 15.10]; Available from: https://www.who.int/cancer/en/.
2. Larsen, I.K., et al., *Cancer in Norway 2016 - Cancer incidence, mortality, survival and prevalence in Norway*. 2017: Oslo: Cancer Registry of Norway.
3. Delaney, G., et al., *The role of radiotherapy in cancer treatment: estimating optimal utilization from a review of evidence-based clinical guidelines.* Cancer, 2005. **104**(6): p. 1129-37.
4. Paganetti, H., *Proton Therapy Physics*. 2012: CRC Press - Taylor & Francis Group.
5. Hall, E.J. and A.J. Giaccia, *Radiobiology for the Radiologist*. 6th ed. 2006: Lippincott Williams & Wilkins.
6. Thariat, J., et al., *Past, present, and future of radiotherapy for the benefit of patients.* Nat Rev Clin Oncol, 2013. **10**(1): p. 52-60.
7. Wilson, R.R., *Radiological use of fast protons.* Radiology, 1946. **47**(5): p. 487-91.
8. Bragg, W.H. and R. Kleeman, *On the ionization curves of radium.* Philosophical Magazine, 1904. **8**(48): p. 726-38.
9. PTCOG. *Particle Therapy Co-Operative Group. Facilities in operation*. 2018 [cited 2018 15.10]; Available from: https://www.ptcog.ch/index.php/facilities-in-operation.
10. PTCOG. *Particle Therapy Co-Operative Group. Patient statistics per end of 2016*. 2016 [cited 2018 15.10]; Available from: https://www.ptcog.ch/index.php/patient-statistics.
11. Dasu, A. and I. Toma-Dasu, *Long-term effects and secondary tumors.* Comprehensive Biomedical Physics, 2014. **9**: p. 223-33.
12. Paganetti, H., et al., *Relative biological effectiveness (RBE) values for proton beam therapy.* Int J Radiat Oncol Biol Phys, 2002. **53**(2): p. 407-21.
13. Paganetti, H., *Relative biological effectiveness (RBE) values for proton beam therapy. Variations as a function of biological endpoint, dose, and linear energy transfer.* Phys Med Biol, 2014. **59**(22): p. R419-72.
14. Leeman, J.E., et al., *Proton therapy for head and neck cancer: expanding the therapeutic window.* Lancet Oncol, 2017. **18**(5): p. e254-65.
15. Ng, J. and I. Shuryak, *Minimizing second cancer risk following radiotherapy: current perspectives.* Cancer Manag Res, 2014. **7**: p. 1-11.
16. Joiner, M. and A. van der Kogel, *Basic Clinical Radiobiology*. 4th ed. 2009: CRC Press - Taylor & Francis Group.
17. Dasu, A. and I. Toma-Dasu, *Models for the risk of secondary cancers from radiation therapy.* Physica Medica, 2017. **42**: p. 232-8.
18. BEIR, *Health risks from exposure to low levels of ionizing radiation: BEIR VII Phase 2*. 2006: Washington D.C.
19. Dhall, G., *Medulloblastoma.* J Child Neurology, 2009. **24**(11): p. 1418-30.
20. Packer, R.J., et al., *Phase III study of craniospinal radiation therapy followed by adjuvant chemotherapy for newly diagnosed average-risk medulloblastoma.* J Clin Oncol, 2006. **24**(25): p. 4202-8.
21. Stavrou, T., et al., *Prognostic factors and secondary malignancies in childhood medulloblastoma.* J Pediatr Hematol Oncol, 2001. **23**(7): p. 431-6.
22. Strodtbeck, K., et al., *Risk of subsequent cancer following a primary CNS tumor.* J Neurooncol, 2013. **112**(2): p. 285-95.

23. Packer, R.J., et al., *Survival and secondary tumors in children with medulloblastoma receiving radiotherapy and adjuvant chemotherapy: results of Children's Oncology Group trial A9961.* Neuro Oncol, 2013. **15**(1): p. 97-103.
24. Miralbell, R., et al., *Potential reduction of the incidence of radiation-induced second cancers by using proton beams in the treatment of pediatric tumors.* International Journal of Radiation Oncology*Biology*Physics, 2002. **54**(3): p. 824-829.
25. Mu, X., et al., *Does electron and proton therapy reduce the risk of radiation induced cancer after spinal irradiation for childhood medulloblastoma? A comparative treatment planning study.* Acta Oncol, 2005. **44**(6): p. 554-62.
26. Newhauser, W.D., et al., *The risk of developing a second cancer after receiving craniospinal proton irradiation.* Phys Med Biol, 2009. **54**(8): p. 2277-91.
27. Zhang, R., et al., *Comparison of risk of radiogenic second cancer following photon and proton craniospinal irradiation for a pediatric medulloblastoma patient.* Phys Med Biol, 2013. **58**(4): p. 807-23.
28. Zhang, R., et al., *A comparative study on the risks of radiogenic second cancers and cardiac mortality in a set of pediatric medulloblastoma patients treated with photon or proton craniospinal irradiation.* Radiother Oncol, 2014. **113**(1): p. 84-8.
29. Stokkevåg, C.H., et al., *Estimated risk of radiation-induced cancer following paediatric cranio-spinal irradiation with electron, photon and proton therapy.* Acta Oncol, 2014. **53**(8): p. 1048-57.
30. Taddei, P.J., et al., *Inter-institutional comparison of personalized risk assessments for second malignant neoplasms for a 13-year-old girl receiving proton versus photon craniospinal irradiation.* Cancers (Basel), 2015. **7**(1): p. 407-26.
31. Taddei, P.J., et al., *Low- and middle-income countries can reduce risks of subsequent neoplasms by referring pediatric craniospinal cases to centralized proton treatment centers.* Biomed Phys Eng Express, 2018. **4**(2): p. 025029.
32. Khan, F.M. and J.P. Gibbons, *Khan's The Physics of Radiation Therapy*. 5th ed. 2014: Lippincott Williams & Wilkins.
33. Leo, W.R., *Techniques for nuclear and particle physics experiments*. 2nd edition ed. 1994: Springer-Verlag.
34. Mohan, R. and D. Grosshans, *Proton therapy - Present and future.* Adv Drug Deliv Rev, 2017. **109**: p. 26-44.
35. Fano, U., *Penetration of protons, alpha particles, and mesons.* Annu. Rev. Nucl. Sci., 1963. **13**: p. 1-66.
36. Schardt, D., T. Elsasser, and D. Schulz-Ertner, *Heavy-ion tumor therapy: Physical and radiobiological benefits.* Rev. Mod. Phys., 2010. **82**(1): p. 383-425.
37. Newhauser, W.D. and R. Zhang, *The physics of proton therapy.* Phys Med Biol, 2015. **60**(8): p. R155-209.
38. Tommasino, F. and M. Durante, *Proton radiobiology.* Cancers (Basel), 2015. **7**(1): p. 353-81.
39. Wilkens, J.J. and U. Oelfke, *A phenomenological model for the relative biological effectiveness in therapeutic proton beams.* Phys Med Biol, 2004. **49**(13): p. 2811-2825.
40. Zirkle, R.E., D.F. Marchbank, and K.D. Kuck, *Exponential and sigmoid survival curves resulting from alpha and x irradiation of Aspergillus spores.* J Cell Physiol Suppl, 1952. **39**(Suppl. 1): p. 78-85.
41. ICRU, *ICRU report no 85. Fundamental quantities and units for ionizing radiation*. 2011, International Commission on Radiation Units and Measurements.

42. Grassberger, C. and H. Paganetti, *Elevated LET components in clinical proton beams.* Phys Med Biol, 2011. **56**(20): p. 6677-91.
43. Guan, F., et al., *Analysis of the track- and dose-averaged LET and LET spectra in proton therapy using the geant4 Monte Carlo code.* Med Phys, 2015. **42**(11): p. 6234-47.
44. Podgorsak, E.B., *Radiation Physics for Medical Physicists*. 2nd ed. 2010: Springer-Verlag Berlin Heidelberg.
45. Knoll, G.F., *Radiation Detection and Measurement*. 4th ed. 2010: John Wiley and Sons, Inc.
46. Cember, H. and T.E. Johnson, *Introduction to Health Physics*. 4th ed. 2009: The McGraw-Hill Companies.
47. ICRP, *The 2007 Recommendations of the International Commission on Radiological Protection. ICRP publication 103.* Ann ICRP, 2007. **37**(2-4): p. 1-332.
48. ICRU, *ICRU report no 78. Prescribing, recording, and reporting proton beam therapy*. 2007, International Commission on Radiation Units and Measurement.
49. Girdhani, S., R. Sachs, and L. Hlatky, *Biological effects of proton radiation: what we know and don't know.* Radiat Res, 2013. **179**(3): p. 257-72.
50. Chang, D.S., et al., *Basic Radiotherapy Physics and Biology*. 2014: Springer.
51. Lea, D.E., *Actions of Radiations on Living Cells*. 1946: Cambridge University Press.
52. Dasu, A. and I. Toma-Dasu, *Impact of variable RBE on proton fractionation.* Med Phys, 2013. **40**(1): p. 011705.
53. Henjum, H., *Optimization of proton therapy plans with respect to biological and physical dose distributions*. 2018.
54. Paganetti, H., *Relating proton treatments to photon treatments via the relative biological effectiveness - should we revise current clinical practice?* Int J Radiat Oncol Biol Phys, 2015. **91**(5): p. 892-4.
55. Stokkevåg, C.H., et al., *Radiation-induced cancer risk predictions in proton and heavy ion radiotherapy.* Phys Med, 2017. **42**: p. 259-62.
56. Wedenberg, M., B.K. Lind, and B. Hårdemark, *A model for the relative biological effectiveness of protons: The tissue specific parameter α/β of photons is a predictor for the sensitivity to LET changes.* Acta Oncol, 2013. **52**(3): p. 580-8.
57. Giovannini, G., et al., *Variable RBE in proton therapy: comparison of different model predictions and their influence on clinical-like scenarios.* Radiat Oncol, 2016. **11**(1): p. 68.
58. Dale, R.G. and B. Jones, *The assessment of RBE effects using the concept of biologically effective dose.* Int J Radiat Oncol Biol Phys, 1999. **43**(3): p. 639-45.
59. Carabe-Fernandez, A., R.G. Dale, and B. Jones, *The incorporation of the concept of minimum RBE (RBE_{min}) into the linear-quadratic model and the potential for improved radiobiological analysis of high-LET treatments.* Int J Radiat Biol, 2007. **83**(1): p. 27-39.
60. McNamara, A.L., J. Schuemann, and H. Paganetti, *A phenomenological relative biological effectiveness (RBE) model for proton therapy based on all published in vitro cell survival data.* Phys Med Biol, 2015. **60**(21): p. 8399-416.
61. Rørvik, E., et al., *A phenomenological biological dose model for proton therapy based on linear energy transfer spectra.* Med Phys, 2017. **44**(6): p. 2586-94.
62. Unkelbach, J., et al., *Reoptimization of intensity-modulated proton therapy plans based on linear energy transfer.* Int J Radiat Oncol Biol Phys, 2016. **96**(5): p. 1097-106.

63. Rørvik, E., et al., *Exploration and application of phenomenological RBE models for proton therapy.* Phys Med Biol, 2018. **63**(18): p. 185013.
64. Miller, K.D., et al., *Cancer treatment and survivorship statistics, 2016.* CA Cancer J Clin, 2016. **66**(4): p. 271-89.
65. Howlader, N., et al. *SEER Cancer Statistics Review, 1975-2012*. 2015 [cited 2018 17.10]; Available from: https://seer.cancer.gov/archive/csr/1975_2012/.
66. Ho, E.S.Q., S.A. Barrett, and L.M. Mullaney, *A review of dosimetric and toxicity modeling of proton versus photon craniospinal irradiation for pediatrics medulloblastoma.* Acta Oncol, 2017. **56**(8): p. 1031-42.
67. St. Clair, W.H., et al., *Advantages of protons compared to conventional X-ray or IMRT in the treatment of a pediatric patient with medulloblastoma.* Int J Radiat Oncol Biol Phys, 2004. **58**(3): p. 727-34.
68. Brodin, N.P., et al., *Radiobiological risk estimates of adverse events and secondary cancer for proton and photon radiation therapy of pediatric medulloblastoma.* Acta Oncol, 2011. **50**(6): p. 806-16.
69. UNSCEAR, *Effects of ionizing radiation, Annex A: Epidemiological studies of radiation and cancer*. 2006, United Nations Scientific Committee on the Effects of Atomic Radiation: Vienna.
70. Schneider, U. and L. Walsh, *Risk of secondary cancers: Bridging epidemiology and modeling.* Physica Medica, 2017. **42**: p. 228-31.
71. Hall, E.J., *Intensity-modulated radiation therapy, protons, and the risk of second cancers.* Int J Radiat Oncol Biol Phys, 2006. **65**(1): p. 1-7.
72. Friedman, D.L., et al., *Subsequent neoplasms in 5-year survivors of childhood cancer: the Childhood Cancer Survivor Study.* J Natl Cancer Inst, 2010. **102**(14): p. 1083-95.
73. Kellerer, A.M., E.A. Nekolla, and L. Walsh, *On the conversion of solid cancer excess relative risk into lifetime attributable risk.* Radiat Environ Biophys, 2001. **40**(4): p. 249-57.
74. Schneider, U., *Modeling the Risk of Secondary Malignancies after Radiotherapy.* Genes, 2011. **2**(4): p. 1033-49.
75. Hall, E.J. and D.J. Brenner, *The dose-rate effect revisited: Radiobiological considerations of importance in radiotherapy.* Int J Radiat Oncol Biol Phys, 1991. **21**(6): p. 1403-14.
76. Schneider, U., et al., *Estimation of radiation-induced cancer from three-dimensional dose distributions: concept of organ equivalent dose.* Int J Radiat Oncol Biol Phys, 2005. **61**(5): p. 1510-5.
77. Schneider, U., M. Sumila, and J. Robotka, *Site-specific dose-response relationships for cancer induction from the combined Japanese A-bomb and Hodgkin cohorts for doses relevant to radiotherapy.* Theor Biol Med Model, 2011. **8**: p. 27-47.
78. Schneider, U., A. Stipper, and J. Besserer, *Dose-response relationship for lung cancer induction at radiotherapy dose.* Z Med Phys, 2010. **20**(3): p. 206-14.
79. Schneider, U. and B. Kaser-Hotz, *Radiation risk estimates after radiotherapy: application of the organ equivalent dose concept to plateau dose-response relationships.* Radiat Environ Biophys, 2005. **44**(3): p. 235-9.
80. Davis, R.H., *Production and killing of second cancer precursor cells in radiation therapy: in regard to Hall and Wuu (Int J Radiat Oncol Biol Phys 2003;56:83-88).* Int J Radiat Oncol Biol Phys, 2004. **59**(3): p. 916.

81. Thompson, D.E., et al., *Cancer incidence in atomic bomb survivors. Part II: Solid tumors, 1958-1987.* Radiat Res, 1994. **137**(2 Suppl): p. S17-67.
82. Schneider, U., *Mechanistic model of radiation-induced cancer after fractionated radiotherapy using the linear-quadratic formula.* Med Phys, 2009. **36**(4): p. 1138-43.
83. Preston, D.L., et al., *Solid cancer incidence in atomic bomb survivors: 1958-1998.* Radiat Res, 2007. **168**(1): p. 1-64.
84. Cancer, I.A.f.R.o. *EPIC thyroid cancer working group*. 2018 [cited 2018 09.11]; Available from: http://epic.iarc.fr/research/cancerworkinggroups/thyroidcancer.php.
85. Cancer, I.A.f.R.o. *EPIC lung cancer working group*. 2018 [cited 2018 09.11]; Available from: http://epic.iarc.fr/research/cancerworkinggroups/lungcancer.php.
86. Ferrari, A., et al., *FLUKA: A multi-particle transport code (Program version 2005)*. 2005.
87. Battistoni, G., et al., *Overview of the FLUKA code.* Annals of Nuclear Energy, 2015. **82**: p. 10-18.
88. Fjæra, L.F., et al., *Linear energy transfer distributions in the brainstem depending on tumour location in intensity-modulated proton therapy of paediatric cancer.* Acta Oncol, 2017. **56**(6): p. 763-8.
89. Fedorov, A., et al., *3D Slicer as an image computing platform for the quantitative imaging network.* Magn Reson Imaging, 2012. **30**(9): p. 1323-41.
90. sentralbyrå, S. *Døde*. 2018 [cited 2018 18.09]; Available from: https://www.ssb.no/befolkning/statistikker/dode.
91. Kehwar, T.S., *Analytical approach to estimate normal tissue complication probability using best fit of normal tissue tolerance doses into the NTCP equation of the linear quadratic model.* J Cancer Res Ther, 2005. **1**(3): p. 168-79.
92. Cox, J.D., *Fractionation: a paradigm for clinical research in radiation oncology.* Int J Radiat Oncol Biol Phys, 1987. **13**(9): p. 1271-81.
93. Bentzen, S.M., J.Z. Skoczylas, and J. Bernier, *Quantitative clinical radiobiology of early and late lung reactions.* Int J Radiat Biol, 2000. **76**(4): p. 453-62.
94. Nguyen, J., M. Moteabbed, and H. Paganetti, *Assessment of uncertainties in radiation-induced cancer risk predictions at clinically relevant doses.* Med Phys, 2015. **42**(1): p. 81-9.
95. Kry, S.F., et al., *Uncertainty in calculated risk estimates for secondary malignancies after radiotherapy.* Int J Radiat Oncol Biol Phys, 2007. **68**(4): p. 1265-71.
96. Fontenot, J.D., et al., *Estimate of the uncertainties in the relative risk of secondary malignant neoplasms following proton therapy and intensitymodulated photon therapy.* Phys Med Biol, 2010. **55**(23): p. 6987-98.
97. Sigurdson, A.J., et al., *Primary thyroid cancer after a first tumour in childhood (the Childhood Cancer Survivor Study): a nested case-control study.* Lancet, 2005. **365**(9476): p. 2014-23.
98. Gilbert, E.S., et al., *Lung cancer after treatment for Hodgkin's disease: focus on radiation effects.* Radiat Res, 2003. **159**(2): p. 161-73.
99. Schneider, U., A. Lomax, and B. Timmermann, *Second cancers in children treated with modern radiotherapy techniques.* Radiother Oncol, 2008. **89**(2): p. 135-40.

Appendix A

Tables for LAR of radiation-induced secondary lung cancer.

Table A.1: Lung risk coefficient *l* expressed in units of %/Gy per person with a 95% confidence interval (in parenthesis), calculated based on LAR table values (given as LAR per 100 000 persons per 0.1 Gy) and procedures from the BEIR VII report.

Patient index	*1*	*2*	*3*	*4*	*5*	*6*	*7*	*8*	*9*	*10*
Sex	Female	Female	Female	Female	Female	Male	Male	Male	Male	Male
Age at exposure	5	6	7	8	9	8	8	8	11	12
LAR table value	608.0	587.2	566.4	545.6	524.8	234.0	234.0	234.0	208.8	201.6
Risk coefficient, l	9.120 (4.380, 18.989)	8.808 (4.230, 18.339)	8.496 (4.081, 17.689)	8.184 (3.931, 17.040)	7.872 (3.781, 16.390)	3.510 (1.564, 7.875)	3.510 (1.564, 7.875)	3.510 (1.564, 7.875)	3.132 (1.396, 7.027)	3.024 (1.348, 6.785)

Table A.2: OED for the lungs (in Gy(RBE)) for each patient, using the different RBE models and dose-response relationships. The lowest values are highlighted in blue and the highest values are highlighted in red.

Patient index	$RBE_{1.1}$	LWD	MCN_{2Gy}	MCN_{10Gy}	$RØR_{2Gy}$	$RØR_{10Gy}$	WIL
Linear							
1	4.77	4.97	5.99	4.85	5.85	4.82	5.93
2	3.77	4.01	4.96	3.89	4.81	3.86	4.95
3	4.33	4.57	5.52	4.44	5.37	4.40	5.51
4	4.83	5.16	6.32	5.00	6.13	4.95	6.34
5	3.34	3.57	4.39	3.46	4.26	3.43	4.40
6	4.83	5.14	6.27	4.99	6.09	4.94	6.29
7	2.65	2.79	3.41	2.71	3.32	2.69	3.38
8	4.61	4.86	5.89	4.73	5.74	4.69	5.87
9	2.17	2.25	2.76	2.20	2.71	2.19	2.71
10	3.17	3.38	4.22	3.28	4.10	3.25	4.22
Linear-exponential							
1	1.25	1.26	1.37	1.27	1.37	1.27	1.35
2	1.06	1.09	1.21	1.09	1.21	1.09	1.19
3	1.06	1.06	1.15	1.07	1.16	1.07	1.13

4	1.25	1.26	1.36	1.27	1.37	1.27	1.34
5	0.89	0.90	0.98	0.90	0.98	0.90	0.96
6	1.22	1.22	1.30	1.23	1.31	1.23	1.28
7	0.76	0.78	0.87	0.78	0.87	0.78	0.86
8	1.20	1.21	1.32	1.22	1.33	1.22	1.30
9	0.77	0.78	0.89	0.78	0.89	0.78	0.86
10	0.99	1.01	1.13	1.01	1.13	1.01	1.11
Plateau							
1	2.29	2.34	2.66	2.32	2.64	2.32	2.63
2	1.87	1.95	2.27	1.92	2.24	1.91	2.25
3	2.00	2.06	2.34	2.04	2.32	2.03	2.32
4	2.31	2.39	2.74	2.36	2.71	2.35	2.72
5	1.62	1.68	1.93	1.66	1.91	1.65	1.92
6	2.29	2.36	2.68	2.33	2.65	2.33	2.66
7	1.32	1.36	1.58	1.35	1.57	1.34	1.56
8	2.20	2.27	2.58	2.24	2.56	2.23	2.56
9	1.20	1.23	1.44	1.22	1.43	1.21	1.41

10	1.66	1.73	2.03	1.71	2.00	1.70	2.01

Table A.3: LAR of secondary lung cancer (in %) for each patient, using the different RBE models and dose-response relationships. The values in parenthesis are the 95% confidence interval. The lowest LAR values are highlighted in blue and the highest values are highlighted in red.

Patient index	$RBE_{1.1}$	LWD	MCN_{2Gy}	MCN_{10Gy}	$RØR_{2Gy}$	$RØR_{10Gy}$	WIL
Linear							
1	**43.50** (20.89, 90.57)	**45.34** (21.78, 94.41)	**54.66** (26.25, 113.81)	**44.24** (21.25, 92.11)	**53.34** (25.62, 111.07)	**43.92** (21.09, 91.45)	**54.06** (25.96, 112.56)
2	**33.23** (15.96, 69.18)	**35.31** (16.96, 73.52)	**43.65** (20.96, 90.89)	**34.31** (16.48, 71.43)	**42.39** (20.36, 88.26)	**34.00** (16.33, 70.79)	**43.57** (20.93, 90.72)
3	**36.75** (17.65, 76.50)	**38.83** (18.65, 80.84)	**46.87** (22.51, 97.59)	**37.70** (18.11, 78.49)	**45.59** (21.90, 94.93)	**37.38** (17.96, 77.83)	**46.78** (22.47, 97.40)
4	**39.50** (18.97, 82.25)	**42.20** (20.27, 87.86)	**51.70** (24.83, 107.65)	**40.88** (19.64, 85.12)	**50.17** (24.10, 104.47)	**40.50** (19.45, 84.33)	**51.88** (24.92, 108.02)
5	**26.29** (12.63, 54.73)	**28.08** (13.49, 58.47)	**34.52** (16.58, 71.88)	**27.22** (13.07, 56.67)	**33.50** (16.09, 69.74)	**26.96** (12.95, 56.14)	**34.62** (16.63, 72.09)
6	**16.95** (7.55, 38.02)	**18.06** (8.05, 40.52)	**22.00** (9.80, 49.37)	**17.50** (7.80, 39.27)	**21.37** (9.52, 47.94)	**17.34** (7.73, 38.91)	**22.07** (9.83, 49.52)
7	**9.30** (4.14, 20.86)	**9.79** (4.36, 21.95)	**11.96** (5.33, 26.84)	**9.52** (4.24, 21.37)	**11.66** (5.20, 26.16)	**9.45** (4.21, 21.20)	**11.87** (5.29, 26.64)
8	**16.19** (7.21, 36.31)	**17.06** (7.60, 38.29)	**20.69** (9.22, 46.41)	**16.59** (7.39, 37.22)	**20.15** (8.98, 45.20)	**16.46** (7.33, 36.92)	**20.60** (9.18, 46.22)
9	**6.80** (3.03, 15.26)	**7.05** (3.14, 15.83)	**8.64** (3.85, 19.38)	**6.90** (3.07, 15.48)	**8.49** (3.78, 19.04)	**6.86** (3.06, 15.40)	**8.48** (3.78, 19.02)
10	**9.57** (4.27, 21.48)	**10.21** (4.55, 22.92)	**12.77** (5.69, 28.65)	**9.92** (4.42, 22.26)	**12.40** (5.53, 27.83)	**9.83** (4.38, 22.06)	**12.76** (5.69, 28.62)
Linear-exponential							
1	**11.38** (5.47, 23.70)	**11.52** (5.53, 23.99)	**12.47** (5.99, 25.96)	**11.54** (5.54, 24.03)	**12.52** (6.01, 26.07)	**11.55** (5.55, 24.06)	**12.31** (5.91, 25.64)
2	**9.37** (4.50, 19.51)	**9.56** (4.59, 19.91)	**10.64** (5.11, 22.16)	**9.57** (4.60, 19.92)	**10.63** (5.11, 22.14)	**9.56** (4.59, 19.91)	**10.48** (5.03, 21.82)
3	**8.98** (4.31, 18.70)	**9.04** (4.34, 18.81)	**9.76** (4.69, 20.33)	**9.08** (4.36, 18.90)	**9.82** (4.72, 20.45)	**9.09** (4.37, 18.93)	**9.59** (4.61, 19.97)

4	**10.25** (4.92, 21.34)	**10.34** (4.97, 21.54)	**11.17** (5.37, 23.26)	**10.39** (4.99, 21.63)	**11.22** (5.39, 23.36)	**10.40** (4.99, 21.65)	**10.99** (5.28, 22.87)
5	**7.00** (3.36, 14.58)	**7.07** (3.40, 14.73)	**7.69** (3.69, 16.02)	**7.10** (3.41, 14.78)	**7.71** (3.70, 16.06)	**7.10** (3.41, 14.79)	**7.56** (3.63, 15.73)
6	**4.27** (1.90, 9.59)	**4.29** (1.91, 9.63)	**4.56** **(2.03, 10.**24)	**4.31** (1.92, 9.68)	**4.59** (2.05, 10.30)	**4.32** (1.93, 9.69)	**4.49** (2.00, 10.07)
7	**2.68** (1.19, 6.01)	**2.72** (1.21, 6.11)	**3.07** (1.37, 6.88)	**2.72** (1.21, 6.11)	**3.07** (1.37, 6.88)	**2.72** (1.21, 6.11)	**3.01** (1.34, 6.75)
8	**4.22** (1.88, 9.46)	**4.26** (1.90, 9.55)	**4.63** (2.06, 10.38)	**4.27** (1.90, 9.58)	**4.65** (2.07, 10.43)	**4.27** (1.90, 9.59)	**4.55** (2.03, 10.21)
9	**2.40** (1.07, 5.39)	**2.44** (1.09, 5.47)	**2.77** (1.24, 6.22)	**2.43** (1.08, 5.45)	**2.78** (1.24, 6.24)	**2.43** (1.08, 5.46)	**2.71** (1.21, 6.08)
10	**3.00** (1.34, 6.74)	**3.06** (1.37, 6.87)	**3.42** (1.52, 7.67)	**3.06** (1.36, 6.87)	**3.42** (1.52, 7.67)	**3.06** (1.36, 6.86)	**3.36** (1.50, 7.55)
Plateau							
1	**20.85** (10.01, 43.41)	**21.38** (10.27, 44.52)	**24.29** (11.66, 50.57)	**21.17** (10.17, 44.07)	**24.09** (11.57, 50.16)	**21.11** (10.14, 43.96)	**24.01** (11.53, 50.00)
2	**16.50** (7.92, 34.35)	**17.14** (8.23, 35.70)	**19.97** (9.59, 41.59)	**16.93** (8.13, 35.25)	**19.72** (9.47, 41.06)	**16.86** (8.10, 35.10)	**19.81** (9.51, 41.24)
3	**17.03** (8.18, 35.46)	**17.52** (8.41, 36.47)	**19.86** (9.54, 41.36)	**17.33** (8.33, 36.09)	**19.69** (9.46, 41.01)	**17.28** (8.30, 35.99)	**19.67** (9.45, 40.96)
4	**18.90** (9.08, 39.36)	**19.58** (9.40, 40.76)	**22.40** (10.76, 46.65)	**19.34** (9.29, 40.28)	**22.16** (10.64, 46.14)	**19.27** (9.26, 40.12)	**22.25** (10.69, 46.32)
5	**12.77** (6.13, 26.58)	**13.23** (6.36, 27.55)	**15.20** (7.30, 31.64)	**13.07** (6.28, 27.21)	**15.02** (7.22, 31.28)	**13.02** (6.25, 27.11)	**15.08** (7.24, 31.40)
6	**8.02** (3.58, 18.00)	**8.28** (3.69, 18.59)	**9.39** (4.18, 21.07)	**8.19** (3.65, 18.37)	**9.30** (4.14, 20.86)	**8.16** (3.64, 18.31)	**9.32** (4.15, 20.92)
7	**4.64** (2.07, 10.42)	**4.79** (2.13, 10.74)	**5.56** (2.48, 12.48)	**4.73** (2.11, 10.62)	**5.51** (2.45, 12.36)	**4.72** (2.10, 10.59)	**5.49** (2.44, 12.31)
8	**7.73** (3.44, 17.34)	**7.95** (3.54, 17.84)	**9.07** (4.04, 20.34)	**7.87** (3.50, 17.65)	**8.99** (4.01, 20.17)	**7.84** (3.50, 17.60)	**8.97** (4.00, 20.13)
9	**3.77** (1.68, 8.45)	**3.85** (1.72, 8.63)	**4.50** (2.01, 10.10)	**3.81** (1.70, 8.55)	**4.48** (2.00, 10.05)	**3.80** (1.70, 8.54)	**4.41** (1.96, 9.88)

10	**5.02** (2.24, 11.27)	**5.22** (2.33, 11.72)	**6.13** (2.73, 13.76)	**5.16** (2.30, 11.57)	**6.05** (2.70, 13.58)	**5.13** (2.29, 11.52)	**6.08** (2.71, 13.63)

Table A.4: The median LAR values (in %) of radiation-induced secondary lung cancer for the whole patient cohort with respects to each RBE model and each dose-response relationship with the range (min and max LAR value) in parenthesis.

RBE model	***Dose-response relationship***		
	Linear	Linear-exponential	Plateau
$RBE_{1.1}$	**21.62** (6.80, 43.50)	**5.64** (2.40, 11.38)	**10.40** (3.77, 20.85)
LWD	**23.07** (7.05, 45.34)	**5.68** (2.44, 11.52)	**10.76** (3.85, 21.38)
MCN_{2Gy}	**28.26** (8.64, 54.66)	**6.16** (2.77, 12.47)	**12.29** (4.50, 24.29)
MCN_{10Gy}	**22.36** (6.90, 44.24)	**5.71** (2.43, 11.54)	**10.63** (3.81, 21.17)
$RØR_{2Gy}$	**27.43** (8.49, 53.34)	**6.18** (2.78, 12.52)	**12.16** (4.48, 24.09)
$RØR_{10Gy}$	**22.15** (6.86, 43.92)	**5.71** (2.43, 11.55)	**10.59** (3.80, 21.11)
WIL	**28.35** (8.48, 54.06)	**6.05** (2.71, 12.31)	**12.20** (4.41, 24.01)

Table A.5: Median increase in LAR of secondary lung cancer with the variable RBE models relative to $RBE_{1.1}$ with the range (min and max relative increase in LAR) in parenthesis.

RBE model	***Dose-response relationship***		
	Linear	Linear-exponential	Plateau
LWD	**1.06** (1.04, 1.07)	**1.01** (1.00, 1.02)	**1.03** (1.02, 1.04)
MCN_{2Gy}	**1.30** (1.26, 1.33)	**1.10** (1.07, 1.15)	**1.19** (1.16, 1.22)
MCN_{10Gy}	**1.03** (1.01, 1.04)	**1.01** (1.01, 1.02)	**1.02** (1.01, 1.03)
$RØR_{2Gy}$	**1.26** (1.23, 1.30)	**1.10** (1.07, 1.16)	**1.18** (1.16, 1.21)
$RØR_{10Gy}$	**1.02** (1.01, 1.03)	**1.01** (1.01, 1.02)	**1.02** (1.01, 1.02)
WIL	**1.29** (1.24, 1.33)	**1.08** (1.05, 1.13)	**1.18** (1.15, 1.21)

Appendix B

Tables for LAR of radiation-induced secondary thyroid cancer.

Table B.1: Thyroid risk coefficient *r* expressed in units of %/Gy per person with a 95% confidence interval (in parenthesis), calculated based on LAR table values (given as LAR per 100 000 persons per 0.1 Gy) and procedures from the BEIR VII report.

Patient index	*1*	*2*	*3*	*4*	*5*	*6*	*7*	*8*	*9*	*10*
Sex	Female	Female	Female	Female	Female	Male	Male	Male	Male	Male
Age at exposure	5	6	7	8	9	8	8	8	11	12
LAR table value	419.0	390.2	361.4	332.6	303.8	60.40	60.40	60.40	46.60	43.20
Risk coefficient, l	6.285 (1.663, 23.748)	5.853 (1.549, 22.116)	5.421 (1.435, 20.483)	4.989 (1.320, 18.851)	4.557 (1.206, 17.219)	0.906 (0.240, 3.423)	0.906 (0.240, 3.423)	0.906 (0.240, 3.423)	0.699 (0.185, 2.641)	0.648 (0.171, 2.448)

Table B.2: OED for the thyroid (in [Gy(RBE)]) for each patient, using the different RBE models and dose-response relationships. The lowest values are highlighted in blue and the highest values are highlighted in red.

Patient index	$RBE_{1.1}$	LWD	MCN_{2Gy}	MCN_{10Gy}	$RØR_{2Gy}$	$RØR_{10Gy}$	WIL
Linear							
1	4.56	5.00	6.58	4.83	6.39	4.78	6.63
2	8.44	9.07	11.26	8.78	10.94	8.70	11.37
3	1.24	1.40	1.99	1.35	1.92	1.33	1.99
4	2.00	2.20	3.05	2.13	2.97	2.11	3.04
5	6.08	6.60	8.45	6.39	8.19	6.33	8.53
6	1.24	1.43	2.17	1.38	2.08	1.36	2.18
7	5.81	6.25	7.94	6.06	7.73	6.01	7.96
8	3.24	3.51	4.79	3.42	4.68	3.39	4.75
9	3.30	3.62	4.95	3.51	4.81	3.48	4.95
10	6.53	6.99	8.82	6.79	8.58	6.73	8.84
Linear-exponential							
1	3.62	3.86	4.80	3.78	4.71	3.75	4.78
2	6.06	6.34	7.32	6.22	7.22	6.19	7.33
3	1.07	1.18	1.62	1.15	1.58	1.14	1.59

4	1.73	1.86	2.47	1.82	2.42	1.81	2.43
5	4.57	4.84	5.81	4.74	5.70	4.71	5.81
6	1.12	1.27	1.84	1.23	1.77	1.21	1.83
7	4.43	4.65	5.57	4.56	5.49	4.54	5.53
8	2.83	3.01	3.92	2.95	3.85	2.93	3.87
9	2.80	3.01	3.91	2.94	3.83	2.92	3.88
10	4.97	5.19	6.14	5.10	6.05	5.07	6.11
Plateau							
1	1.26	1.28	1.35	1.27	1.35	1.27	1.35
2	1.42	1.43	1.44	1.42	1.44	1.42	1.44
3	0.61	0.64	0.80	0.63	0.79	0.63	0.78
4	0.87	0.90	1.04	0.89	1.03	0.89	1.02
5	1.31	1.33	1.38	1.32	1.38	1.32	1.38
6	0.63	0.67	0.84	0.66	0.83	0.66	0.83
7	1.34	1.35	1.40	1.35	1.40	1.35	1.39
8	1.21	1.24	1.33	1.23	1.33	1.23	1.32
9	1.17	1.19	1.30	1.18	1.29	1.18	1.29

10	1.38	1.39	1.42	1.39	1.42	1.39	1.42

Table B.3: Lifetime attributable risk of secondary thyroid cancer (in %) for each patient, using the different RBE models and dose-response relationships. The values in parenthesis are the 95% confidence interval. The lowest LAR values are highlighted in blue and the highest values are highlighted in red.

Patient index	$RBE_{1.1}$	LWD	MCN_{2Gy}	MCN_{10Gy}	$RØR_{2Gy}$	$RØR_{10Gy}$	WIL
Linear							
1	**28.64** (7.58, 108.23)	**31.40** (8.31, 118.66)	**41.37** (10.95, 156.31)	**30.38** (8.04, 114.78)	**40.13** (10.62, 151.64)	**30.07** (7.96, 113.62)	**41.69** (11.03, 157.54)
2	**49.39** (13.07, 186.63)	**53.09** (14.05, 200.59)	**65.93** (17.45, 249.12)	**51.41** (13.61, 194.28)	**64.04** (16.95, 241.98)	**50.95** (13.48, 192.52)	**66.54** (17.61, 251.42)
3	**6.74** (1.78, 25.46)	**7.57** (2.00, 28.60)	**10.79** (2.86, 40.77)	**7.31** (1.94, 27.63)	**10.43** (2.76, 39.42)	**7.23** (1.91, 27.30)	**10.77** (2.85, 40.70)
4	**9.96** (2.63, 37.62)	**10.99** (2.91, 41.52)	**15.20** (4.02, 57.45)	**10.65** (2.82, 40.22)	**14.79** (3.91, 55.90)	**10.55** (2.79, 39.85)	**15.16** (4.01, 57.28)
5	**27.70** (7.33, 104.65)	**30.08** (7.96, 113.65)	**38.51** (10.19, 145.53)	**29.12** (7.71, 110.02)	**37.34** (9.88, 141.10)	**28.83** (7.63, 108.92)	**38.87** (10.29, 146.89)
6	**1.12** (0.30, 4.24)	**1.29** (0.34, 4.89)	**1.97** (0.52, 7.44)	**1.25** (0.33, 4.73)	**1.88** (0.50, 7.11)	**1.23** (0.33, 4.65)	**1.97** (0.52, 7.46)
7	**5.26** (1.39, 19.89)	**5.66** (1.50, 21.38)	**7.19** (1.91, 27.18)	**5.49** (1.45, 20.74)	**7.00** (1.85, 26.45)	**5.44** (1.44, 20.56)	**7.21** (1.91, 27.26)
8	**2.94** (0.78, 11.09)	**3.18** (0.84, 12.01)	**4.34** (1.15, 16.41)	**3.10** (0.82, 11.70)	**4.24** (1.12, 16.01)	**3.07** (0.81, 11.61)	**4.30** (1.14, 16.26)
9	**2.30** (0.61, 8.71)	**2.53** (0.67, 9.56)	**3.46** (0.92, 13.08)	**2.46** (0.65, 9.28)	**3.36** (0.89, 12.71)	**2.43** (0.64, 9.19)	**3.46** (0.92, 13.08)
10	**4.23** (1.12, 15.98)	**4.53** (1.20, 17.11)	**5.71** (1.51, 21.58)	**4.40** (1.16, 16.61)	**5.56** (1.47, 20.99)	**4.36** (1.15, 16.47)	**5.73** (1.51, 21.65)
Linear-exponential							
1	**22.75** (6.02, 85.96)	**24.27** (6.42, 91.69)	**30.15** (7.98, 113.92)	**23.74** (6.28, 89.70)	**29.62** (7.84, 111.90)	**23.58** (6.24, 89.11)	**30.03** (7.95, 113.46)
2	**35.47** (9.39, 134.04)	**37.11** (9.82, 140.23)	**42.86** (11.34, 161.96)	**36.41** (9.63, 137.56)	**42.23** (11.18, 159.57)	**36.21** (9.58, 136.84)	**42.90** (11.35, 162.10)
3	**5.82** (1.54, 22.01)	**6.37** (1.69, 24.07)	**8.78** (2.32, 33.16)	**6.22** (1.65, 23.50)	**8.57** (2.27, 32.40)	**6.17** (1.63, 23.30)	**8.62** (2.28, 32.57)

4	**8.64** (2.29, 32.66)	**9.30** (2.46, 35.13)	**12.30** (3.25, 46.48)	**9.09** (2.41, 34.35)	**12.09** (3.20, 45.69)	**9.03** (2.39, 34.13)	**12.11** (3.20, 45.74)
5	**20.82** (5.51, 78.69)	**22.04** (5.83, 83.30)	**26.46** (7.00, 99.99)	**21.59** (5.71, 81.57)	**26.00** (6.88, 98.23)	**21.45** (5.68, 81.05)	**26.46** (7.00, 99.98)
6	**1.01** (0.27, 3.82)	**1.15** (0.30, 4.33)	**1.67** (0.44, 6.29)	**1.11** (0.30, 4.21)	**1.61** (0.43, 6.07)	**1.10** (0.29, 4.15)	**1.65** (0.44, 6.25)
7	**4.01** (1.06, 15.16)	**4.21** (1.12, 15.91)	**5.04** (1.34, 19.05)	**4.13** (1.09, 15.60)	**4.97** (1.32, 18.78)	**4.11** (1.09, 15.52)	**5.01** (1.33, 18.94)
8	**2.56** (0.68, 9.67)	**2.73** (0.72, 10.32)	**3.55** (0.94, 13.42)	**2.67** (0.71, 10.10)	**3.49** (0.92, 13.18)	**2.66** (0.70, 10.05)	**3.51** (0.93, 13.25)
9	**1.95** (0.52, 7.39)	**2.10** (0.56, 7.95)	**2.73** (0.72, 10.32)	**2.06** (0.54, 7.77)	**2.68** (0.71, 10.12)	**2.04** (0.54, 7.71)	**2.71** (0.72, 10.25)
10	**3.22** (0.85, 12.17)	**3.37** (0.89, 12.72)	**3.98** (1.05, 15.02)	**3.30** (0.87, 12.48)	**3.92** (1.03, 14.80)	**3.29** (0.87, 12.41)	**3.96** (1.04, 14.95)
Plateau							
1	**7.95** (2.10, 30.03)	**8.05** (2.13, 30.41)	**8.51** (2.25, 32.15)	**8.01** (2.12, 30.27)	**8.50** (2.25, 32.11)	**8.01** (2.12, 30.25)	**8.46** (2.24, 31.98)
2	**8.33** (2.20, 31.47)	**8.35** (2.21, 31.54)	**8.43** (2.23, 31.85)	**8.34** (2.21, 31.51)	**8.43** (2.23, 31.84)	**8.34** (2.21, 31.51)	**8.42** (2.23, 31.83)
3	**3.29** (0.87, 12.43)	**3.46** (0.91, 13.06)	**4.33** (1.15, 16.36)	**3.41** (0.90, 12.90)	**4.28** (1.13, 16.17)	**3.40** (0.90, 12.85)	**4.24** (1.12, 16.00)
4	**4.36** (1.15, 16.46)	**4.47** (1.18, 16.90)	**5.18** (1.37, 19.56)	**4.43** (1.17, 16.76)	**5.16** (1.36, 19.49)	**4.43** (1.17, 16.73)	**5.09** (1.35, 19.22)
5	**5.98** (1.58, 22.58)	**6.04** (1.60, 22.83)	**6.30** (1.67, 23.81)	**6.02** (1.59, 22.76)	**6.29** (1.66, 23.77)	**6.02** (1.59, 22.74)	**6.28** (1.66, 23.74)
6	**0.57** (0.15, 2.14)	**0.61** (0.16, 2.29)	**0.76** (0.20, 2.88)	**0.60** (0.16, 2.26)	**0.75** (0.20, 2.83)	**0.59** (0.16, 2.24)	**0.75** (0.20, 2.84)
7	**1.21** (0.32, 4.59)	**1.22** (0.32, 4.62)	**1.27** (0.34, 4.78)	**1.22** (0.32, 4.61)	**1.26** (0.34, 4.78)	**1.22** (0.32, 4.60)	**1.26** (0.33, 4.76)
8	**1.10** (0.29, 4.16)	**1.12** (0.30, 4.23)	**1.21** (0.32, 4.56)	**1.11** (0.29, 4.20)	**1.20** (0.32, 4.55)	**1.11** (0.29, 4.20)	**1.20** (0.32, 4.53)
9	**0.82** (0.22, 3.08)	**0.83** (0.22, 3.15)	**0.91** (0.24, 3.43)	**0.83** (0.22, 3.13)	**0.90** (0.24, 3.42)	**0.83** (0.22, 3.12)	**0.90** (0.24, 3.40)

10	**0.90** (0.24, 3.39)	**0.90** (0.24, 3.40)	**0.92** (0.24, 3.47)	**0.90** (0.24, 3.39)	**0.92** (0.24, 3.47)	**0.90** (0.24, 3.39)	**0.92** (0.24, 3.46)

Table B.4: The median LAR values (in %) of radiation-induced secondary thyroid cancer for the whole patient cohort with respects to each RBE model and each dose-response relationship with the range (min and max LAR value) in parenthesis.

RBE model	***Dose-response relationship***		
	Linear	Linear-exponential	Plateau
$RBE_{1.1}$	**6.00** (1.12, 49.39)	**4.92** (1.01, 35.47)	**2.25** (0.57, 8.33)
LWD	**6.61** (1.29, 53.09)	**5.29** (1.15, 37.11)	**2.34** (0.61, 8.35)
MCN_{2Gy}	**8.99** (1.97, 65.93)	**6.91** (1.67, 42.86)	**2.80** (0.76, 8.51)
MCN_{10Gy}	**6.40** (1.25, 51.41)	**5.17** (1.11, 36.41)	**2.32** (0.60, 8.34)
$RØR_{2Gy}$	**8.72** (1.88, 64.04)	**6.77** (1.61, 42.23)	**2.77** (0.75, 8.50)
$RØR_{10Gy}$	**6.33** (1.23, 50.95)	**5.14** (1.10, 36.21)	**2.31** (0.59, 8.34)
WIL	**8.99** (1.97, 66.54)	**6.82** (1.65, 42.90)	**2.75** (0.75, 8.46)

Table B.5: Median increase in LAR of secondary thyroid cancer with the variable RBE models relative to $RBE_{1.1}$ with the range (min and max relative increase in LAR) in parenthesis.

RBE model	***Dose-response relationship***		
	Linear	Linear-exponential	Plateau
LWD	**1.10** (1.07, 1.15)	**1.07** (1.05, 1.13)	**1.02** (1.00, 1.07)
MCN_{2Gy}	**1.46** (1.33, 1.76)	**1.36** (1.21, 1.65)	**1.09** (1.01, 1.35)
MCN_{10Gy}	**1.06** (1.04, 1.12)	**1.04** (1.03, 1.10)	**1.01** (1.00, 1.05)
$RØR_{2Gy}$	**1.42** (1.30, 1.68)	**1.33** (1.19, 1.59)	**1.08** (1.01, 1.32)
$RØR_{10Gy}$	**1.05** (1.03, 1.10)	**1.04** (1.02, 1.09)	**1.01** (1.00, 1.05)
WIL	**1.47** (1.35, 1.76)	**1.35** (1.21, 1.64)	**1.08** (1.01, 1.32)

Appendix C

Tables for EAR of radiation-induced secondary lung cancer.

Table C.1: Risk coefficient for radiation-induced lung cancer expressed in units of (10000 PY Gy)$^{-1}$ including a 90% confidence interval (in parenthesis), calculated with equation (5.4), based on patient data and table values from Table 5.3.

Patient index	*1*	*2*	*3*	*4*	*5*	*6*	*7*	*8*	*9*	*10*
Sex	Female	Female	Female	Female	Female	Male	Male	Male	Male	Male
Age at exposure (agex)	5	6	7	8	9	8	8	8	11	12
Risk coefficient, r	20.272 (14.257, 26.732)	20.312 (14.286, 26.785)	20.353 (14.314, 26.839)	20.394 (14.343. 26.893)	20.434 (14.371, 26.947)	11.337 (4.346, 20.785)	11.337 (4.346, 20.785)	11.337 (4.346, 20.785)	11.406 (4.372, 20.910)	11.428 (4.381, 20.952)

Table C.2: OED for the lungs (in Gy(RBE)) for each patient, using the different RBE models and dose-response relationships. The lowest values are highlighted in blue and the highest values are highlighted in red.

Patient index	$RBE_{1.1}$	LWD	MCN_{2Gy}	MCN_{10Gy}	$RØR_{2Gy}$	$RØR_{10Gy}$	WIL
Linear							
1	4.77	4.97	5.99	4.85	5.85	4.82	5.93
2	3.77	4.01	4.96	3.89	4.81	3.86	4.95
3	4.33	4.57	5.52	4.44	5.37	4.40	5.51
4	4.83	5.16	6.32	5.00	6.13	4.95	6.34
5	3.34	3.57	4.39	3.46	4.26	3.43	4.40
6	4.83	5.14	6.27	4.99	6.09	4.94	6.29
7	2.65	2.79	3.41	2.71	3.32	2.69	3.38
8	4.61	4.86	5.89	4.73	5.74	4.69	5.87
9	2.17	2.25	2.76	2.20	2.71	2.19	2.71
10	3.17	3.38	4.22	3.28	4.10	3.25	4.22
Bell-shaped							
1	3.22	3.31	3.77	3.27	3.74	3.26	3.73
2	2.61	2.72	3.18	2.68	3.14	2.67	3.16
3	2.85	2.94	3.33	2.90	3.30	2.89	3.30

4	3.27	3.40	3.90	3.35	3.86	3.34	3.88
5	2.29	2.39	2.75	2.35	2.72	2.34	2.73
6	3.26	3.38	3.84	3.33	3.80	3.32	3.82
7	1.83	1.89	2.19	1.87	2.17	1.86	2.17
8	3.10	3.20	3.65	3.16	3.62	3.15	3.62
9	1.61	1.65	1.93	1.63	1.92	1.62	1.89
10	2.28	2.39	2.82	2.35	2.78	2.34	2.80
Plateau							
1	3.07	3.15	3.60	3.12	3.57	3.11	3.56
2	2.49	2.60	3.04	2.56	3.00	2.55	3.02
3	2.71	2.80	3.18	2.76	3.15	2.75	3.15
4	3.11	3.23	3.72	3.19	3.68	3.17	3.70
5	2.18	2.27	2.62	2.24	2.59	2.23	2.61
6	3.10	3.21	3.66	3.17	3.62	3.15	3.64
7	1.75	1.81	2.10	1.78	2.08	1.78	2.07
8	2.96	3.05	3.49	3.01	3.46	3.00	3.46
9	1.54	1.58	1.85	1.56	1.84	1.56	1.81

10	2.18	2.28	2.70	2.24	2.66	2.23	2.68
Full model							
1	2.98	3.06	3.52	3.02	3.48	3.01	3.48
2	2.41	2.52	2.97	2.48	2.92	2.47	2.95
3	2.64	2.73	3.12	2.69	3.08	2.68	3.09
4	3.02	3.14	3.64	3.09	3.59	3.08	3.62
5	2.11	2.20	2.56	2.17	2.52	2.16	2.55
6	3.00	3.12	3.58	3.07	3.54	3.06	3.56
7	1.70	1.76	2.05	1.73	2.03	1.72	2.03
8	2.87	2.97	3.42	2.92	3.38	2.91	3.38
9	1.49	1.53	1.80	1.51	1.79	1.51	1.77
10	2.11	2.21	2.62	2.17	2.58	2.16	2.60

Table C.3: Excess absolute risk of secondary lung cancer (per 10000 PY) for each patient, using the different RBE models and dose-response relationships. The values in parenthesis are the 90% confidence interval. The lowest EAR values are highlighted in blue and the highest values are highlighted in red.

Patient index	$RBE_{1.1}$	LWD	MCN_{2Gy}	MCN_{10Gy}	$RØR_{2Gy}$	$RØR_{10Gy}$	WIL
Linear							
1	**96.69** (68.00, 127.50)	**100.79** (70.89, 132.91)	**121.50** (85.45, 160.22)	**98.34** (69.16, 129.67)	**118.58** (83.39, 156.36)	**97.63** (68.66, 128.75)	**120.16** (84.51, 158.45)
2	**76.62** (53.89, 101.04)	**81.43** (57.28, 107.39)	**100.66** (70.80, 132.74)	**79.11** (55.64, 104.32)	**97.76** (68.76, 128.91)	**78.40** (55.14, 103.39)	**100.48** (70.67, 132.50)
3	**88.03** (61.91, 116.08)	**93.01** (65.41, 122.65)	**112.29** (78.97, 148.07)	**90.31** (63.52, 119.09)	**109.22** (76.82, 144.03)	**89.55** (62.98, 118.08)	**112.07** (78.82, 147.79)
4	**98.44** (69.23, 129.81)	**105.15** (73.95, 138.66)	**128.84** (90.61, 169.90)	**101.88** (71.65, 134.35)	**125.03** (87.93, 164.87)	**100.93** (70.98, 133.09)	**129.28** (90.92, 170.48)
5	**68.24** (47.99, 89.99)	**72.89** (51.27, 96.13)	**89.61** (63.02, 118.17)	**70.65** (49.69, 93.17)	**86.95** (61.15, 114.67)	**69.99** (49.22, 92.29)	**89.88** (63.21, 118.52)
6	**54.74** (20.98, 100.35)	**58.33** (22.36, 106.94)	**71.07** (27.25, 130.30)	**56.53** (21.67, 103.64)	**69.02** (26.46, 126.53)	**56.01** (21.47, 102.70)	**71.28** (27.33, 130.69)
7	**30.03** (11.51, 55.05)	**31.61** (12.12, 57.94)	**38.64** (14.81, 70.85)	**30.76** (11.79, 56.40)	**37.67** (14.44, 69.06)	**30.53** (11.70, 55.96)	**38.35** (14.70, 70.31)
8	**52.28** (20.04, 95.85)	**55.12** (21.13, 101.05)	**66.82** (25.62, 122.51)	**53.58** (20.54, 98.24)	**65.07** (24.94, 119.30)	**53.15** (20.38, 97.45)	**66.54** (25.51, 121.99)
9	**24.77** (9.49, 45.41)	**25.69** (9.85, 47.09)	**31.46** (12.06, 57.67)	**25.12** (9.63, 46.05)	**30.90** (11.85, 56.66)	**25.00** (9.58, 45.83)	**30.87** (11.83, 56.59)
10	**36.18** (13.87, 66.32)	**38.60** (14.80, 70.77)	**48.25** (18.50, 88.47)	**37.49** (14.37, 68.73)	**46.87** (17.97, 85.94)	**37.15** (14.24, 68.12)	**48.21** (18.48, 88.38)
Bell-shaped							
1	**65.37** (45.98, 86.21)	**67.12** (47.20, 88.51)	**76.49** (53.80, 100.87)	**66.36** (46.67, 87.50)	**75.89** (53.37, 100.08)	**66.17** (46.54, 87.26)	**75.67** (53.22, 99.78)
2	**53.07** (37.33, 69.98)	**55.31** (38.90, 72.94)	**64.67** (45.48, 85.28)	**54.51** (38.34, 71.88)	**63.84** (44.90, 84.18)	**54.26** (38.16, 71.55)	**64.23** (45.17, 84.69)
3	**58.04** (40.82, 76.53)	**59.78** (42.04, 78.83)	**67.69** (47.60, 89.26)	**59.08** (41.55, 77.91)	**67.18** (47.25, 88.59)	**58.90** (41.43, 77.67)	**67.08** (47.18, 88.46)

4	**66.69** (46.90, 87.95)	**69.30** (48.74, 91.39)	**79.56** (55.96, 104.92)	**68.35** (48.07, 90.13)	**78.71** (55.36, 103.80)	**68.06** (47.87, 89.75)	**79.06** (55.60, 104.25)
5	**46.86** (32.96, 61.80)	**48.75** (34.29, 64.29)	**56.18** (39.51, 74.09)	**48.06** (33.80, 63.37)	**55.53** (39.05, 73.23)	**47.84** (33.64, 63.09)	**55.81** (39.25, 73.60)
6	**36.93** (14.16, 67.71)	**38.27** (14.67, 70.16)	**43.55** (16.69, 79.84)	**37.76** (14.47, 69.22)	**43.14** (16.54, 79.08)	**37.61** (14.42, 68.95)	**43.26** (16.58, 79.30)
7	**20.76** (7.96, 38.07)	**21.43** (8.22, 39.29)	**24.87** (9.53, 45.59)	**21.16** (8.11, 38.80)	**24.64** (9.45, 45.18)	**21.10** (8.09, 38.68)	**24.55** (9.41, 45.01)
8	**35.19** (13.49, 64.52)	**36.27** (13.91, 66.51)	**41.40** (15.87, 75.90)	**35.84** (13.74, 65.70)	**41.07** (15.74, 75.29)	**35.72** (13.69, 65.50)	**41.00** (15.72, 75.16)
9	**18.36** (7.04, 33.66)	**18.79** (7.20, 34.44)	**22.03** (8.45, 40.39)	**18.56** (7.12, 34.03)	**21.91** (8.40, 40.17)	**18.53** (7.10, 33.98)	**21.57** (8.27, 39.54)
10	**26.10** (10.00, 47.85)	**27.28** (10.46, 50.01)	**32.27** (12.37, 59.17)	**26.85** (10.29, 49.23)	**31.82** (12.20, 58.35)	**26.72** (10.24, 48.98)	**32.02** (12.27, 58.70)
Plateau							
1	**62.25** (43.78, 82.09)	**63.94** (44.97, 84.32)	**73.05** (51.37, 96.33)	**63.20** (44.44, 83.33)	**72.40** (50.92, 95.47)	**63.01** (44.32, 83.09)	**72.25** (50.81, 95.27)
2	**50.59** (35.58, 66.71)	**52.73** (37.09, 69.53)	**61.79** (43.46, 81.47)	**51.96** (36.55, 68.52)	**60.93** (42.86, 80.35)	**51.72** (36.37, 68.20)	**61.36** (43.15, 80.91)
3	**55.22** (38.83, 72.81)	**56.92** (40.03, 75.06)	**64.72** (45.52, 85.35)	**56.23** (39.54, 74.14)	**64.14** (45.11, 84.58)	**56.04** (39.41, 73.90)	**64.17** (45.13, 84.61)
4	**63.45** (44.62, 83.67)	**65.97** (46.39, 86.99)	**75.96** (53.42, 100.17)	**65.03** (45.74, 85.76)	**75.05** (52.78, 98.97)	**64.75** (45.54, 85.38)	**75.51** (53.11, 99.58)
5	**44.58** (31.35, 58.78)	**46.38** (32.62, 61.17)	**53.58** (37.68, 70.66)	**45.71** (32.15, 60.28)	**52.91** (37.21, 69.77)	**45.50** (32.00, 60.00)	**53.25** (37.45, 70.22)
6	**35.11** (13.46, 64.37)	**36.39** (13.95, 66.72)	**41.54** (15.92, 76.15)	**35.89** (13.76, 65.81)	**41.09** (15.75, 75.33)	**35.75** (13.70, 65.54)	**41.28** (15.82, 75.68)
7	**19.82** (7.60, 36.33)	**20.46** (7.84, 37.52)	**23.82** (9.13, 43.67)	**20.20** (7.74, 37.04)	**23.57** (9.04, 43.22)	**20.13** (7.72, 36.91)	**23.52** (9.02, 43.12)
8	**33.51** (12.85, 61.43)	**34.56** (13.25, 63.37)	**39.57** (15.17, 72.56)	**34.13** (13.08, 62.57)	**39.21** (15.03, 71.88)	**34.02** (13.04, 62.37)	**39.20** (15.03, 71.86)
9	**17.59** (6.74, 32.25)	**18.00** (6.90, 33.01)	**21.13** (8.10, 38.74)	**17.79** (6.82, 32.61)	**21.01** (8.05, 38.52)	**17.76** (6.81, 32.56)	**20.69** (7.93, 37.94)

10	**24.91** (9.55, 45.68)	**26.03** (9.98, 47.73)	**30.83** (11.82, 56.52)	**25.63** (9.83, 46.99)	**30.38** (11.65, 55.70)	**25.50** (9.78, 46.76)	**30.59** (11.73, 56.08)
Full model							
1	**60.39** (42.47, 79.63)	**62.12** (43.69, 81.91)	**71.31** (50.15, 94.03)	**61.32** (43.12, 80.86)	**70.57** (49.63, 93.06)	**61.11** (42.98, 80.59)	**70.52** (49.60, 92.99)
2	**49.03** (34.48, 64.65)	**51.19** (36.01, 67.51)	**60.27** (42.39, 79.48)	**50.38** (35.44, 66.44)	**59.36** (41.75, 78.27)	**50.12** (35.25, 66.10)	**59.88** (42.11, 78.96)
3	**53.68** (37.75, 70.78)	**55.47** (39.01, 73.15)	**63.45** (44.62, 83.67)	**54.70** (38.47, 72.13)	**62.76** (44.14, 82.76)	**54.49** (38.32, 71.86)	**62.94** (44.27, 83.00)
4	**61.52** (43.27, 81.13)	**64.12** (45.10, 84.56)	**74.26** (52.23, 97.92)	**63.11** (44.39, 83.22)	**73.25** (51.51, 96.59)	**62.81** (44.17, 82.82)	**73.88** (51.96, 97.43)
5	**43.16** (30.35, 56.92)	**45.02** (31.66, 59.37)	**52.33** (36.80, 69.01)	**44.30** (31.16, 58.42)	**51.58** (36.28, 68.02)	**44.08** (31.00, 58.13)	**52.04** (36.60, 68.63)
6	**34.02** (13.04, 62.37)	**35.36** (13.55, 64.82)	**40.60** (15.57, 74.44)	**34.81** (13.35, 63.83)	**40.09** (15.37, 73.51)	**34.66** (13.29, 63.54)	**40.39** (15.48, 74.04)
7	**19.23** (7.37, 35.26)	**19.90** (7.63, 36.48)	**23.28** (8.92, 42.67)	**19.62** (7.52, 35.97)	**23.00** (8.82, 42.17)	**19.54** (7.49, 35.83)	**22.99** (8.81, 42.15)
8	**32.54** (12.47, 59.65)	**33.63** (12.89, 61.66)	**38.72** (14.84, 70.98)	**33.16** (12.71, 60.79)	**38.29** (14.68, 70.21)	**33.04** (12.66, 60.57)	**38.36** (14.71, 70.34)
9	**17.03** (6.53, 31.22)	**17.45** (6.69, 31.99)	**20.56** (7.88, 37.70)	**17.23** (6.60, 31.58)	**20.42** (7.83, 37.44)	**17.19** (6.59, 31.52)	**20.14** (7.72, 36.91)
10	**24.08** (9.23, 44.15)	**25.20** (9.66, 46.21)	**29.98** (11.49, 54.96)	**24.79** (9.50, 45.44)	**29.51** (11.31, 54.10)	**24.65** (9.45, 45.20)	**29.76** (11.41, 54.56)

Table C.4: The median EAR values (per 10000 PY) of radiation-induced secondary lung cancer for the whole patient cohort with respects to each RBE model and each dose-response relationship with the range (min and max EAR value) in parenthesis.

RBE model	***Dose-response relationship***			
	Linear	Bell-shaped	Plateau	Full model
$RBE_{1.1}$	**61.49** (24.77, 98.44)	**41.90** (18.36, 66.69)	**39.84** (17.59, 63.45)	**38.59** (17.03, 61.52)
LWD	**65.61** (25.69, 105.15)	**43.51** (18.79, 69.30)	**41.39** (18.00, 65.97)	**40.19** (17.45, 64.12)
MCN_{2Gy}	**80.34** (31.46, 128.84)	**49.87** (22.03, 79.56)	**47.56** (21.13, 75.96)	**46.47** (20.56, 74.26)
MCN_{10Gy}	**63.59** (25.12, 101.88)	**42.91** (18.56, 68.35)	**40.80** (17.79, 65.03)	**39.56** (17.23, 63.11)
$RØR_{2Gy}$	**77.98** (30.90, 125.03)	**49.33** (21.91, 78.71)	**47.00** (21.01, 75.05)	**45.84** (20.42, 73.25)
$RØR_{10Gy}$	**63.00** (25.00, 100.93)	**42.72** (18.53, 68.06)	**40.63** (17.76, 64.75)	**39.37** (17.19, 62.81)
WIL	**80.58** (30.87, 129.28)	**49.53** (21.57, 79.06)	**47.26** (20.69, 75.51)	**46.21** (20.14, 73.88)

Table C.5: Median increase in EAR of secondary lung cancer with the variable RBE models relative to $RBE_{1.1}$ with the range (min and max relative increase in EAR) in parenthesis.

RBE model	***Dose-response relationship***			
	Linear	Bell-shaped	Plateau	Full model
LWD	**1.06** (1.04, 1.07)	**1.04** (1.02, 1.05)	**1.04** (1.02, 1.04)	**1.04** (1.02, 1.05)
MCN_{2Gy}	**1.30** (1.26, 1.33)	**1.20** (1.17, 1.24)	**1.20** (1.17, 1.24)	**1.21** (1.18, 1.24)
MCN_{10Gy}	**1.03** (1.01, 1.04)	**1.02** (1.01, 1.03)	**1.02** (1.01, 1.03)	**1.02** (1.01, 1.03)
$RØR_{2Gy}$	**1.26** (1.23, 1.30)	**1.18** (1.16, 1.22)	**1.19** (1.16, 1.22)	**1.20** (1.17, 1.23)
$RØR_{10Gy}$	**1.02** (1.01, 1.03)	**1.02** (1.01, 1.02)	**1.02** (1.01, 1.02)	**1.02** (1.01, 1.02)
WIL	**1.29** (1.24, 1.33)	**1.18** (1.16, 1.23)	**1.19** (1.16, 1.23)	**1.20** (1.17, 1.24)

Appendix D

Comparison of results from this thesis with that of other studies, and adjustment of results from other studies with the highest median relative risk estimates by variable RBE models in this thesis.

Comparison of results (Table D.1): In the study by Mu et al., the lifetime risk of lung and thyroid cancer was not estimated individually but could be recreated using the method described in the article with the organ absorbed doses listed. As the dose to the thyroid was 0 Gy(RBE) in both Miralbell et al. and Mu et al., the calculations could only be done for the lungs. These two studies only used a linear model to estimate risks for 1 and 5 paediatric medulloblastoma patients, respectively, while Stokkevåg et al. used a linear, linear-exponential and plateau model to estimate risks for 6 paediatric medulloblastoma patients. All studies used a DDREF in their estimations, which was removed for the comparison (2 from the ICRP 60 recommendations for Miralbell et al. and Mu et al., and 1.5 from the BEIR VII recommendations for Stokkevåg et al.). The dose of 36 Gy(RBE) used in Miralbell et al. was adjusted to a 23.4 Gy(RBE) regime as well as using the median lifetime of this study (92 years) with their calculated risk in yearly rate (in %) to yield lifetime risk. The tissue weighting factor for lungs of 0.12 was also removed.

Table D.1: Comparison of lifetime risk of radiation-induced secondary cancer following proton CSI with pencil beam scanning from different studies. The lifetime risks from the chosen studies have been modified to be comparable with the results in this thesis.

Study *Dose-response relationship*

	Linear		Linear-exponential		Plateau	
	Lung	Thyroid	Lung	Thyroid	Lung	Thyroid
Miralbell et al. (2002)	10.0	-	-	-	-	-
Mu et al. (2005)	9.9	-	-	-	-	-
Stokkevåg et al. (2014)	15.0	1.5	3.0	1.2	6.0	0.9
Thesis	21.3 (6.8, 43.5)	6.0 (1.1, 49.4)	5.6 (2.4, 11.4)	4.9 (1.0, 35.5)	10.4 (3.8, 20.9)	2.3 (0.6, 8.3)

Table D.2 and D.3: Results from several studies that have compared secondary cancer risk estimates for proton therapy and photon therapy for paediatric medulloblastoma patients receiving CSI [24-31]. The risk estimates in each of these studies presented in Table D.2 are adjusted by the highest median relative risk made by the variable RBE models in this thesis. The corresponding resulting risk relative to the photon risk estimates are presented in Table D.3 for comparison.

Table D.2: Lifetime risk of radiation-induced secondary cancer values in [%] for proton therapy from different studies comparing photon and proton risk estimations. Each value is adjusted by the highest median relative risks found in this thesis, corresponding to the dose-response relationship and organ at risk of each study.

Study	Dose-response relationship and modality	Lung	Lung (variable RBE)	Thyroid	Thyroid (variable RBE)
Miralbell et al. (2002)[a]	Linear, IMPT	0.01	0.013	-	-
Mu et al. (2005)[b]	Linear, IMPT (incl. neutrons)	4.9	6.4	-	-
Newhauser et al. (2009)[a]	Linear, IMPT	0.011	0.014	0.004	0.006
	Linear, PS	0.014	0.018	0.005	0.007
Zhang et al. (2013)[c]	Linear, PS	11.4	14.8	0.5	0.7
Zhang et al. (2014)[d]	Linear, PS median (range)	12.0 (4.0, 36.0)	15.6 (5.2, 46.8)	1.0 (0.2, 4.0)	1.5 (0.3, 5.9)
Stokkevåg et al. (2014)[e]	Linear, IMPT (PS)	10.0 (7.8)	13.0 (10.1)	1.0 (0.8)	1.5 (1.2)
	Lin-exp, IMPT (PS)	2.0 (1.0)	2.2 (1.1)	0.8 (0.9)	1.1 (1.2)
	Plateau, IMPT (PS)	4.0 (2.2)	4.8 (2.6)	0.6 (1.0)	0.7 (1.1)
Taddei et al. (2015)[c]	Linear, PS (incl. neutrons)	12.3 (16.8)	16.0 (21.8)	1.5 (3.9)	2.2 (5.7)
Taddei et al. (2018)[c]	Linear, PS (incl. neutrons)	11.7 (13.0)	15.2 (16.9)	1.5 (2.4)	2.2 (3.5)

[a] Photon risk estimates were done for either CRT or IMRT or both – for both, ratio is listed as CRT/IMRT
[a] Risk given in yearly rate [%], thus given more decimals to show change with variable RBE
[b] Estimated organ-specific lifetime risk from article information (average organ dose in table II) and the ICRP 103 report (table A.4.2)
[c] Estimated organ-specific LAR from article information and the BEIR VII report (table 12D-1)
[d] Calculated median LAR from supplementary material to the article
[e] Average LAR eye measured from Figure 6 in article

Table D.3: The ratio of adjusted proton risk estimates normalised to photon risk estimates are given for each organ. Photon risk estimates were done for either CRT or IMRT or both – for both, ratio is listed as CRT/IMRT

Study	Dose-response relationship and modality	Lung ratio	Adjusted lung ratio	Thyroid ratio	Adjusted thyroid ratio
Miralbell et al. (2002)[a]	Linear, IMPT	0.14	0.19/0.19	-	-
Mu et al. (2005)[b]	Linear, IMPT (incl. neutrons)	0.91/0.42	0.96/0.44	-	-
Newhauser et al. (2009)[a]	Linear, IMPT	0.16/0.16	0.20/0.20	0.02/0.07	0.03/0.10
	Linear, PS	0.20/0.20	0.26/0.26	0.03/0.08	0.04/0.12
Zhang et al. (2013)[c]	Linear, PS	0.63	0.82	0.04	0.05
Zhang et al. (2014)[d]	Linear, PS median (range)	0.75	0.98	0.06	0.08
Stokkevåg et al. (2014)[e]	Linear, IMPT (PS)	0.56 (0.43)	0.72 (0.56)	0.03 (0.003)	0.05 (0.04)
	Lin-exp, IMPT (PS)	0.40 (0.20)	0.44 (0.22)	0.05 (0.01)	0.07 (0.08)
	Plateau, IMPT (PS)	0.48 (0.27)	0.58 (0.31)	0.09 (0.14)	0.10 (0.16)
Taddei et al. (2015)[c]	Linear, PS (incl. neutrons)	0.32 (0.44)	0.42 (0.58)	0.03 (0.07)	0.04 (0.10)
Taddei et al. (2018)[c]	Linear, PS (incl. neutrons)	0.66 (0.73)	0.86 (0.95)	0.04 (0.06)	0.06 (0.09)

[a] Photon risk estimates were done for either CRT or IMRT or both – for both, ratio is listed as CRT/IMRT
[a] Risk given in yearly rate [%], thus given more decimals to show change with variable RBE
[b] Estimated organ-specific lifetime risk from article information (average organ dose in table II) and the ICRP 103 report (table A.4.2)
[c] Estimated organ-specific LAR from article information and the BEIR VII report (table 12D-1)
[d] Calculated median LAR from supplementary material to the article
[e] Average LAR eye measured from Figure 6 in article